ESTABLISH HIGHWAY BRIDGE NETWORK RESILIENCE VIA MULTI-HAZARDS SUSCEPTIBILITY MODELING

by

Sophia Lin

A dissertation submitted to the faculty of
The University of North Carolina at Charlotte
in partial fulfillment of the requirements
for the degree of Doctor of Philosophy in
Infrastructure and Environmental Systems

Charlotte

2024

Approved by:

_____
Dr. Shen-En Chen

_____
Dr. Wenwu Tang

_____
Dr. Nicole Braxtan

_____
Dr. Wei Fan

_____
Dr. Yuting Chen

ABSTRACT

SOPHIA LIN. Establish highway bridge network resilience via multi-hazards susceptibility modeling. (Under the direction of DR. SHEN-EN CHEN)

Climate change presents a pressing challenge for natural disaster management, to quantify its effects and associated disasters is a persistent challenge for regional climate risk studies. As climate-induced hazards escalate in intensity and frequency, infrastructure in hazard-prone regions faces growing risks – A situation especially critical to transportation infrastructures. Recent events, such as Hurricane Helene in 2024, which caused widespread damage to life supporting infrastructures including washing out bridges resulting in roadway closures, underscore the urgency of addressing these combined hazards. This dissertation assesses multi-hazard risks to bridge infrastructure in North Carolina's mountainous regions, focusing on the interplay between landslide, flooding, wildfire, and earthquake risks. We approach the multi-hazard issue using landslide as the basic quantifier and investigate the nesting effect of earthquake and rainfall triggered landslides.

Because forest fire has the potential of diminishing soil moisture and can encourage landslides, wildfire risk is also included as a predictor. Analysis identified key wildfire-related variables, such as distance to roads, elevation, and proximity to populated areas, as significant contributors to landslide susceptibility, highlighting the role of remote sensing data in extreme weather event prediction. Soil type, included in the landslide model, had limited impact, suggesting the need for refined soil classification methods in future studies.

Utilizing logistic regression (LR) and random forest (RF) models, this study develops predictive maps for landslide and wildfire susceptibility, achieving accuracy rates

of 75.7% and 83.9% for landslide prediction and 68.5% and 72.9% for wildfire prediction, respectively. The higher sensitivity of the RF model, as shown in a ROC curve analysis, demonstrates its effectiveness for multi-hazard risk modeling.

The wildfire susceptibility map is then incorporated as an independent variable in predicting landslide occurrences, revealing critical interactions between wildfire and landslide risks. The result are two different landslide susceptibility maps. Finally, a novel index, the Assumed Flooding Potential (AFP), is introduced to quantify flood risk to a bridge. Since it is hard to establish flooding scenarios for bridges in mountain regions. AFP is calculated as the mid-span clearance for bridges. Furthermore, using a 30m radius as site topology calculation, bridges-in-valleys are identified for high flooding risk analysis.

The integration of multi-hazard data allows for a dynamic understanding of bridge vulnerability, resulting in a shift in risk probability for certain structures. Specifically, the number of bridges with over a 50% probability of multi-hazard risk exposure decreased from 47 to 26, while four new bridges emerged in high-risk zones due to the addition of wildfire susceptibility data. These findings provide actionable insights for decision-makers, enabling proactive mitigation strategies tailored to bridges that face increased vulnerability from wildfire-triggered landslides.

This research delivers a high-resolution multi-hazard risk map and model for infrastructure resilience planning, offering critical tools for bridge engineers and policymakers. The 2024 Hurricane Helene landslides and bridge damage data from the state have been used to validate the risk maps. The results indicated reasonable accurate predictions, thus, ascertaining the study contributed to the potential to anticipate future multi-hazard risks. However, it also highlighted the need to address the complex

interactions between environmental and anthropogenic factors and the urgency for future studies to advance our understanding of climate effects and to enhance our ability to anticipate and mitigate multi-hazard impacts on critical infrastructure in the face of evolving climate challenges.

ACKNOWLEDGMENTS

It is a fantasy journal for pursuing Ph.D. First and foremost, I would like to sincerely thank my advisor, Dr. Sen-En Chen. He has shared a wealth of knowledge, provided invaluable advice, and guided me throughout this journey, enabling me to achieve my goals. I deeply appreciate all of Dr. Chen's support during this transformative experience.

I am also immensely grateful to Dr. Wenwu Tang for offering me opportunities to work with CAGIS and for involving me in the Geo-Frit project. To my committee members—Dr. Tang, Dr. Nicole Braxtan, Dr. Wei Fan, and Dr. Yuting Chen—I am truly thankful for your valuable comments and guidance.

I would like to acknowledge my funding support from the North Carolina Department of Transportation (NCDOT) and the support of the NCDOT Steering and Implementation Committee, including Dana Magliola, John W. Kirby, Mike Schoen, Mark Johnston, Tysean Wooten, Austin Chamberlain, Nazia Sarder, Chris Paslgrove, Patrick Flanagan, Josh Kellen, Karyl Fuller, James Salmons, Meredith McDiarmid, Nastasha E. Young, Matthew Lauffer, Colin Melior, and Curtis Bradley. I am also thankful to Nastasha Earle-Young for her assistance with data support.

I want to extend my heartfelt thanks to the Geo-Frit project team members, Dr. Tianyang Chen and Zachery Slocum, for their advice and encouragement. Special thanks go to Dr. Tarini Shukla and Dr. Yu Lan for their tremendous help in supporting me throughout my Ph.D. journey. I am also sincerely grateful to Dr. Jy S. Wu, Dr. John Diemer, Dr. Eric M. Delmelle, and Dr. William L. Saunders, Jr., for their guidance and support along the way.

Finally, I would like to express my eternal gratitude to my family. I am forever grateful to my loving parents, Chih-Sen and Ming-Yueh, and to my brother and sister-in-law, Karl and Chia-Jung. To my two adorable nephews, Lyon and Zareck, thank you for your love and support.

Lastly, to the most important person in my life, my boyfriend, Yu-Kai: thank you for your patience, love, and unwavering support, which have allowed me to pursue my Ph.D. without hesitation and regret. I am endlessly grateful to you.

DEDICATION

To my parents, brother, sister-in-law, my nephews, and my boyfriend.

TABLE OF CONTENTS

LIST OF TABLES

LIST OF FIGURES

LIST OF ABBREVIATIONS

AFP	Assuming Flooding Potential
AIC	Akaike Information Criterion
AUC	Area Under Curve
BRT	Boosted Regression Tree
DEM	Digital Elevation Model
DOTs	Departments of Transportation
FAHP	Fuzzy Analytical Hierarchy Process
FHWA	Federal Highway Administration
FPR	False Positive Rate
GCM	Global Climate Models
GIS	Geographic Information Systems
GLC	Global Landslide Catalog
IDW	Inverse Distance Weighted
LR	Logistic Regression
MaxEnt	Maximum Entropy
ML	Machine Learning
NASA	National Aeronautics and Space Administration
NC	North Carolina
NCDHHS	NC Department of Health and Human Services
NCDOT	North Carolina Department of Transportation
NCFS	North Carolina Forest Service
NCGS	North Carolina Geological Survey

NHD	National Hydrography Dataset
NMH	Nested Multi-Hazard
NOAA	National Oceanic and Atmospheric Administration
OOB	Out of Bag
RF	Random Forest
ROC	Receiver Operating Characteristic
SVM	Support Vector Machine
TPR	True Positive Rate
USDA	U.S. Department of Agriculture
USGS	U.S. Geological Survey

Chapter 1: Introduction

1.1 Introduction

Climate change is a critical issue for natural disaster management, and quantification of climate effects and the associated disasters have always been a challenge for regional risk studies. The frequency and intensity of these events are expected to continue rising in the future, posing significant challenges to infrastructure resilience and public safety (Argyroudis & Mitoulis, 2021; Liang & Xiong, 2019). As a result, there is a growing need for accurate predictions and risk assessments to identify high-risk areas and prioritize mitigation efforts (Kavzoglu & Teke, 2022; Kim et al., 2021; Lee et al., 2017; Wubalem & Meten, 2020).

Climate extremes can result in several disaster scenarios ranging from extreme flooding, torrential rain, intense earthquakes, draught, forest fires and landslides. Some of the climate disasters are interrelated, for example, torrential rain can induce ground saturation and result in more landslides, and draught can induce forest fires and result in soil's lack of ability to hold moisture which increase landslide risk. To better define the effects of climate change on natural disasters, we focus our efforts in a more traditional approach, namely, to collect historical data on significant events and study natural disasters that include hurricanes, floods, wildfires, and landslides (Chen et al., 2020; Kavzoglu & Teke, 2022; Lee et al., 2017; Milanović et al., 2021; Taalab et al., 2018).

To establish the causality of different disasters, geospatial, geomorphic, and meteorological variables along with historical storm and seismicity data have been collected, analyzed, and used for disaster risk (Chen et al., 2020; Kavzoglu & Teke, 2022; Milanović et al., 2021; Sun et al., 2021; Taalab et al., 2018; Wubalem & Meten, 2020).

Different machine learning tools, including random forest (RF), have been used in the modeling of disaster risks (Milanović et al., 2021; Taalab et al., 2018). The outcomes can be applied to enhance the resilience of highway infrastructures, such as freight routings and bridges (Argyroudis & Mitoulis, 2021; Pervaiz & Hummel, 2023) .

From the infrastructure management perspective, state departments of transportation (DOTs) across the country are facing increased maintenance costs and resource strains due to more frequent and intense extreme weather events, including floods, coastal storms, and heat waves, with impacts varying by regions (Nasr et al., 2021; Rowan et al., 2013). For the past three years, extreme events in frequency, intensity, and duration have been studied at UNC Charlotte and the outcomes have been applied to various highway infrastructures such as bridges and freight routings (Wenwu Tang, 2023). Bridges are critical components of transportation infrastructure, supporting economies and societies worldwide (Koks et al., 2019; Li et al., 2020). However, roads and bridges are vulnerable to various hazards, and their failure can significantly disrupt transport networks (Argyroudis & Mitoulis, 2021; Pervaiz & Hummel, 2023).

The escalating impacts of climate change, including more frequent extreme weather events and harsh environmental conditions, significantly challenge the resilience and durability of transportation infrastructure, particularly bridges, highlighting an urgent need for more research and adaptive strategies (Hunt & Watkiss, 2011; Mondoro et al., 2018; Pachauri et al., 2014; Schulz et al., 2017). As uncertainties in the life-cycle of civil infrastructure systems accumulate, there is a growing recognition among researchers, policymakers, and insurers of the critical importance of enhancing risk mitigation measures

and improving the performance and recovery capabilities of bridges to minimize losses (Biondini & Frangopol, 2016; Li et al., 2020).

The concept of resilience has gained prominence in discussions about infrastructure management following significant damages to U.S. infrastructure by Hurricanes Katrina, Sandy, and Harvey (Minaie & Moon, 2017; Serre & Heinzlef, 2018). These events highlighted the critical role of transportation networks, particularly highway bridges, in maintaining the economic and social well-being of the nation (Andersson et al., 2021; Zhang et al., 2017). Bridges, identified as particularly vulnerable to climate changes, are crucial to the robustness and recovery of transportation systems during extreme hazards such as earthquakes, wind storms, floods, and landslides (Dong & Frangopol, 2016; Minaie & Moon, 2017; Zhang et al., 2017). Damage to these structures not only increases community vulnerability but also impedes emergency responses, such as effective evacuation and recovery efforts that heavily depend on reliable road infrastructure (Minaie & Moon, 2017).

Resilience in infrastructure refers to the ability of infrastructure systems, such as utilities, communication system, medical facility and transportation system, to resist, absorb, recover from, and adapt to adverse events (Dong & Frangopol, 2016). Resilience is characterized by four key dimensions: a) Robustness, which is the ability to withstand extreme events and maintain a certain level of service afterwards; b) rapidity, referring to the speed at which recovery from a disaster occurs; c) redundancy, which involves having substitutable components within the system to ensure continuity; and d) resourcefulness, defined as the availability of resources to effectively respond to a disaster (Zhang et al., 2017). In other words, robustness and rapidity are the objectives of resilience, while

redundancy and resourcefulness are the means to achieve the desired level of resilience (Minaie & Moon, 2017). Minaie and Moon (2017) defined a bridge resilience framework that includes disaster events including flood and earthquake.

1.2 Statement of work

This dissertation aims to assess multi-hazard risks, in particular, landslides and flooding, affecting bridge infrastructure in North Carolina's mountainous regions. Specifically, it will develop a predictive model to map susceptibility to these hazards, using data from the USGS, NCDOT, and USDA. The scope is limited to roadway bridges situated in valleys, with special attention to those exposed to potential landslide and flooding risks. The methodology includes model risk using logistic regression (LR) and random forest (RF) modeling techniques, conducted in ArcGIS Pro and R, then validate model validation based on recent hurricane data. Major tasks include data collection, model development, validation, and analysis, leading to the delivery of a susceptibility model, a risk map, and investigation of potential bridge damage models. The findings are expected to ultimately provide resource for proactive bridge maintenance strategies, contributing to safer and more resilient infrastructure in climate-vulnerable areas.

1.3 Problem Statement and Purpose

With the increasing frequency and intensity of extreme weather events due to climate change, transportation infrastructure, particularly bridges, is facing unprecedented risks. In North Carolina (NC), bridges in mountainous regions are exposed to multi-hazard scenarios, including landslides, wildfire, earthquake and flooding, only limited research has specifically addressed the vulnerability of these bridges to the combined effect of all the extreme weather events. Despite advances in risk assessment for single hazards, there

is a critical gap in multi-hazard assessment that integrates both landslide and flooding risks for infrastructure resilience planning. Addressing this gap is essential for developing proactive maintenance and mitigation strategies that can improve bridge resilience in hazard-prone areas.

The purpose of this study is to develop a nested multi-hazard susceptibility model for assessing landslide and flooding risks to bridges in NC's mountainous regions. By integrating geospatial data and employing logistic regression and random forest modeling techniques, this research will create a high-fidelity risk map identifying bridges at high risk of multi-hazard exposure. The findings will provide valuable insights for bridge engineers and policymakers, enabling more effective infrastructure resilience planning and hazard mitigation in the face of increasing climate-related risks.

1.4 Research of Objectives

Through our prior post-disaster studies in Puerto Rico after 2017 Hurricane Maria, we recognized the effects of bridge location and the multiple hazard impacts. Specifically, several bridges in Puerto Rico were damaged or washed out because they geographically situated in valleys and as a result, they suffered from the combined flooding from torrential rain and from congested stream bed from landslides. The goals of this study are to predict landslide, wildfire, and flood events in NC and to recognize the high risk bridges to enhance disaster response. The specific objectives of this research are expected to have several significant implications in NC and are defined as:

1. Develop predictors of multi-hazard susceptibility risk maps as functions of landslide for NC mountain region;

2. Using multi-hazard maps to identify critical highway bridges based on the physical locations;
3. Investigate recent Hurricane Helene-induced slides and flooding scenarios; and
4. Interpret bridge damage based on Helene landslide and flooding.

The 2024 Hurricane Helene provided valuable opportunity to assess the product of current research. This natural disaster has enhanced the contributions of current study that included the following:

1. Landslide, wildfire, and flood susceptibility maps for NC, are generated, thus, enabling more effective strategies and systems for disaster response and mitigation;
2. This study offers first observation and assessment of the landside prediction after Hurricane Helene;
3. Based on the variable consideration and the available data collected from state resource show the possibility of using ML for multi-hazard risk modeling for the western NC's mountain region; and finally
4. This study provides an insight to the possible damage mechanisms of the 79 bridges.

1.5 Research Methodology

This study employs geospatial and statistical methods to analyze landslide susceptibility and bridge vulnerability within mountainous regions of North Carolina. Using datasets from the USGS, NCDOT, FHWA, and other agencies, we compiled a comprehensive landslide and bridge inventory. The landslide inventory includes 4,794 points and 6,653 polygons, while the bridge dataset comprises 22,812 bridges.

Key conditioning factors for landslide susceptibility were determined, including elevation, slope, aspect, rainfall, and distances to faults and rivers, all derived using ArcGIS Pro tools. Elevation and slope were calculated from USGS DEM data, while rainfall totals were interpolated using the Inverse Distance Weighted method with NOAA data. To account for the influence of seismicity, distances to faults were included, and proximity to rivers was used to represent potential erosion risks.

Two statistical models, Logistic Regression (LR) and Random Forest (RF), were applied to estimate landslide susceptibility. Logistic Regression was used to establish the probability of landslide occurrence, while the Random Forest model provided enhanced predictive accuracy and robust model validation through ROC curve analysis.

For bridge susceptibility, we identified structures located in valleys using various ArcGIS Pro tools, calculating an Approximate Flooding Potential (AFP) for each bridge based on elevation data from DEM. This analysis considers landform classifications derived from geomorphons, slope, and elevation differences to determine vulnerability.

Through these methods, the study provides a spatial analysis framework that combines environmental conditioning factors with advanced statistical models to assess multi-hazard risks to bridges in North Carolina's mountainous terrain.

1.6 Scope of Work

This study assesses multi-hazard risks, specifically landslides, wildfires, and their impact on bridge infrastructure within North Carolina's mountainous regions. As a southeastern coastal state, North Carolina (NC) is vulnerable to Atlantic hurricanes, similar to Puerto Rico, which exposes the state to related hazards. The study area encompasses one

regions of NC: Appalachian Mountains, with particular emphasis on the mountainous region where landslides and wildfires are prevalent.

Landslides are a significant hazard in the Appalachian Mountains (26,572 km²), affecting infrastructure and leading to events like the 2005 Pigeon River Gorge rockslide, which incurred over $15 million in costs. Despite this risk, specific landslide assessments targeting roadway bridges are limited. To address this, we utilized landslide data from 1900 to 2021, collected by the USGS, focusing on high-confidence landslide areas rated between 5 and 8 on a susceptibility scale.

Wildfire is another common hazard in NC, influenced by factors such as fuel accumulation, seasonal precipitation variability, and frequent droughts. Defined as "an unplanned and uncontrolled fire spreading through vegetative fuels" (Intini et al., 2019), wildfires have occurred annually from 1928 to 2023, as documented by the North Carolina Forest Service (NCFS). For this study, wildfire data from the U.S. Department of Agriculture (USDA) from 1995 to 2018 were compiled, focusing on human-induced and naturally occurring wildfire events, with undetermined causes excluded. The dataset contains 112,454 wildfire events across NC, including significant incidents like the 2011 Pains Bay fire, one of the largest natural wildfire events in the state.

Through this multi-hazard approach, the study aims to identify the susceptibility of bridges in NC's mountainous region to landslides and wildfires, providing critical insights for infrastructure resilience and hazard management.

1.7 Dissertation Outline

This dissertation is organized into seven chapters, each addressing critical aspects of multi-hazard risks to transportation infrastructure in North Carolina, with a focus on

landslides and flooding vulnerabilities affecting bridges. Following this Introduction chapter, Chapter 2 assesses landslide and flooding risks to bridges located in valleys across North Carolina using logistic regression and random forest models, introducing the AFP metric to aid in risk visualization for bridge engineers. Building on Chapter 2, Chapter 3 develops a nested multi-hazard model to assess susceptibility to landslides and flooding, refining AFP to prioritize high-risk bridges in the mountainous regions of North Carolina. Chapter 4 documents the structural impacts of Hurricane Helene on North Carolina bridges, highlighting vulnerabilities in bridge design exposed by landslide-induced flooding from extreme weather events. Chapter 5 provides that landslide events from Hurricane Helene are used to validate the susceptibility model, providing empirical support for the model's reliability in predicting multi-hazard risks. Chapter 6 synthesizes the research findings, emphasizing their implications for multi-hazard risk management in bridge engineering and infrastructure resilience. The final Chapter 7 suggests avenues for expanding the research, including additional hazard types and refined flood risk analysis, to enhance infrastructure resilience strategies.

Reference

Andersson, J., Grassi, V., Mirandola, R., & Perez-Palacin, D. (2021). A conceptual framework for resilience: fundamental definitions, strategies and metrics. *Computing, 103*(4), 559-588. doi:10.1007/s00607-020-00874-x

Argyroudis, S. A., & Mitoulis, S. A. (2021). Vulnerability of bridges to individual and multiple hazards- floods and earthquakes. *Reliability Engineering & System Safety, 210*, 107564. doi:https://doi.org/10.1016/j.ress.2021.107564

Biondini, F., & Frangopol, D. M. (2016). Life-Cycle Performance of Deteriorating Structural Systems under Uncertainty: Review. *Journal of Structural Engineering, 142*(9), F4016001. doi:doi:10.1061/(ASCE)ST.1943-541X.0001544

Chen, W., Li, Y., Xue, W., Shahabi, H., Li, S., Hong, H., . . . Ahmad, B. B. (2020). Modeling flood susceptibility using data-driven approaches of naïve Bayes tree, alternating decision tree, and random forest methods. *Science of The Total Environment, 701*, 134979. doi:https://doi.org/10.1016/j.scitotenv.2019.134979

Dong, Y., & Frangopol, D. M. (2016). Probabilistic Time-Dependent Multihazard Life-Cycle Assessment and Resilience of Bridges Considering Climate Change. *Journal of Performance of Constructed Facilities, 30*(5), 04016034. doi:doi:10.1061/(ASCE)CF.1943-5509.0000883

Hunt, A., & Watkiss, P. (2011). Climate change impacts and adaptation in cities: a review of the literature. *Climatic Change, 104*(1), 13-49. doi:10.1007/s10584-010-9975-6

Intini, P., Ronchi, E., Gwynne, S., & Pel, A. (2019). Traffic Modeling for Wildland–Urban Interface Fire Evacuation. *Journal of Transportation Engineering, Part A: Systems, 145*(3), 04019002. doi:doi:10.1061/JTEPBS.0000221

Kavzoglu, T., & Teke, A. (2022). Predictive Performances of Ensemble Machine Learning Algorithms in Landslide Susceptibility Mapping Using Random Forest, Extreme Gradient Boosting (XGBoost) and Natural Gradient Boosting (NGBoost). *Arabian Journal for Science and Engineering, 47*(6), 7367-7385. doi:10.1007/s13369-022-06560-8

Kim, H., Lee, J.-H., Park, H.-J., & Heo, J.-H. (2021). Assessment of temporal probability for rainfall-induced landslides based on nonstationary extreme value analysis.

Engineering Geology, 294, 106372. doi:https://doi.org/10.1016/j.enggeo.2021.106372

Koks, E. E., Rozenberg, J., Zorn, C., Tariverdi, M., Vousdoukas, M., Fraser, S. A., . . . Hallegatte, S. (2019). A global multi-hazard risk analysis of road and railway infrastructure assets. *Nature communications, 10*(1), 2677.

Lee, S., Kim, J.-C., Jung, H.-S., Lee, M. J., & Lee, S. (2017). Spatial prediction of flood susceptibility using random-forest and boosted-tree models in Seoul metropolitan city, Korea. *Geomatics, Natural Hazards and Risk, 8*(2), 1185-1203. doi:10.1080/19475705.2017.1308971

Li, Y., Dong, Y., Frangopol, D. M., & Gautam, D. (2020). Long-term resilience and loss assessment of highway bridges under multiple natural hazards. *Structure and Infrastructure Engineering, 16*(4), 626-641. doi:10.1080/15732479.2019.1699936

Liang, Y., & Xiong, F. (2019). Quantification of debris flow vulnerability of typical bridge substructure based on impact force simulation. *Geomatics, Natural Hazards and Risk, 10*(1), 1839-1862. doi:10.1080/19475705.2019.1641564

Milanović, S., Marković, N., Pamučar, D., Gigović, L., Kostić, P., & Milanović, S. D. (2021). Forest Fire Probability Mapping in Eastern Serbia: Logistic Regression versus Random Forest Method. *Forests, 12*(1), 5. Retrieved from https://www.mdpi.com/1999-4907/12/1/5

Minaie, E., & Moon, F. (2017). Practical and Simplified Approach for Quantifying Bridge Resilience. *Journal of Infrastructure Systems, 23*(4), 04017016. doi:doi:10.1061/(ASCE)IS.1943-555X.0000374

Mondoro, A., Frangopol, D. M., & Liu, L. (2018). Bridge Adaptation and Management under Climate Change Uncertainties: A Review. *Natural Hazards Review, 19*(1), 04017023. doi:doi:10.1061/(ASCE)NH.1527-6996.0000270

Nasr, A., Björnsson, I., Honfi, D., Larsson Ivanov, O., Johansson, J., & Kjellström, E. (2021). A review of the potential impacts of climate change on the safety and performance of bridges. *Sustainable and Resilient Infrastructure, 6*(3-4), 192-212. doi:10.1080/23789689.2019.1593003

Pachauri, R. K., Allen, M. R., Barros, V. R., Broome, J., Cramer, W., Christ, R., . . . Dasgupta, P. (2014). *Climate change 2014: synthesis report. Contribution of*

Working Groups I, II and III to the fifth assessment report of the Intergovernmental Panel on Climate Change: Ipcc.

Pervaiz, F., & Hummel, M. A. (2023). Effects of Climate Change and Urbanization on Bridge Flood Vulnerability: A Regional Assessment for Harris County, Texas. *Natural Hazards Review, 24*(3), 04023025. doi:doi:10.1061/NHREFO.NHENG-1720

Rowan, E., Evans, C., Riley-Gilbert, M., Hyman, R., Kafalenos, R., Beucler, B., . . . Schultz, P. (2013). Assessing the Sensitivity of Transportation Assets to Extreme Weather Events and Climate Change. *Transportation Research Record, 2326*(1), 16-23. doi:10.3141/2326-03

Schulz, A., Zia, A., & Koliba, C. (2017). Adapting bridge infrastructure to climate change: institutionalizing resilience in intergovernmental transportation planning processes in the Northeastern USA. *Mitigation and Adaptation Strategies for Global Change, 22*(1), 175-198. doi:10.1007/s11027-015-9672-x

Serre, D., & Heinzlef, C. (2018). Assessing and mapping urban resilience to floods with respect to cascading effects through critical infrastructure networks. *International Journal of Disaster Risk Reduction, 30*, 235-243. doi:https://doi.org/10.1016/j.ijdrr.2018.02.018

Sun, D., Wen, H., Zhang, Y., & Xue, M. (2021). An optimal sample selection-based logistic regression model of slope physical resistance against rainfall-induced landslide. *Natural Hazards, 105*(2), 1255-1279. doi:10.1007/s11069-020-04353-6

Taalab, K., Cheng, T., & Zhang, Y. (2018). Mapping landslide susceptibility and types using Random Forest. *Big Earth Data, 2*(2), 159-178. doi:10.1080/20964471.2018.1472392

Wubalem, A., & Meten, M. (2020). Landslide susceptibility mapping using information value and logistic regression models in Goncha Siso Eneses area, northwestern Ethiopia. *SN Applied Sciences, 2*(5), 807. doi:10.1007/s42452-020-2563-0

Zhang, W., Wang, N., & Nicholson, C. (2017). Resilience-based post-disaster recovery strategies for road-bridge networks. *Structure and Infrastructure Engineering, 13*(11), 1404-1413. doi:10.1080/15732479.2016.1271813

Chapter 2: Landslide Risks to Bridges-in-Valley in North Carolina

2.1 Abstract

This research delves into the intricate dynamics of landslides, emphasizing their consequences on transportation infrastructure, specifically highway and roadway bridges in North Carolina. Based on prior investigation of bridges in Puerto Rico after Hurricane Maria, we found bridges above water and situated in valleys can be exposed to both landslide and flooding risks. These bridges faced heightened vulnerability to combined landslides and flooding events due to their low depth to water surface and the potential of raised flood height due to upstream landslides. Leveraging a dataset spanning more than a century and inclusive of landslide and bridge infor-mation, we employed logistic regression (LR) and random forest (RF) models to predict land-slide susceptibility in North Carolina. The study considered conditioning factors such as eleva-tion, aspect, slope, rainfall, distance to faults, and distance to rivers, yielding LR and RF models with accuracy rates of 76.3% and 82.7%, respectively.

To establish the bridge location is in the bottom of a valley, data including landform, slope and elevation difference near the bridge location were combined to delineate bridge-in-valley. The difference between bridge height and the lowest river elevation is established as an assumed flooding potential (AFP), which is then used to quantify the flooding risk. Compared to tradi-tional flood risk values, the AFP, reported in elevation differences, is more straightforward and helps bridge engineers visualize the flood risk to a bridge. Specifically, a bridge (NCDOT ID: 740002) is found susceptible to both landslide (92%) and flooding (AFT of 6.61 m) risks and has been validated by field investigation, which is currently being retrofitted by North Carolina DOT with slope reinforcements (soil nailing

and grouting). This paper is a first report in evalu-ating the multi-hazard issue for bridges-in-valleys. The resulting high-fidelity risk map for North Carolina can help bridge engineers in proactive maintenance planning. Future endeavors will extend the analysis to incorporate actual flooding risk susceptibility analysis, thus enhanc-ing our understanding of multi-hazard impacts and guiding the resilient mitigation strategies on transportation infrastructure.

Keywords: bridges in valleys, landslide risk, flooding risk, multi-hazards

2.2 Introduction

Landslides are influenced by geological, geomorphological, topographical, and hydrological factors and represent a substantial natural hazard with evolving consequences for hillslope morphology and human activities (Pourghasemi et al., 2018; Regmi et al., 2014; Sun et al., 2021). According to the Global Landslide Catalog (GLC), which presents landslide events caused only by rainfall conditions, landslides can occur in any country (Kirschbaum et al., 2015; Kirschbaum et al., 2010). Figure 2-1 shows the distribution of landslides occurring around the world according to the GLC. The United States of America has the highest occurrence of landslides in the world. Reports from landslide-prone regions documenting substantial economic losses have been recorded in the United States, Italy, Japan, India, China, and Germany(Chen, Zhang, et al., 2018; Nhu et al., 2020). Impacts including fatalities, injuries, and extensive damage to infrastructure and land, as seen in Europe, Ethiopia, and China, underscore the widespread and varied consequences of these events(Chen, Zhang, et al., 2018; Ganga et al., 2022; Nhu et al., 2020; Wubalem & Meten, 2020). For example, landslides cause in excess of $1 billion in damage and more than 25 fatalities in the United States each year (USGS, 2023b).

A landslide can be exacerbated by factors like seismic activity and global warming-induced rainstorms, leading to escalating occurrence of landslides (Kim et al., 2018). The complex and challenging task of predicting landslides has driven the international focus on evaluating landslide susceptibility, leading to the development of diverse methods, including statistical, data mining, and soft computing-based techniques within geographic information systems (GIS), aiming to spatially identify vulnerable areas by establishing the

connection between landslide occurrence and relevant environmental factors (Pourghasemi et al., 2018).

Landslides are typically caused by triggering mechanisms including: heavy rainfall, snowmelt, changes in ground water levels and discharge, earthquakes, volcanic activity, and disturbance by human activities (Highland & Bobrowsky, 2008). Climate change resulted in increased magnitude and intensity of precipitation events and increased the risk of landslides and posed significant hazards towards infrastructure damage, human casualties, and economic losses (Ganga et al., 2022; Ozturk & Uzel-Gunini, 2022; Pourghasemi et al., 2018). For example, in 2017 elevated sea surface temperatures fueled the intensification of Hurricane Maria which triggered more than 40,000 landslides in Puerto Rico (Bessette-Kirton et al., 2019). Figure 2-2 and Figure 2-3 show examples of landslides triggered by Hurricane Maria.

The inspiration for current paper is from the damaged bridges in Puerto Rico after Hurricane Maria as reported by FEMA (Ortiz, 2020). Hurricane Maria's intensity has been linked to climate change and is indicative of current tropical storm scenarios predicted by climate modeling, which predict fewer but more severe tropical storms with significantly increased precipitation (Keellings & Hernández Ayala, 2019).

Figure 2-4 shows the torrential rain that resulted in flooding and caused the washout of a bridge structure and failure of river embankments in Las Marias, Puerto Rico. In this particular case, the neighborhood near the bridge was totally cut off from the outside for several weeks and the villagers relied on cables suspended across the river to receive their food and supplies.

Close examination of the bridge in Figure 2-4 shows a combination of local scour from massive flooding and embankment slope failures that resulted in the bridge washout. (The bridge in Figure 2-4a andFigure 2-4b is a replacement bridge under construction). With a central mountain range (the Cordillera Central) that has a maximum elevation of 1,338 m above sea level, Puerto Rico's landscape is characterized by steep slopes in most central parts of the island and relatively flat coastal plains on the perimeter of the island. As a result, the landslides triggered by Maria were complicated by the mountainous riverine network.

The Las Marias bridge (Figure 2-4) was exposed to severe flooding brought about by the torrential rain and congested water flow from the upstream landslides, resulted in the bridge failure. The bridge is situated in the bottom of a valley or gully, which created a situation for combination of flooding and landslide risks. Thus, it may be possible to estimate the risk to a bridge by differentiating where the bridge is situated, whether in the bottom of a valley, in the middle of a valley or at a ridge top.

Current study focuses on landslide impacts to highways and roadway bridges (Miele et al., 2021; Schlögl et al., 2019). When occurring near roadways landslides can suddenly block traffic, causing collisions and even direct loss of lives. The debris can further create unsafe road conditions, causing accidents due to drivers encountering obstacles. Large landslides can cause the total collapse of bridges and overpasses, directly endangering vehicles and occupants, elevating the risk of accidents due to road closures, obstacles, and damaged infrastructure. Therefore, landslides are critical geohazards that can undermine the structural stability of transportation infrastructure, which demand the

need to develop effective monitoring and new infrastructure resiliency strategies(Miele et al., 2021).

An accurate landslide risk map would be extremely helpful to regional Departments of Transportation (DOTs) to improve maintenance planning, routing decision making, and future site preparation. Ultimately, the outcomes of those improvements can be lifesaving. However, existing landslide risk analyses do not differentiate bridge locations in terms of whether they are in valleys or on ridge tops. Hence, this paper attempts to determine the major storm risks to the bridges in North Carolina by combining the North Carolina landslide risk information and highway and roadway bridge locations to help identify critical bridges that may be exposed to the damaging effects of landslides. These bridges can be differentiated into higher risk bridges depending on their geographical locations. As such, we can identify bridges that are likely to experience the combined risks of flooding and landslides.

This paper explains the mapping methodology of the bridge landslide risks by identifying their geographical situations and validated by site visits. The following section describes the study areas and the generation of the landslide database.

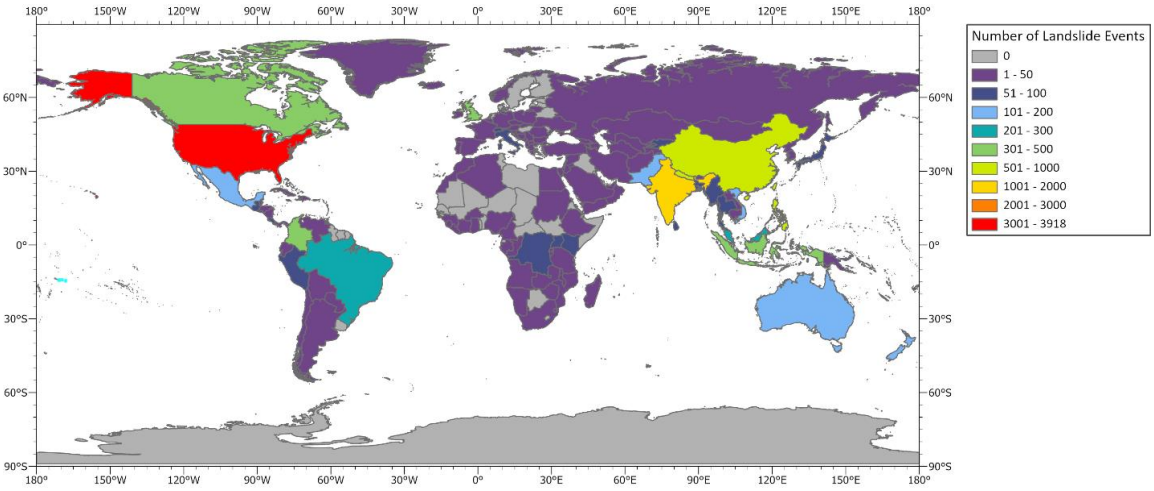

Figure 2-1. Number of landslide events from 2007 to 2023 by country (generated from NASA data).

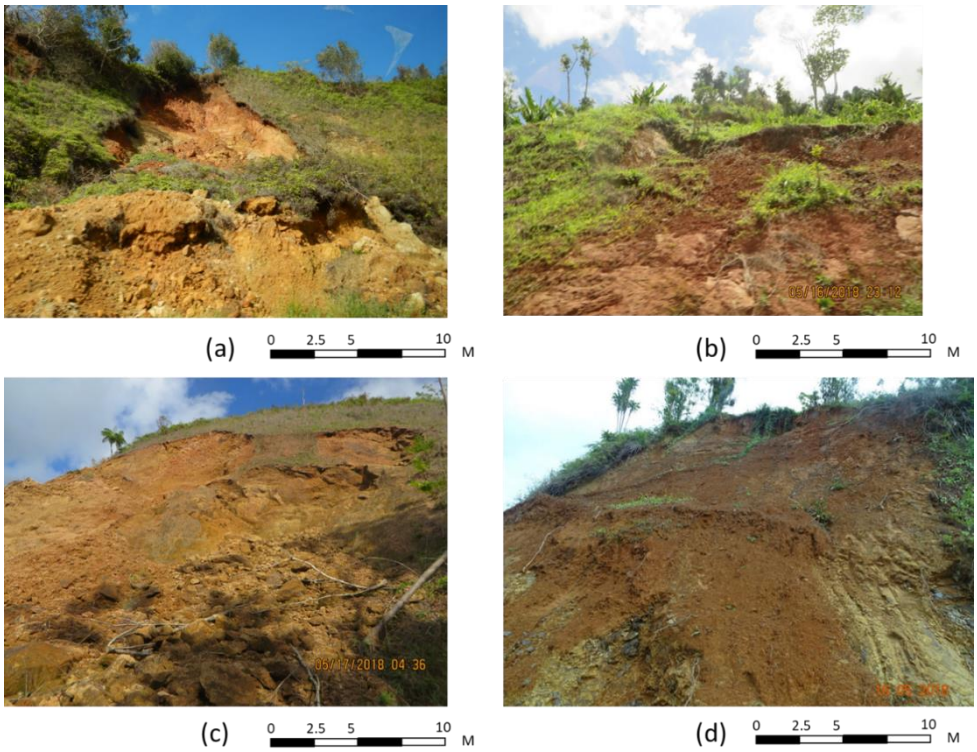

Figure 2-2. Landslide in Puerto Rico after 2017 Hurricane Maria: Surface observations indicated rotational slope failures with debris flows (Bedrock is mostly volcaniclastic sandstone and siltstone of Yauco formation and soils are Maricao Ultisols). (Photo credit: Shen-En Chen)

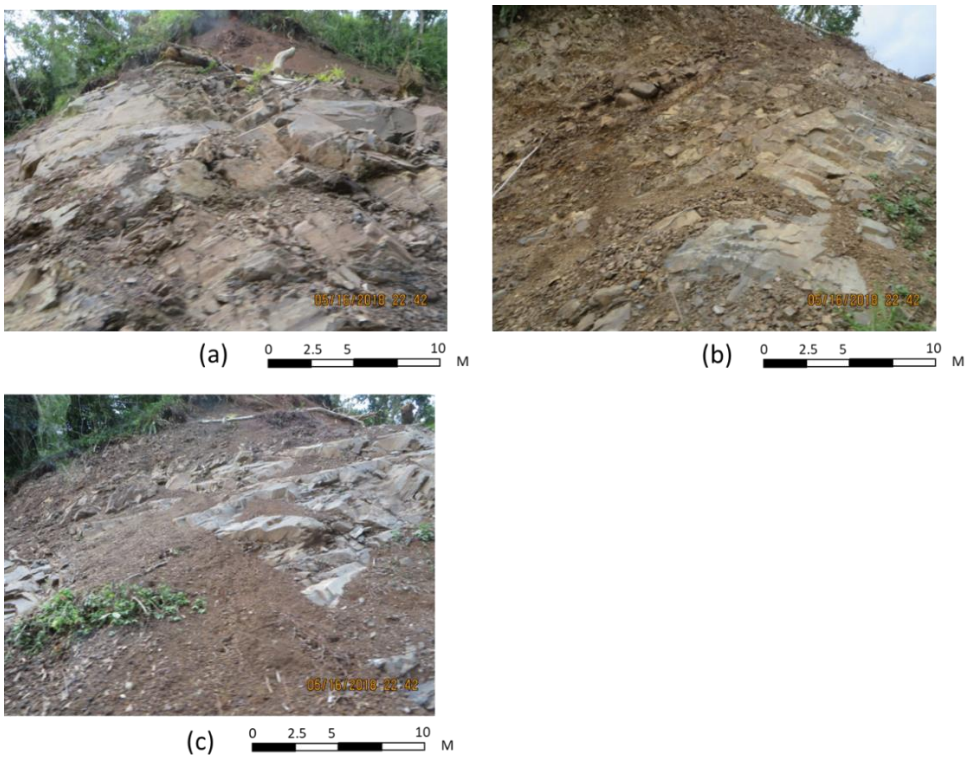

Figure 2-3. Landslide in Puerto Rico after 2017 Hurricane Maria: Surface observations indicated failure of rocky slopes (Bedrock is mostly serpentinite, chert and calcareous sandstone). (Photo credit: Shen-En Chen)

Figure 2-4. A new bridge under construction in Las Marias - Heavy flooding resulted in localized landslides and the washout of the original bridge. (Photo credit: Shen-En Chen)

2.3 Study Area and Landslide Data

As one of the US southeastern coastal states, North Carolina is often impacted by the same Atlantic hurricanes that hit Puerto Rico (such as the case of hurricane Maria). Because of the likelihood of exposing to the Atlantic hurricanes, we are interested in studying the same multi-hazard risks to bridges in North Carolina (NC).

Figure 2-5a shows the three physiographic regions in North Carolina. North Carolina's geography is composed of the eastern Coastal Plain Region (Figure 2-5d), the central Piedmont (Figure 2-5c), and the western Appalachian Mountains (Figure 2-5b).

The mountain area (26,572 km^2) encompasses the Blue Ridge and the Great Smoky Mountains (State, 2024). The Eastern Continental Divide separates the rivers that flow eastward into the Atlantic Ocean from those flowing westward towards the Tennessee and Ohio rivers (State, 2024). The Coastal Plain (59,363 km^2) refers to the low-lying areas extending from the sandy farmland in the east to the Outer Banks, featuring barrier islands and three capes (State, 2024). Last, the Piedmont (43,288 km^2), typically described as "the foothills," is characterized by rolling hills ranging from 90 to 450 m in elevation (State, 2024).

Landslides are a common hazard in the western mountains of NC. For example, the 2005 Pigeon River Gorge rockslide event had direct (e.g. road repair, stabilization costs, etc.) and indirect (e.g. interruption of business, commerce, tourism because of lengthy detours, etc.) costs that exceeded $15 million (NCGS, 2006). To date, no attempt has been made to discern the probable landslide risks in North Carolina to specific roadway bridge structures.

To evaluate landslide risks, the landslide data from 1900 to 2021 were collected from the U.S. Geological Survey (USGS). The NC landslide prone area is roughly 320 km^2, and approximately 99.7% of the landslides occurred in the western mountains with only 0.03% of the landslides occurring in the Piedmont (Belair et al., 2022). Belair et al. (2022) developed the US landslide database (version 2.0) and based on the confidence levels, quality of input data, as well as the method used for identification and mapping of each landslide, they suggested a scale system for slope susceptibility to landslides (Mirus et al., 2020). In their database, the authors recommended that the lowest susceptibility value (1) is for "Possible landslide in the area" and the highest value (8) is for "High confidence in extent or nature of landslide" (Mirus et al., 2020). In our study, landslide areas with values 5 (Confident consequential landslide at this location) to 8 were used.

2.4 Materials and Methods

2.4.1 Landslide and Bridges Inventory

The landslide inventory used in this study is the USGS dataset (Belair et al., 2022). The dataset contains 4,794 landslide points and 6,653 landslide polygons from 1991 to 2021 (Figure 2-6). The database is collected and maintained by different agencies and institutions, such as the National Aeronautics and Space Administration (NASA), USGS, and the North Carolina Geological Survey (NCGS).

The bridges inventory for current study is collected from the North Carolina Department of Transportation (NCDOT) dataset and the Federal Highway Administration (FHWA) dataset. We used the bridge's ID to combine the two datasets for our analysis. The combined dataset, updated to 2023, contains 22,812 bridges (Figure 2-7).

2.4.2 Conditioning Factors

In defining a likely landslide area, we selected several variables known to influence the susceptibility of a slope to fail, including elevation, aspect, slope, rainfall, distance to faults, and distance to rivers for landslides (Abella & Van Westen, 2007; Chau & Chan, 2005; Feizizadeh et al., 2013; Lee & Pradhan, 2007; Mondini, 2017).

Elevation can significantly affect landslide occurrence; it can also interact with other factors, and their combined effects impact the probability of occurrence (Chau & Chan, 2005; Dai & Lee, 2002; Mousavi et al., 2011). Elevation data were obtained from the Digital Elevation Model (DEM) provided by the USGS (USGS, 2023a) at a resolution of 1 arc-second (Figure 2-8a). Contour lines that contain elevation values were used to construct a DEM layer with cell size of 30 m × 30m (USGS, 2023a).

Using the DEM, we calculated the aspect variable with the ArcGIS Pro aspect tool (Figure 2-8b) and the slope variable with the slope tool (Figure 2-8c). Aspect related parameters such as exposure to sunlight, drying winds, and discontinuities may influence the occurrence of landslides (Feizizadeh et al., 2013). Following Ayalew and Yamagishi (2005) and Lee and Pradhan (2007), we reclassified the aspect variable and divided the aspect into nine classes: flat (-1°), north (0°–22.5° and 337.5°–360°), northeast (22.5°–67.5°), east (67.5°–112.5°), southeast (112.5°–157.5°), south (157.5°–202.5°), southwest (202.5°–247.5°), northwest (247.5°–292.5°), and west (292.5°–337.5°). Based on the order of the classes, we assigned aspect values from 1 to 9 to each class. Aspect value is especially critical to landslide susceptibility of steep slopes.

High rainfall amounts typically result in high hazard index values for landslides(Abella & Van Westen, 2007). Rainfall totals were calculated using observation

data from the National Oceanic and Atmospheric Administration (NOAA) and the Inverse Distance Weighted (IDW) tool in ArcGIS Pro (Figure 2-8d).

It is important to recognize that several of the geological, geomorphological and hydrological factors are implied in the aspect variable [31]. As a result, the only other major factor in triggering landslides that needs to be explicitly investigated is seismicity(Ganga et al., 2022). Therefore, the distance to faults is an important susceptibility criterion (Feizizadeh et al., 2013) (Figure 2-8e). We used the Euclidean distance tool in ArcGIS Pro to generate distances to faults (NCDEQ, 2022).

Slopes located closer to rivers are generally more vulnerable to landslides due to factors such as increased water infiltration, erosion, and the destabilizing effect of flowing water (Cebulski, 2022; Gómez & Kavzoglu, 2005). We used Euclidean distance tool to generate distance to river in ArcGIS Pro. The river data were collected from the USGS National Hydrography Dataset (NHD) (USGS, 2023c).

Figure 2-9 illustrates the schematic of the workflow for our models and calculations, which will be further explained in the following section.

2.4.3 Logistic Regression Model

Logistic Regression (LR) allows for estimating the relationship between a categorical variable (e.g., occurrence and no occurrence of an extreme event) and its influential factors (Bai et al., 2010; VanderWeele & Knol, 2014). It is a useful tool to calculate the probability of occurrence of an event (Bai et al., 2010; Budimir et al., 2015; Kleinbaum et al., 2002). Kleinbaum et al. (2002) described the logistic model as:

$$p = \frac{e^z}{1+e^z} = \frac{1}{1+e^{-z}} \tag{2.1}$$

where p is the probability of event occurrence (1: occurrence; 0: no occurrence). Logit z is assumed as a linear combination of the independent variables, and is defined as:

$$z = \beta_0 + \beta_1 x_1 + \beta_2 x_2 + \ldots + \beta_i x_i \quad (2.2)$$

where β_0 is the intercept of the model, x_i is the i_{th} variable, and β_i is the coefficient of the variable x_i. We used random forest tool in R (open-source statistical software) for the LR modeling and generated the probability map of event occurrence (Eq. 2.1) in NC in ArcGIS Pro 3.1.2.

The Receiver Operating Characteristic (ROC) curve is a representation of the performance of a binary classification model (Nahm, 2022). Zhang et al. (2016) used ROC curve to determine the optimal discrimination threshold for predicting event occurrence. The ROC curve is created by plotting the True Positive Rate (TPR) against the False Positive Rate (FPR) for various threshold values of a model's predicted probabilities (Milanović et al., 2021; Park et al., 2004). Zhang et al. (2016) and Milanović et al. (2021) further used the Area Under Curve (AUC) values between 0.5–0.7 to indicate poor precision, values between 0.7–0.8 to indicate acceptable precision, values between 0.8–0.9 to indicate excellent precision, and values higher than 0.9 to indicate outstanding model precision. We used R to fit the LR models and produced the LR results, ROC curve and AUC values. This model validation approach is used in the current study in the LR modeling. These model validation approaches will also be used in the Random Forest (RF) modeling as explained in the following section.

2.4.4 Random Forest Model

According to Alzubi et al. (2018), Machine Learning (ML) is about making computers modify their actions in order to improve the actions to attain more accuracy,

where accuracy is measured in terms of the number of times the chosen actions that results in correct values. ML can be defined as a category of artificial intelligence that enables computers to learn and do what comes naturally to humans, such as learn from past experiences (Alzubi et al., 2018). ML techniques have been extensively applied in spatial statistical analysis to predict and model extreme events (Chen, Peng, et al., 2018; Jain et al., 2020; Kavzoglu & Teke, 2022).

Introduced by Breiman (2001), Random Forest (RF) is a computationally effectual ensemble ML method that constructs the combination of many decision trees that can be used to model the spatial distribution of extreme events and has been applied in geomorphological research, susceptibility mapping, and remote sensing data modelling (Breiman, 2001; Kavzoglu & Teke, 2022; Taalab et al., 2018). RF has strong algorithmic advantages such as rapid processing capability, easy hyper-parameter optimization, and success in achieving high predictive performance (Kavzoglu & Teke, 2022). This technique has been applied to spatial regression analysis to predict the likelihood of extreme events occurring in different regions(Chen et al., 2017; Milanović et al., 2021; Park & Kim, 2019; Taalab et al., 2018). It has been combined with multiple decision trees to improve the accuracy and robustness of the model (Breiman, 2001).

An RF model can deal with a large amount of data, including both categorical and numerical data, and it can account for complex interactions and validate the predictions (Taalab et al., 2018). The data requirement is for data that represent both occurrence and non-occurrence areas (Taalab et al., 2018). Therefore, we assigned a value of 1 to occurrence landslide points and a value of 0 to non-occurrence landslide points in our dataset (Park & Kim, 2019). Identifying the areas and sample conditions from GIS spatial

locations is straightforward (Kim et al., 2018). However, the accuracy of data mining models, often considered 'black box,' should be rigorously tested due to the challenge of defining variable relationships (Taalab et al., 2018). In our study, it involved splitting the entire dataset into two parts where 80% of dataset was used for training, and the remaining 20% of dataset was employed for validation (Kim et al., 2018; Taalab et al., 2018).

The study by Kim et al. (2018), focused on landslide susceptibility mapping using ML models, specifically RF and boosted tree models. The performance of the models was evaluated using ROC analysis and AUC values. The results of the study showed that both the RF and boosted tree models performed well in predicting landslide susceptibility, with the RF model outperforming the boosted tree model in terms of accuracy. The study demonstrated the effectiveness of RF and boosted tree models for landslide susceptibility mapping and emphasized the importance of slope in landslide susceptibility analysis. Chen et al. (Chen, Zhang, et al., 2018) also tested the performance of RF to quantify landslide susceptibilities and concluded that RF can reach 95% confidence level with high AUC values (Chen, Zhang, et al., 2018).

In this study, we used R software for the RF modelling and produced the RF result, the out of bag (OOB) error, the accuracy value, the ROC curve, the AUC values and finally, a map of the probability of landslide event occurrence in NC.

2.4.5 North Carolina Highway Bridges

In this study, we focused on bridges situated above water, with a length more than 6 m, and excluded those bridges over pipes and culverts or those designed as ramps. A significant number of the bridges on the NC highway system are prestressed concrete stringer bridges and steel girder bridges with very few other bridge types. However, bridge

construction materials are not the focus of current study. The elevation of the bridge plays a crucial role in determining its susceptibility to damage by streams and rivers. Our previous investigation in Puerto Rico revealed that bridges located in the bottom of valleys are particularly vulnerable to multi-hazard risks that include landslide and flooding events. Hence, similar to the bridge in Las Marias (Figure 2-4), the combined hazards can lead to bridge washout. Thus, we further identified bridges likely to be affected by landslides and selectively examined those situated in or near the bottom of valleys.

Throughout this research, we employed various tools in ArcGIS Pro to automatically calculate the bridge's assumed flooding potential (AFP) based on their geographical locations. These tools included the buffer tool, zonal statistics tool, extract multi-values to points tool, split line to points tool, and bearing distance to line tool. We utilized these tools to generate elevation data for both banks of a bridge and the elevation of the river. Subsequently, these elevation data were incorporated into the bridge's AFP calculation, defined by the following equation:

$$B_i = \frac{E_{1i}+E_{2i}}{2} - E_{Li} \tag{2.3}$$

where B_i represents the bridge's AFP, i denotes the bridge ID, E_{1i} and E_{2i} correspond to the elevations of the two sides of the bridge and E_{Li} represents the elevation of the river. AFP is different from bridge clearance as it is physically the approximate bridge height (averaged from the two banks) minus the river elevation from DEM at the location of the bridge. Hence, AFP is not the exact bridge height to the water level, but the approximate bridge height to the DEM elevation. Ignored are the actual heights from the bridge bottom to the bridge deck surface. We utilized ArcGIS Pro tools to compute the AFP results (Eq. 2.3) and identified bridge locations within valleys in NC.

To identify bridge locations within a valley, we used several criteria, such as AFP value, landform, slope, and elevation difference. The landform were classified using the 'Geomorphon Landforms' tool in ArcGIS Pro, which categorizes calculated geomorphons into common landform types(ESRI, 2023). Jasiewicz and Stepinski (2013) studied classification and mapping of landform elements and described geomorphon as the landscape representation based on elevation differences around a target cell. Comprising 498 geomorphons, their data set encompassed all conceivable morphological terrain types, encompassing both common landscape elements and rare, unconventional forms found infrequently on natural terrestrial surfaces (Jasiewicz & Stepinski, 2013). The data were then classified into 10 common landform types: flat, peak, ridge, shoulder, spur, slope, hollow, footslope, valley, and pit (ESRI, 2023; Jasiewicz & Stepinski, 2013).

In the current study, the slope values were determined based on the maximum slope degrees (see section 2.4.2) within a 30 m search area around the bridge. The elevation differences were calculated from the maximum elevation within the same 30 m search area around the bridge, compared to the bridge's elevation.

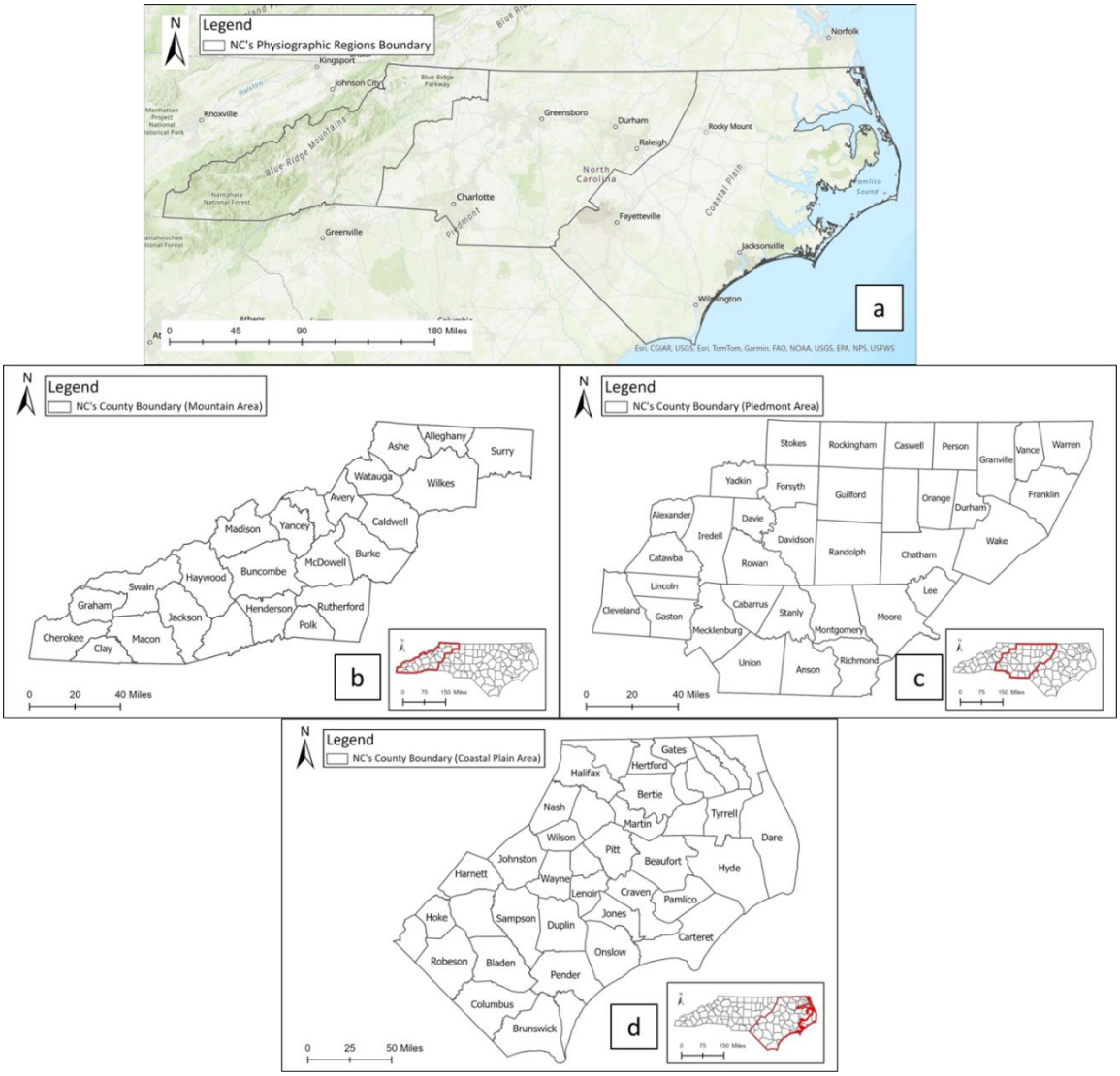

Figure 2-5. Study area with location map illustrating North Carolina's three distinct physiographic regions. a. North Carolina distinct physiographic regions distribution, b. Blue Ridge Mountain area, c. Piedmont area, and d. Coastal Plain area.

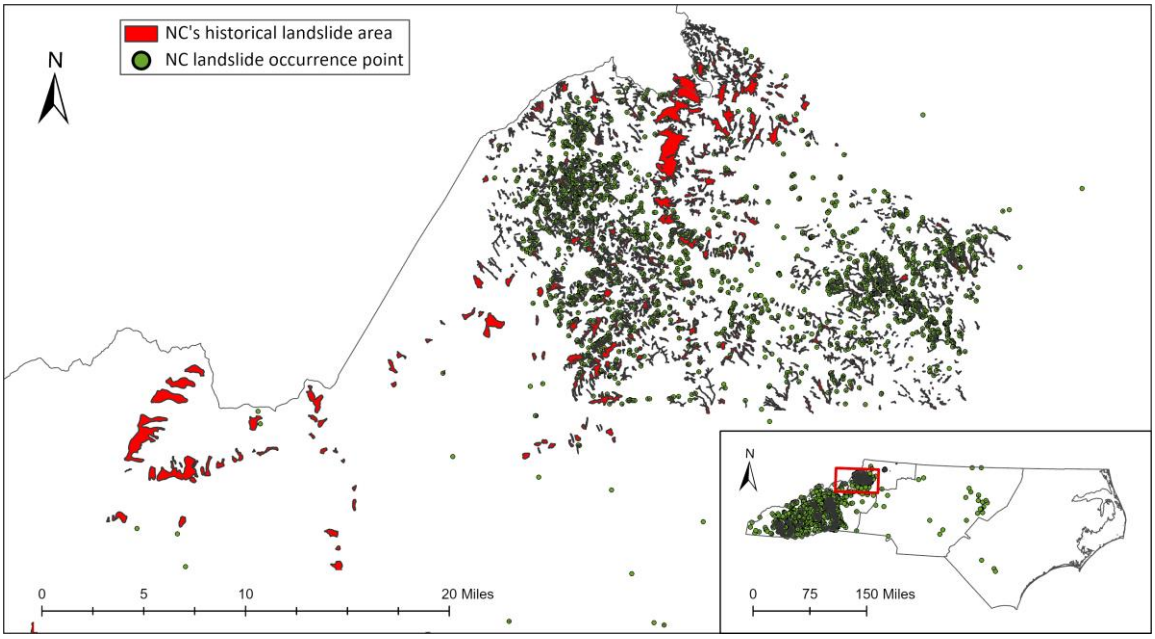

Figure 2-6. Location of landslide points and polygons within the study area. a. Showing closer version in Ashe County, Watauga County, and Avery County. b. Showing NC statewide results.

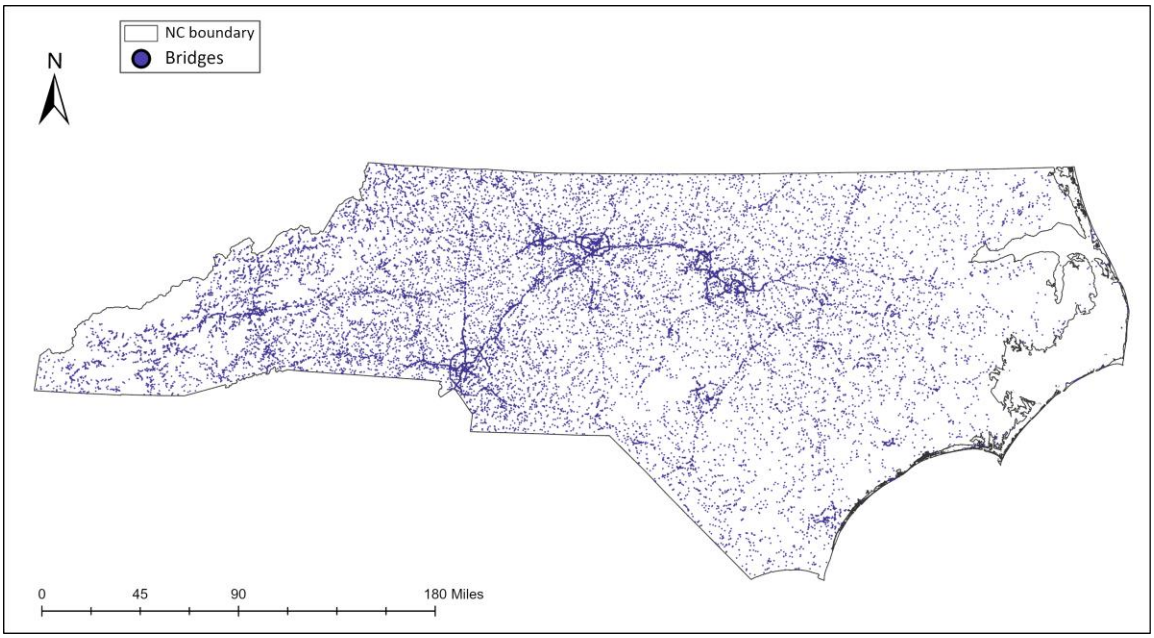

Figure 2-7. Location of bridges within the study area.

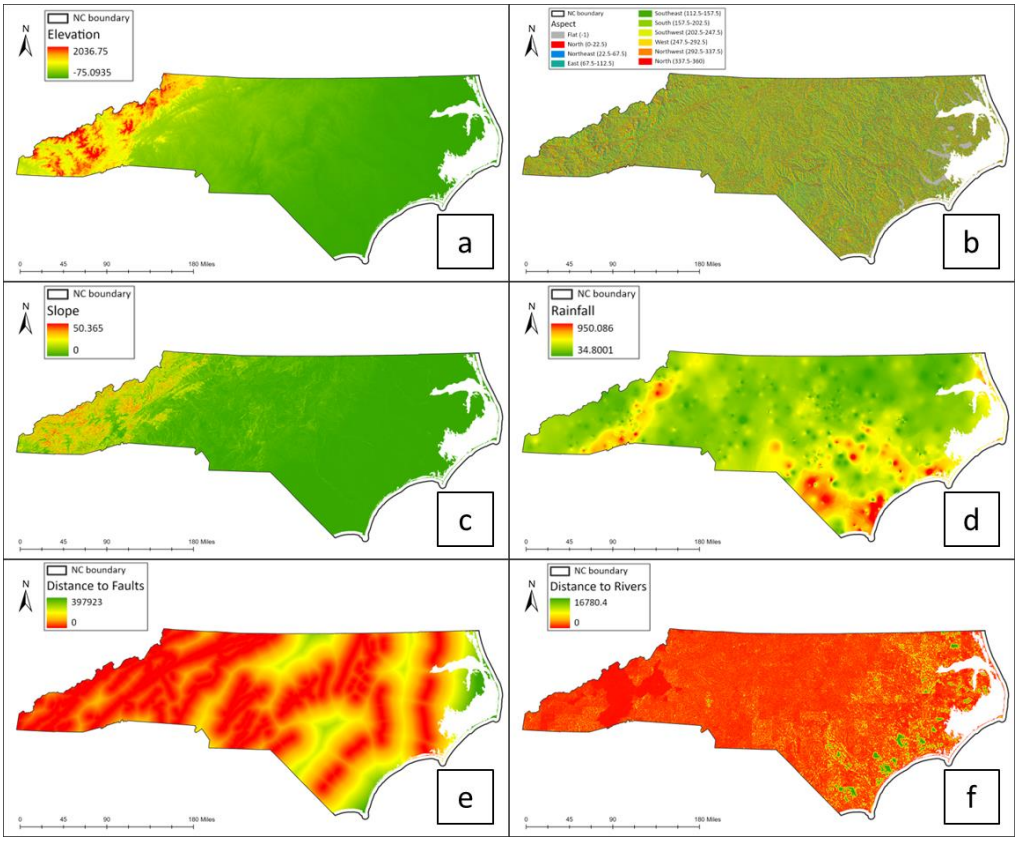

Figure 2-8. Landslide conditioning factors used in this study: a. Elevation, b. Aspect, c. Slope, d. Rainfall, e. Distance to fault, f. Distance to river.

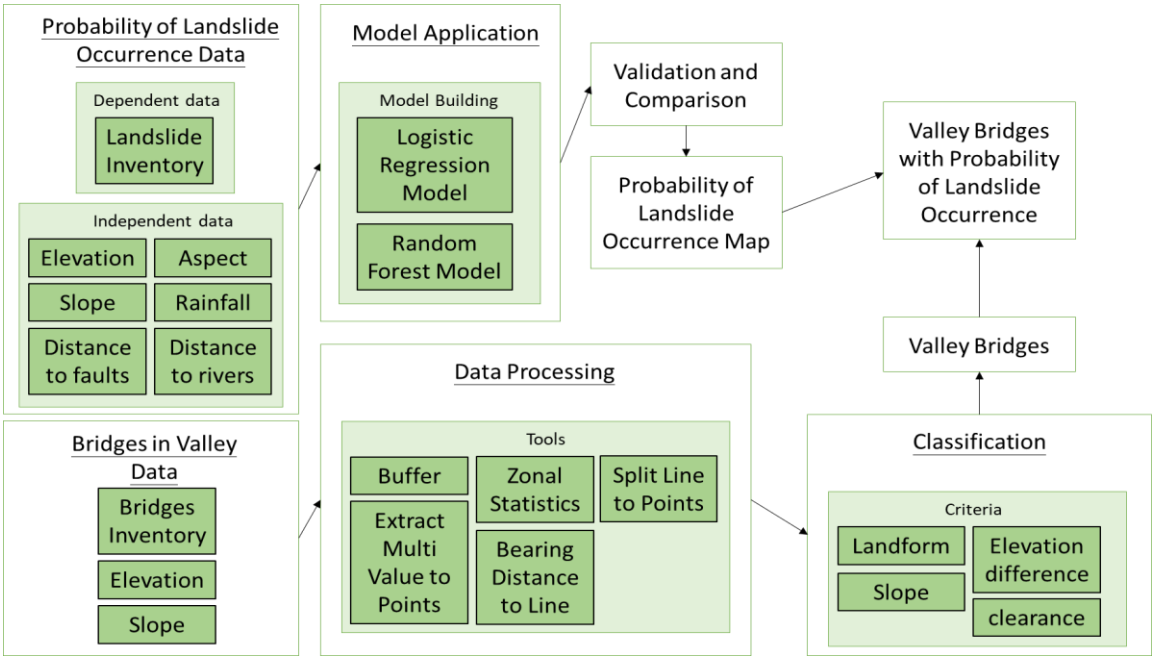

Figure 2-9. A schematic of the calculation workflow for the probability of landslide occurrence map and bridges in the valley.

2.5 Results and Discussions

We utilized 9,794 sample points for the LR and RF modelling (4,794 for historical landslide occurrences and 5,000 for no landslide occurrences). In our data set, we used random points tool in ArcGIS Pro to generate 5,000 points that had no landslide occurrences.

2.5.1 Statistical results

The variables of elevation, aspect, slope, rainfall, distance to faults, and distance to rivers were used in our analysis. The results for the LR model are shown in Table 2-1. We used the slope interaction with the elevation model to analyze the landside sample points. The results for the LR model show that the elevation, aspect, rainfall, slope, aspect 2 to aspect 6 and the distance to rivers are considered positive and significant variables. This means that the landslides would occur more frequently in areas where the elevation is higher, the slope is steeper, the rainfall is larger, the location is far away from a river, and the facing slope is north (aspect 2), northeast (aspect 3), east (aspect 4), southeast (aspect 5), or south (aspect 6). On the other hand, distances to faults and slope interaction elevation are negative and significant meaning that the high occurrence of landslide in the area is closer to the fault lines. In this case, negative slope interaction means that when the slope is steeper, the elevation will be lower. Furthermore, aspect 7 and aspect 8 are both identified as negative, but only aspect 8 is significant. The interpretation is that landslides will not frequently occur where the facing slope is westward (aspect 8). Finally, it is not conclusive if landslides will likely occur for southwest (aspect 7) facing slopes.

Table 2-1**.** Coefficient values for LR in the case of each predictor variable in landslide.

Variable	Unit	Aspect (Reclass) interact slope	Significance
Elevation*	m	2.264e-03	***
Slope	Degree	6.346e-01	***
Rainfall	mm/year	3.399e-03	***
Distance to faults	m	-1.069e-05	***
Distance to rivers	m	1.515e-04	**
Aspect2		5.706e-01	***
Aspect3		1.175e+00	***
Aspect4		1.362e+00	***
Aspect5		9.241e-01	***
Aspect6		5.366e-01	***
Aspect7		-1.296e-01	
Aspect8		-2.987e-01	*
Slope: Elevation		-3.752e-04	***
Intercept		-5.523e+00	***

* Significance codes: 0 ‘***’ 0.001 ‘**’ 0.01 ‘*’ 0.05 ‘.’ 0.1 ‘ ’ 1.

2.5.2 Validation and comparison of models

In Table 2-2, the LR model predicts a percentage of 76.3%, which is a measure of how well the model predicts the correct outcome. Further, in a sensitivity analysis, the model has identified an accuracy of 77.4% indicating the percentage of positive model identification. In the case of AIC (Akaike information criteria) values, a lower AIC value indicates a better model fit. In our case, the 8,116.8 value is considered high (Typical reported AIC values are in the range of 200 (Quesada-Román, 2021) to 1,000,000 (Nowicki Jessee et al., 2018). As mentioned in Section 3.4, the ROC curve and AUC value have been widely used to validate the performance of the RF and LR models (Chen et al., 2019). A higher AUC value indicates better model performance, as it can distinguish between positive and negative cases. In our model, the AUC has a reported accuracy of 84.3%, indicating acceptable model performance.

The OOB error estimate with lower values indicates better model performance, suggesting that the model can generalize well for new data. Users should optimize two a priori hyper-parameters: The number of trees in the forest (ntree) and the number of

variables tested at each node (mtry) and the optimization aimed to minimize the OOB error and achieve good model performance(Park & Kim, 2019).

In our RF model, the optimized values were 500 for ntree and 3 for mtry, resulting in an OOB error of 16.5%. Our RF model correctly predicted outcomes with an accuracy of 82.7% meaning the model accurately predicted the outcomes. In a sensitivity test, the model correctly identified 86%, a measure of how well it identifies true positive cases. A higher AUC value indicated better model performance, with an accuracy of 90.9%, signifying outstanding model performance.

In our research, we compare the LR model and RF model to select the best-performing model. The choice of the best model often depends on the specific characteristics of the problem and the data at hand [54]. Based on the accuracy value, AUC value, and ROC curve (Figure 2-10), the RF model demonstrated superior performance in predicting landslide occurrence. Consequently, we chose the random forest model to generate the probability of landslide occurrence map.

Table 2-2. Summary of model performances for LR model and RF model for landslides.

Models	Evaluation	Value
Logistic Regression	AIC[1]	8116.8
	Accuracy	0.763
	Sensitivity	0.7736
	AUC	0.8431
Random Forest	OOB	16.52%
	Accuracy	0.8269
	Sensitivity	0.8592
	AUC	0.9092

[1] AIC: Akaike information criterion.

2.5.3 Predicted probabilities and the susceptibility map

In order to compare to the LR model, we used the trained RF model to generate the probability of landslide occurrence map and susceptibility map. We trained the RF model using R to map the predicted probability of landslide occurrence.

Figure 2-11. Landslide risk map in North Carolina.shows that the red color represents a higher probability of landslide occurrence, yellow indicates a medium probability, and green signifies a low probability. Figure 2-12 reveals that 47 bridges likely will experience over 50% of the landslide occurrences in the NC mountain region. Landslides are predicted to occur in over 80% of the area around Watauga County, Jackson County, Henderson County, and Polk County.

2.5.4 Bridge-in-valley

After bridge data were retrieved from NCDOT and the FHWA databases, 9,462 bridges were identified in North Carolina.

Several of the bridges (Figure 2-13 to Figure 2-17) were visited in September 2023. Figure 2-13 and Figure 2-14 showcase bridges situated at ridge tops. Figure 2-13a, Figure 2-13b, Figure 2-14a, and Figure 2-14b depict the bridge structure, while Figure 2-13c, Figure 2-13d, and Figure 2-14d illustrate the river bedding. Figure 2-14c provides a representation of the situation next to the bridge. Despite a high landslide risk (95%), these bridges, built at higher elevations, exhibit a lower susceptibility to landslide impacts. Figure 2-15a, Figure 2-15b, Figure 2-16a, Figure 2-16c, and Figure 2-17a showing the bridge structure, while Figure 2-15c, Figure 2-16b, Figure 2-16d, and Figure 2-17b illustrate the circumstances of the river bed. Figure 2-15 illustrates a bridge constructed at an elevation high above a valley, presenting a 60% probability of landslide occurrence. Figure 2-16a, Figure 2-16b, and Figure 2-17 depict a specific area where several landslides occurred. These two bridges are considered to be bridges at the bottom of valleys in our study. One of these bridges (Bridge ID: 740002) (Figure 2-17) has experienced landslides

in its vicinity and slope repair works using soil nails were on-going during the field visit (Figure 2-17c and Figure 2-17d).

To establish whether a bridge is in a valley or on a ridge, several criteria were established including landform (e.g., valley and pit) data, slope (e.g., above 9 degrees), elevation difference (e.g., above 15 meters), and AFP value (e.g., under 7 meters). The results showed that 21 bridges were in a valley bottom setting (Figure 2-18). It should be noted that AFP can be a misnomer because it does not exactly project the flooding level. Instead, in the current study, AFP is used by assuming the flooding will reach its full value. Hence, to assess the number of bridges that may be exposed to flooding danger, AFP up to 30 m have been applied to the bridge data (Figure 2-19).

Finally, we combine the bridge-in-valley data with the probability of landslide occurrence, indicating a bridges' landslide and flooding risk (Figure 2-18 and Figure 2-19). According to Figure 2-18, the results showed that three bridges have a lower than 10% chance of landslide occurrence; 12 bridges have a 10% to 20% chance of landslide occurrence; and 5 bridges have a 24% to 32% chance of landslide occurrence. One bridge (ID: 740002) has a 92% chance of landslide occurrence (Figure 2-18, red square symbol). Bridge 740002 is a steel stringers/multiple girder bridge with a concrete deck. This bridge was built in 2010 and the last routine inspection of the structure was in September 2021. According to the inspection results, the deck, superstructure, and substructure were still in good condition in 2021.

The risks posed to bridge 740002 are likely landslides near the bridge foundations as well as upstream and downstream, which may result in increased flood heights from congestions of the channel stream flow during torrential rains. Such multi-hazard analysis

has not been previously attempted and should be included in evaluation of bridges in similar geographical settings. This is especially important in addressing climate extremes where unprecedented storms are projected for the Carolinas.

Further research was conducted on bridge data in valleys, combined with the probability of landslide occurrence and AFP (Figure 2-19 and Appendix A). In Figure 2-19, the bridges with AFP below 10 m indicate that 23 bridges have a 10% to 20% chance of landslide occurrence, 6 bridges have a 20% to 50% chance of landslide occurrence, and one bridge has a 50% to 100% chance of landslide occurrence. Appendix A shows the details of the bridge information, including bridge ID, longitude, latitude, AFP, our assessment (using four criteria for classification), extra observations (confirming the classification method), and the probability of landslide occurrence. When considering AFP, additional field observations were made (Appendix A), which indicates that bridges with AFP above 7 m and below 30 m are not necessarily located in the bottom of a valley. As observed in Figure 2-13 and Figure 2-14, these bridges may be better classified as either bridges at mid-height of a valley or at a ridge top. The field observations were used to validate the bridges-in-valley in Appendix A, where only bridge 020021 does not fit our criteria for a bridge-in-valley (AFP less than 7 m). The classification method used in the current study achieved a 97% accuracy rate in bridge-in-valley selection.

2.6 Conclusions

The 2018 Hurricane Maria resulted in more than 40,000 landslides and damaged 388 bridges in Puerto Rico. Close examination of several of the damaged bridges revealed the danger of multi-hazard risks (landslide + flooding) for bridges-in-valleys. North Carolina, on the east coast of the U.S., is also exposed to the impacts of seasonal Atlantic

hurricanes. Hence, to investigate similar risks to bridges in North Carolina, a landslide risk susceptibility analysis has been conducted. In this study, we identified that the majority of landslides occur in the mountainous region of North Carolina, thus posing a potential threat to numerous bridges in that region.

Using Logistic Regression (LR) and Random Forest (RF) modeling, a landslide risk susceptibility map was created. Conditioning factors included in current study are aspect variable and seismicity (distance to faults). The geomorphic, geological and hydrological considers are inclusive in the aspect variable of the conditioning factors. The results from the two models have accuracy rates of 76.3% and 82.7% for LR and RF models, respectively. Using the ROC curves, RF model is also shown to be more sensitive than the LR model in predicting landslide risks. Combining highway and roadway bridge data, bridges of high landslide risk are then identified.

Further analysis using landform data and bridge assumed flooding potential (AFP) helped identify bridges-in-valleys. The results showed 37 bridges exposing to both landslide and flooding risks. One particular bridge (ID: 740002) have been found to be exposed to high landslide and flooding risks. Observations from a field visit indicated that ongoing construction efforts have been carried out to address localized landslides near the bridge location. This confirmed our analysis result (Figure 2-18, red square symbol), and the observations on bridge 740002 (Figure 2-17) align with our findings, indicating the potential exposure to multi-hazard (landslide with flooding) dangers. This observation reinforced our confidence that the landslide risk map is accurate and can serve as a valuable tool for managers and decision-makers, enabling proactive measures to prevent potential bridge damage in the future.

The development of a landslide risk prediction model poses a challenge, if we are consideration of the complex nature of geo-environments, encompassing factors such as the geology, hydrology, topography, and human activities (land use) (Kirschbaum et al., 2015). The current study covers a large area and only considered aspect variable and seismicity; hence, future work aiming for increased precision can delve into additional factors such as geology and lithology.

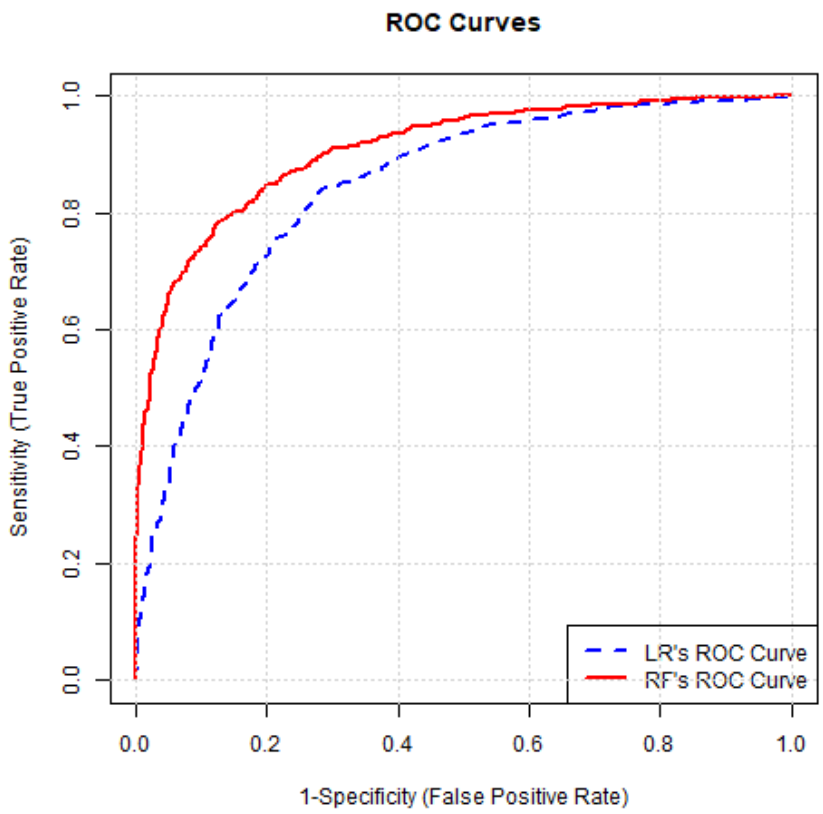

Figure 2-10. ROC curves of the LR model and RF model.

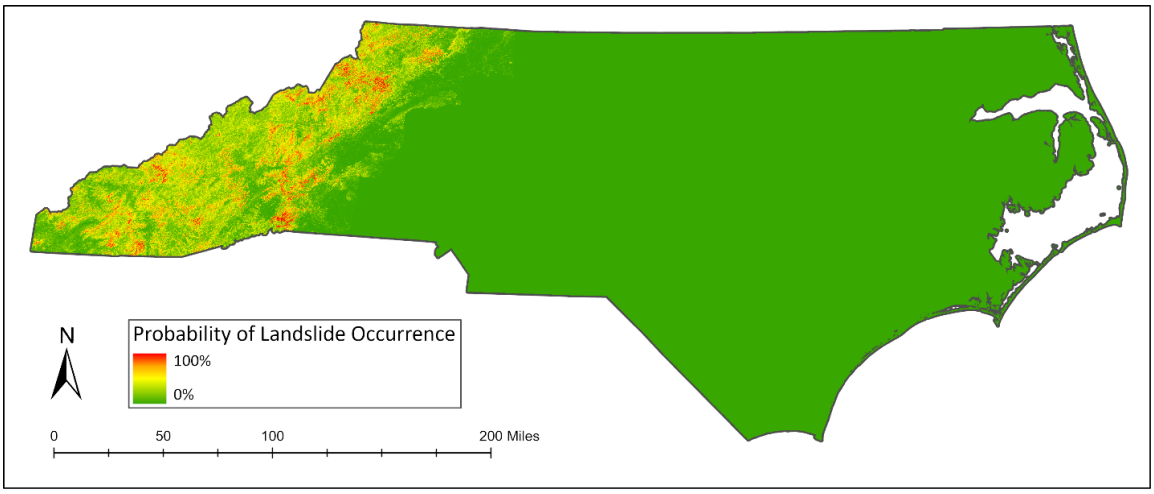

Figure 2-11. Landslide risk map in North Carolina.

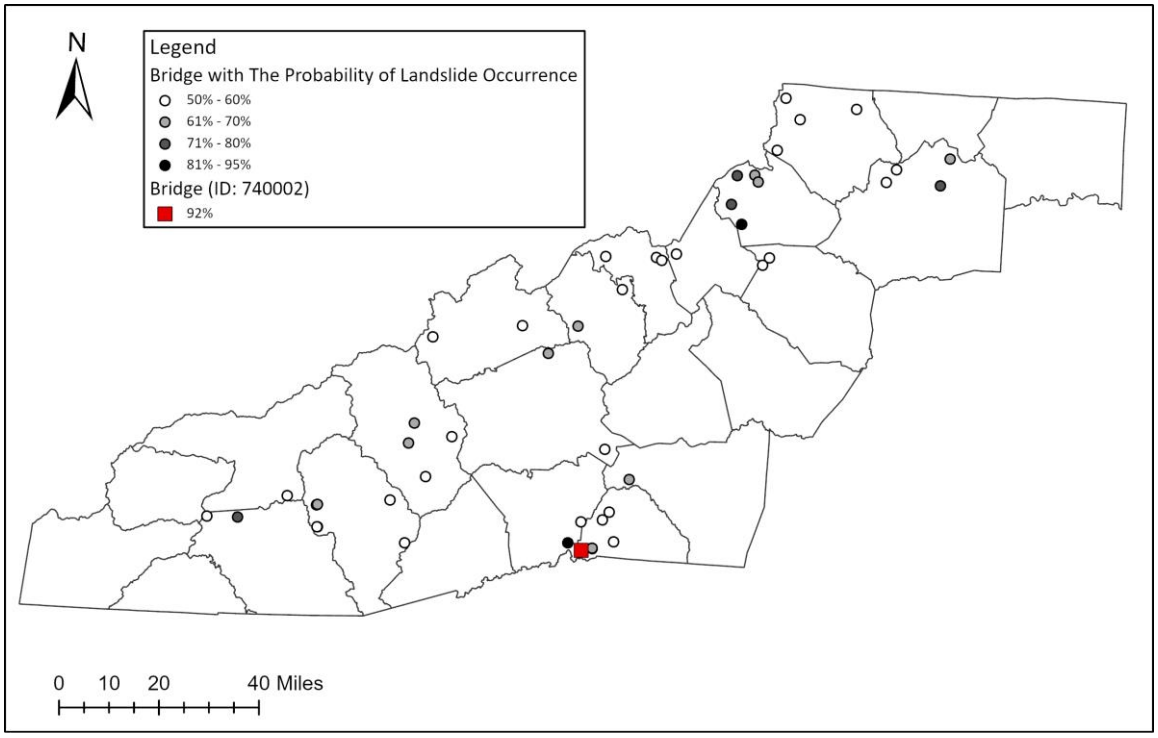

Figure 2-12. Bridges with landslide risk map in NC's mountain area. Showing the bridges with a 50% or greater probability of being impacted by a landslide.

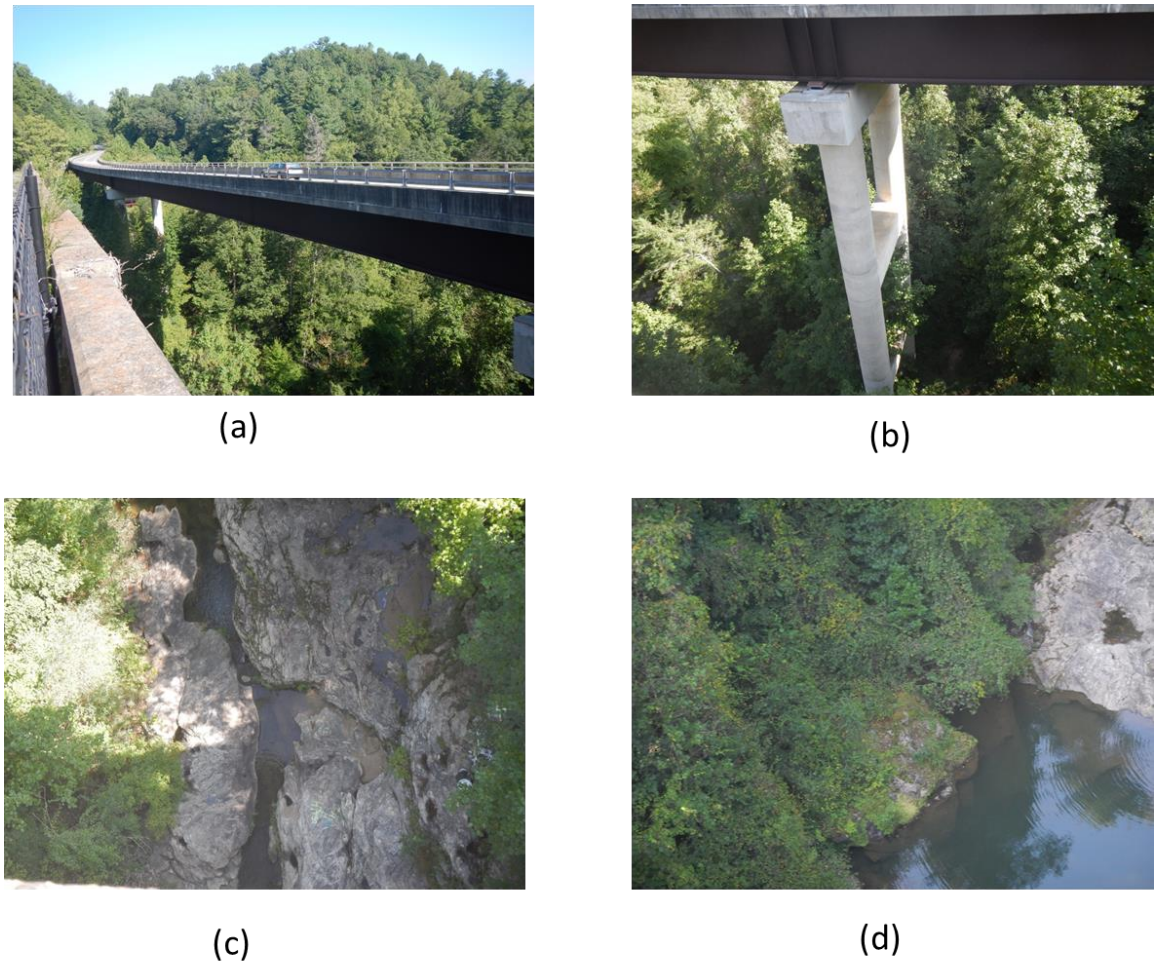

Figure 2-13. Example of bridge at ridge top (Bridge ID: 440375, a steel girder bridge). (Photo credit: Shen-En Chen and Sophia Lin)

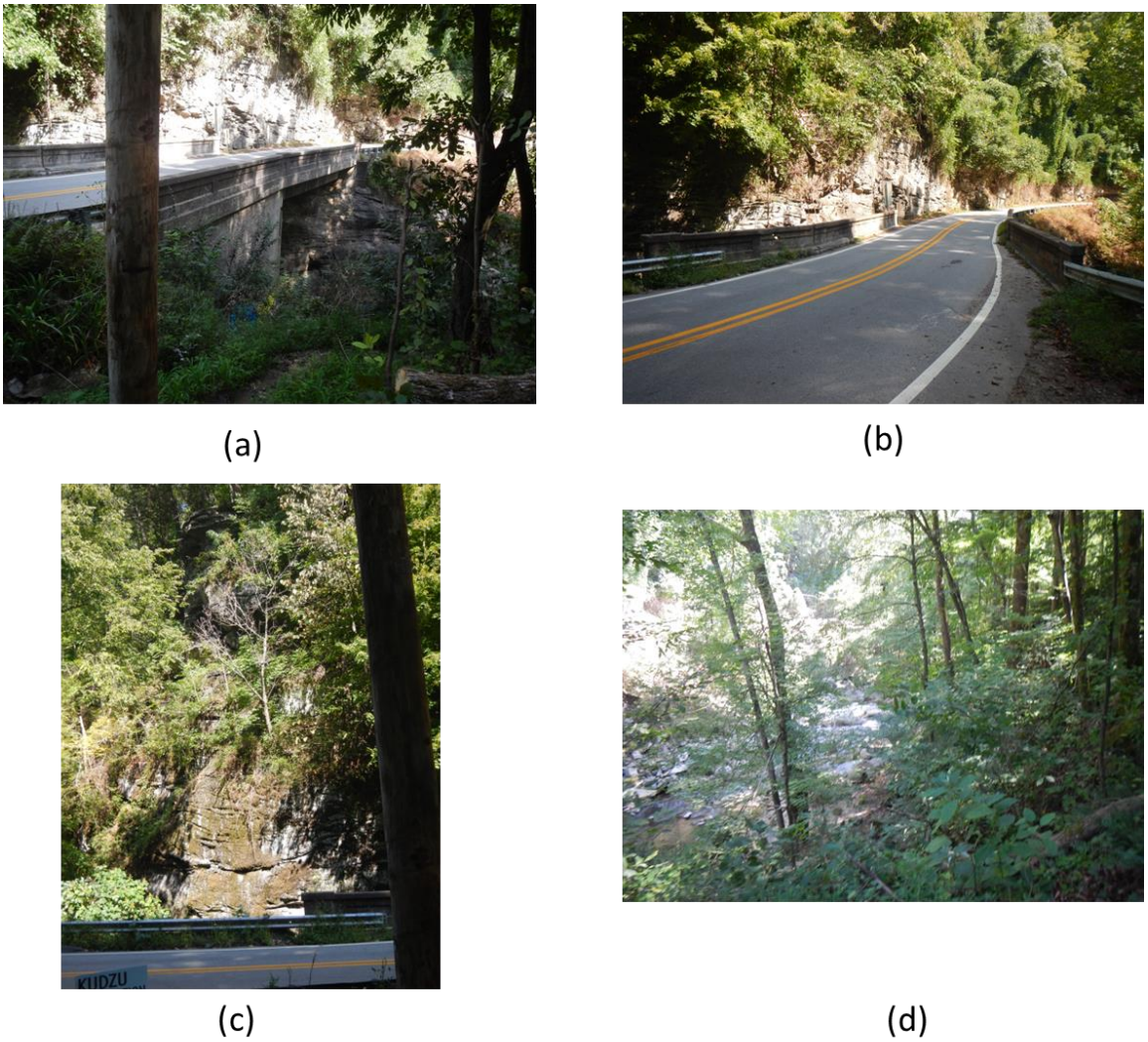

Figure 2-14. Example of bridge sufficiently higher than the valley region (Bridge ID: 740031, a prestressed concrete stringer bridge). (Photo credit: Shen-En Chen and Sophia Lin)

(a)

(b)

(c)

Figure 2-15. Example of bridge-in-valley (Bridge ID: 740027, a steel girder bridge). (Photo credit: Shen-En Chen and Sophia Lin)

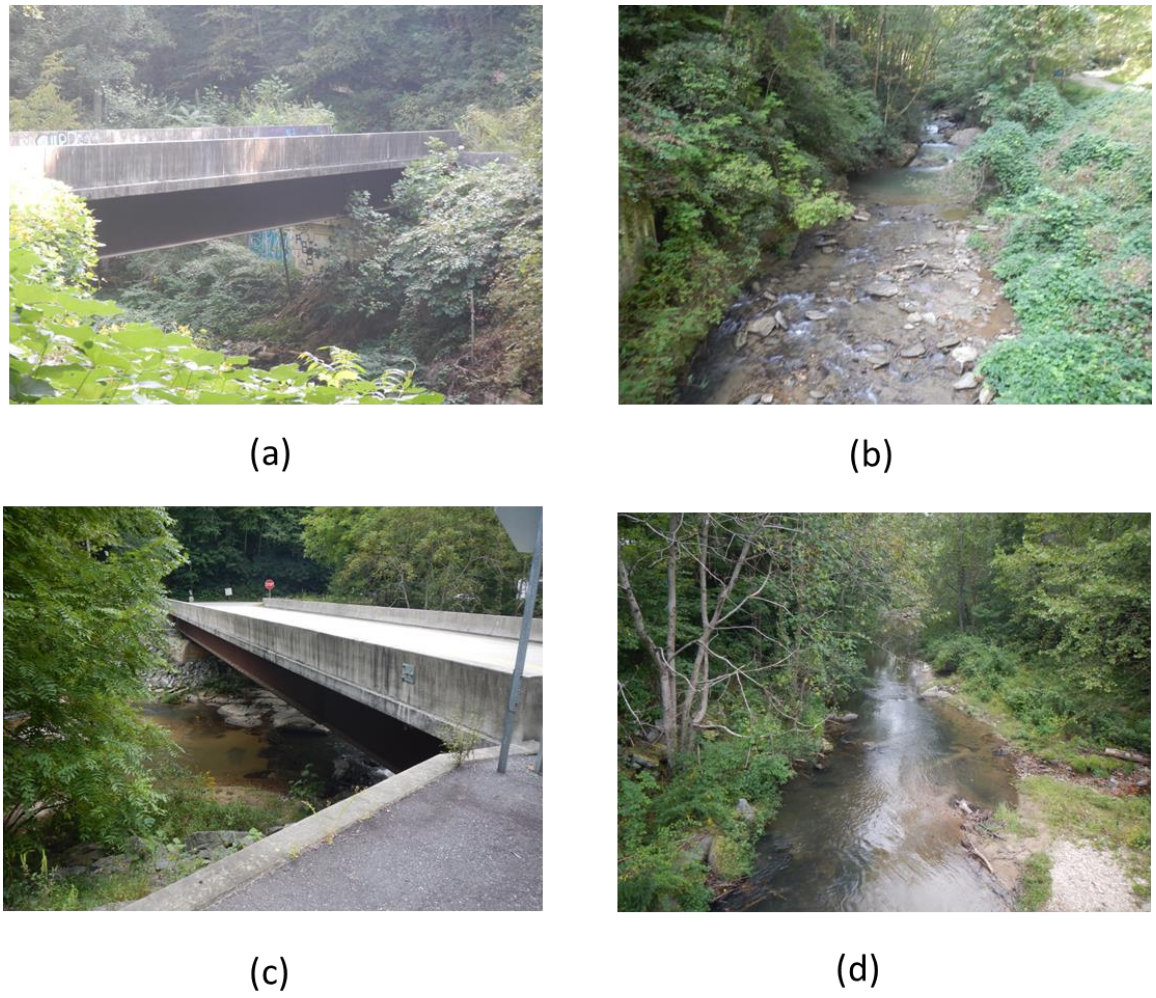

Figure 2-16. Example of bridge-in-valley (Bridge ID: 100653, a steel girder bridge). (Photo credit: Shen-En Chen and Sophia Lin)

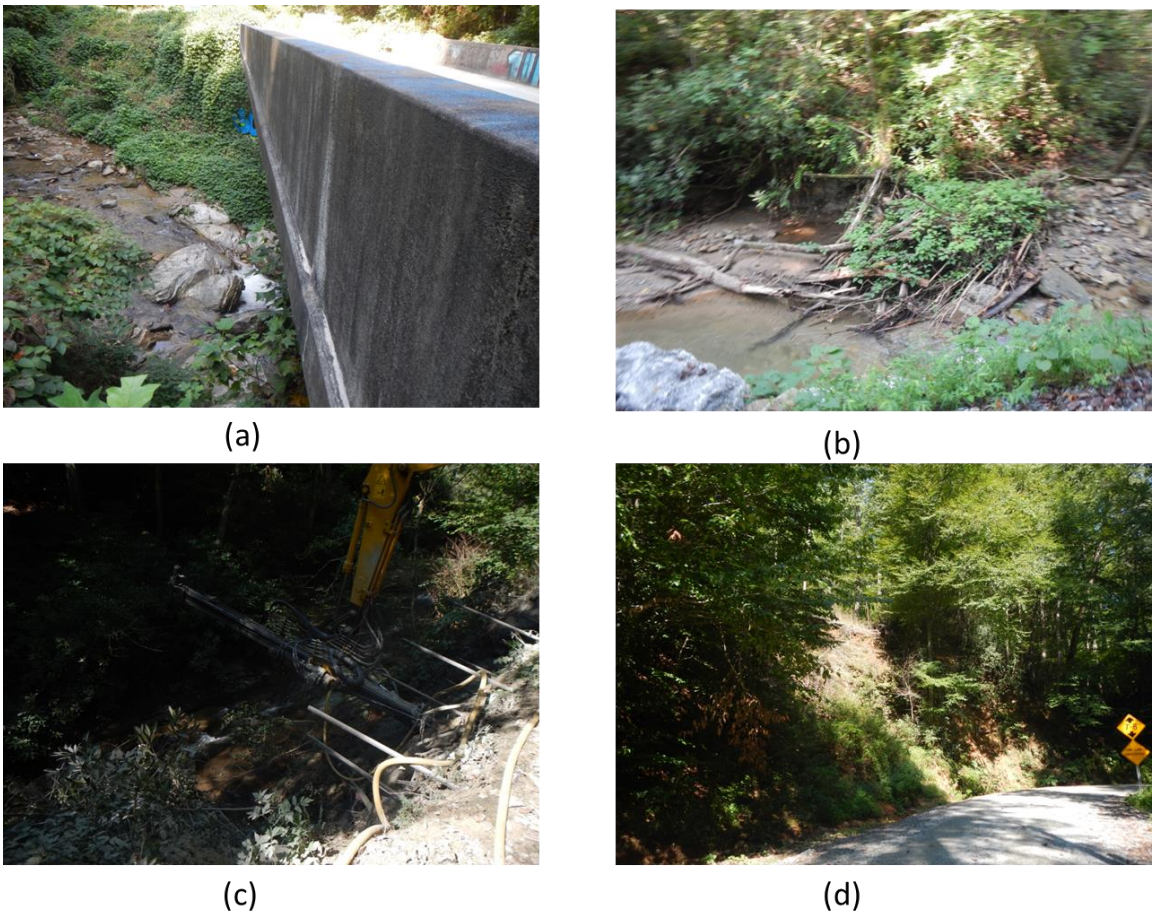

Figure 2-17. Example of valley bridge near a landslide with visible debris flow and rock slide (Bridge ID: 740002, a prestressed concrete stringer bridge). (Photo credit: Shen-En Chen and Sophia Lin)

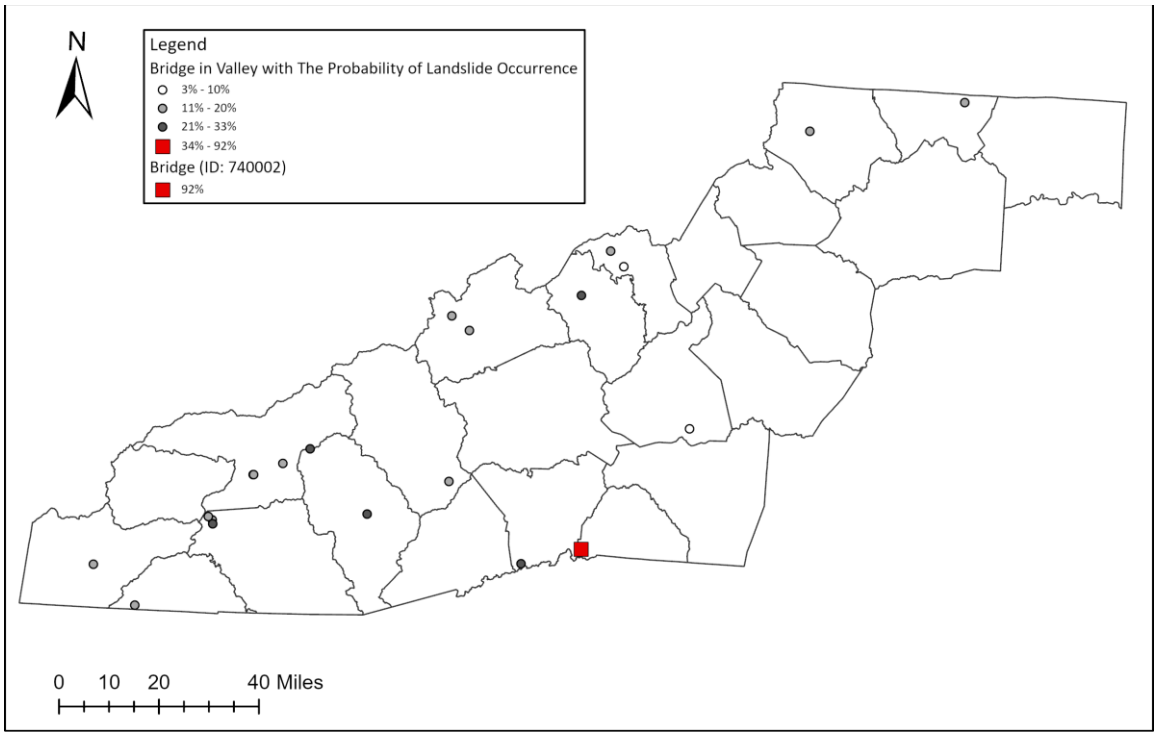

Figure 2-18. Bridges in valley under 7m above stream elevation assuming flooding potential (AFP) in NC's mountain area, indicating the potential of exposing to multi-hazard (landslide with flooding) dangers.

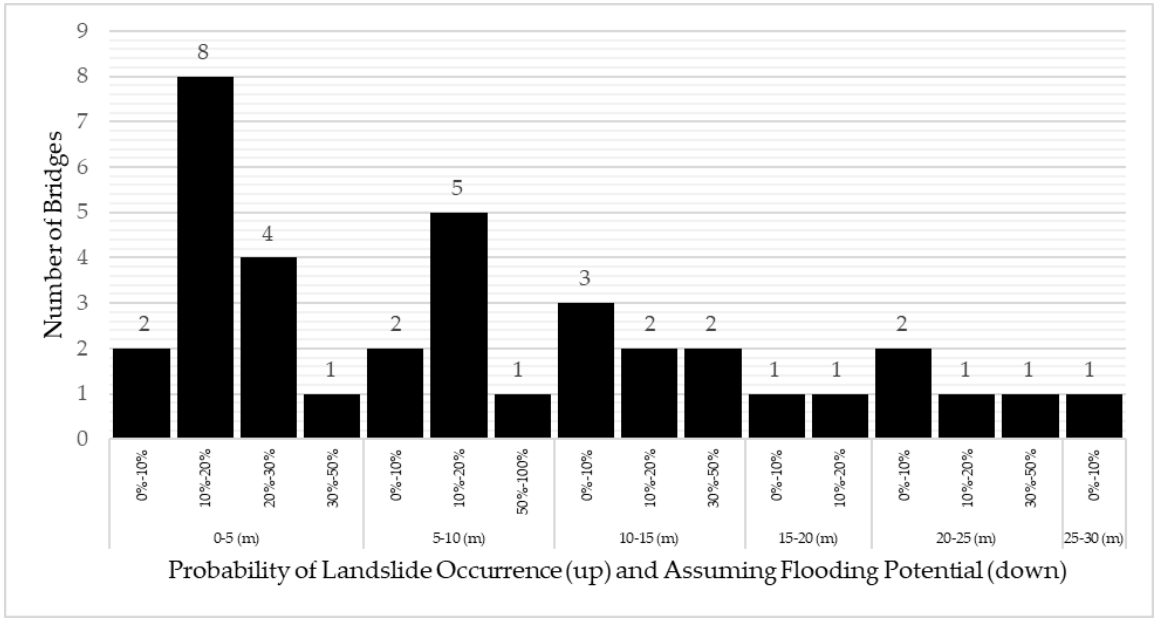

Figure 2-19. Probability of landslide occurrence combine with AFP.

Reference

Abella, E. A. C., & Van Westen, C. J. (2007). Generation of a landslide risk index map for Cuba using spatial multi-criteria evaluation. *Landslides, 4*(4), 311-325. doi:10.1007/s10346-007-0087-y

Alzubi, J., Nayyar, A., & Kumar, A. (2018). Machine Learning from Theory to Algorithms: An Overview. *Journal of Physics: Conference Series, 1142*(1), 012012. doi:10.1088/1742-6596/1142/1/012012

Ayalew, L., & Yamagishi, H. (2005). The application of GIS-based logistic regression for landslide susceptibility mapping in the Kakuda-Yahiko Mountains, Central Japan. *Geomorphology, 65*(1), 15-31. doi:https://doi.org/10.1016/j.geomorph.2004.06.010

Bai, S.-B., Wang, J., Lü, G.-N., Zhou, P.-G., Hou, S.-S., & Xu, S.-N. (2010). GIS-based logistic regression for landslide susceptibility mapping of the Zhongxian segment in the Three Gorges area, China. *Geomorphology, 115*(1), 23-31. doi:https://doi.org/10.1016/j.geomorph.2009.09.025

Belair, G. M., Jones, E. S., Slaughter, S. L., & Mirus, B. B. (2022). *Landslide Inventories across the United States version 2: U.S. Geological Survey data release*.

Bessette-Kirton, E. K., Cerovski-Darriau, C., Schulz, W. H., Coe, J. A., Kean, J. W., Godt, J. W., . . . Hughes, K. S. (2019). Landslides triggered by Hurricane Maria: Assessment of an extreme event in Puerto Rico. *GSA Today, 29*(6), 4-10.

Breiman, L. (2001). Random Forests. *Machine Learning, 45*(1), 5-32. doi:10.1023/A:1010933404324

Budimir, M. E. A., Atkinson, P. M., & Lewis, H. G. (2015). A systematic review of landslide probability mapping using logistic regression. *Landslides, 12*(3), 419-436. doi:10.1007/s10346-014-0550-5

Cebulski, J. (2022). Impact of river erosion on variances in colluvial movement and type for landslides in the Polish Outer Carpathians. *CATENA, 217*, 106415. doi:https://doi.org/10.1016/j.catena.2022.106415

Chau, K. T., & Chan, J. E. (2005). Regional bias of landslide data in generating susceptibility maps using logistic regression: Case of Hong Kong Island. *Landslides, 2*(4), 280-290. doi:10.1007/s10346-005-0024-x

Chen, W., Peng, J., Hong, H., Shahabi, H., Pradhan, B., Liu, J., . . . Duan, Z. (2018). Landslide susceptibility modelling using GIS-based machine learning techniques for Chongren County, Jiangxi Province, China. *Science of The Total Environment, 626*, 1121-1135.

Chen, W., Sun, Z., & Han, J. (2019). Landslide Susceptibility Modeling Using Integrated Ensemble Weights of Evidence with Logistic Regression and Random Forest Models. *Applied Sciences, 9*(1), 171. Retrieved from https://www.mdpi.com/2076-3417/9/1/171

Chen, W., Xie, X., Wang, J., Pradhan, B., Hong, H., Bui, D. T., . . . Ma, J. (2017). A comparative study of logistic model tree, random forest, and classification and regression tree models for spatial prediction of landslide susceptibility. *CATENA, 151*, 147-160. doi:https://doi.org/10.1016/j.catena.2016.11.032

Chen, W., Zhang, S., Li, R., & Shahabi, H. (2018). Performance evaluation of the GIS-based data mining techniques of best-first decision tree, random forest, and naïve Bayes tree for landslide susceptibility modeling. *Science of The Total Environment, 644*, 1006-1018.

Dai, F. C., & Lee, C. F. (2002). Landslide characteristics and slope instability modeling using GIS, Lantau Island, Hong Kong. *Geomorphology, 42*(3), 213-228. doi:https://doi.org/10.1016/S0169-555X(01)00087-3

ESRI. Geomorphon Landforms (Spatial Analyst).

Feizizadeh, B., Blaschke, T., Nazmfar, H., & Rezaei Moghaddam, M. H. (2013). Landslide Susceptibility Mapping for the Urmia Lake basin, Iran: A multi- Criteria Evaluation Approach using GIS. *International Journal of Environmental Research, 7*, 319-336.

Ganga, A., Elia, M., D'Ambrosio, E., Tripaldi, S., Capra, G. F., Gentile, F., & Sanesi, G. (2022). Assessing Landslide Susceptibility by Coupling Spatial Data Analysis and Logistic Model. *Sustainability, 14*(14), 8426. Retrieved from https://www.mdpi.com/2071-1050/14/14/8426

Gómez, H., & Kavzoglu, T. (2005). Assessment of shallow landslide susceptibility using artificial neural networks in Jabonosa River Basin, Venezuela. *Engineering Geology, 78*(1), 11-27. doi:https://doi.org/10.1016/j.enggeo.2004.10.004

Highland, L. M., & Bobrowsky, P. (2008). *The landslide handbook-A guide to understanding landslides*: US Geological Survey.

Jain, P., Coogan, S. C. P., Subramanian, S. G., Crowley, M., Taylor, S., & Flannigan, M. D. (2020). A review of machine learning applications in wildfire science and management. *Environmental Reviews, 28*(4), 478-505. doi:10.1139/er-2020-0019

Jasiewicz, J., & Stepinski, T. F. (2013). Geomorphons — a pattern recognition approach to classification and mapping of landforms. *Geomorphology, 182*, 147-156. doi:https://doi.org/10.1016/j.geomorph.2012.11.005

Kavzoglu, T., & Teke, A. (2022). Predictive Performances of Ensemble Machine Learning Algorithms in Landslide Susceptibility Mapping Using Random Forest, Extreme Gradient Boosting (XGBoost) and Natural Gradient Boosting (NGBoost). *Arabian Journal for Science and Engineering, 47*(6), 7367-7385. doi:10.1007/s13369-022-06560-8

Keellings, D., & Hernández Ayala, J. J. (2019). Extreme Rainfall Associated With Hurricane Maria Over Puerto Rico and Its Connections to Climate Variability and Change. *Geophysical Research Letters, 46*(5), 2964-2973. doi:https://doi.org/10.1029/2019GL082077

Kim, J.-C., Lee, S., Jung, H.-S., & Lee, S. (2018). Landslide susceptibility mapping using random forest and boosted tree models in Pyeong-Chang, Korea. *Geocarto International, 33*(9), 1000-1015. doi:10.1080/10106049.2017.1323964

Kirschbaum, D., Stanley, T., & Zhou, Y. (2015). Spatial and temporal analysis of a global landslide catalog. *Geomorphology, 249*, 4-15. doi:https://doi.org/10.1016/j.geomorph.2015.03.016

Kirschbaum, D. B., Adler, R., Hong, Y., Hill, S., & Lerner-Lam, A. (2010). A global landslide catalog for hazard applications: method, results, and limitations. *Natural Hazards, 52*(3), 561-575. doi:10.1007/s11069-009-9401-4

Kleinbaum, D. G., Dietz, K., Gail, M., Klein, M., & Klein, M. (2002). *Logistic regression*: Springer.

Lee, S., & Pradhan, B. (2007). Landslide hazard mapping at Selangor, Malaysia using frequency ratio and logistic regression models. *Landslides, 4*(1), 33-41. doi:10.1007/s10346-006-0047-y

Miele, P., Di Napoli, M., Guerriero, L., Ramondini, M., Sellers, C., Annibali Corona, M., & Di Martire, D. (2021). Landslide Awareness System (LAwS) to Increase the Resilience and Safety of Transport Infrastructure: The Case Study of Pan-American Highway (Cuenca–Ecuador). *Remote Sensing, 13*(8), 1564. Retrieved from https://www.mdpi.com/2072-4292/13/8/1564

Milanović, S., Marković, N., Pamučar, D., Gigović, L., Kostić, P., & Milanović, S. D. (2021). Forest Fire Probability Mapping in Eastern Serbia: Logistic Regression versus Random Forest Method. *Forests, 12*(1), 5. Retrieved from https://www.mdpi.com/1999-4907/12/1/5

Mirus, B. B., Jones, E. S., Baum, R. L., Godt, J. W., Slaughter, S., Crawford, M. M., . . . McCoy, K. M. (2020). Landslides across the USA: occurrence, susceptibility, and data limitations. *Landslides, 17*(10), 2271-2285. doi:10.1007/s10346-020-01424-4

Mondini, A. C. (2017). Measures of Spatial Autocorrelation Changes in Multitemporal SAR Images for Event Landslides Detection. *Remote Sensing, 9*(6), 554. Retrieved from https://www.mdpi.com/2072-4292/9/6/554

Mousavi, S. Z., Kavian, A., Soleimani, K., Mousavi, S. R., & Shirzadi, A. (2011). GIS-based spatial prediction of landslide susceptibility using logistic regression model. *Geomatics, Natural Hazards and Risk, 2*(1), 33-50. doi:10.1080/19475705.2010.532975

Nahm, F. S. (2022). Receiver operating characteristic curve: overview and practical use for clinicians. *Korean J Anesthesiol, 75*(1), 25-36. doi:10.4097/kja.21209

NCDEQ. (2022). *Geologic Faults*. Retrieved from: https://data-nconemap.opendata.arcgis.com/datasets/nconemap::geologic-faults/explore?location=35.380206%2C-80.335448%2C7.97

NCGS. (2006). Introduction to landslides in North Carolina. *Landslides.* Retrieved from https://www.deq.nc.gov/about/divisions/energy-mineral-and-land-resources/north-carolina-geological-survey/geologic-hazards/landslides

Nhu, V. H., Shirzadi, A., Shahabi, H., Singh, S. K., Al-Ansari, N., Clague, J. J., . . . Ahmad, B. B. (2020). Shallow Landslide Susceptibility Mapping: A Comparison between Logistic Model Tree, Logistic Regression, Naïve Bayes Tree, Artificial Neural

Network, and Support Vector Machine Algorithms. *Int J Environ Res Public Health, 17*(8). doi:10.3390/ijerph17082749

Nowicki Jessee, M., Hamburger, M. W., Allstadt, K., Wald, D. J., Robeson, S. M., Tanyas, H., . . . Thompson, E. M. (2018). A global empirical model for near-real-time assessment of seismically induced landslides. *Journal of Geophysical Research: Earth Surface, 123*(8), 1835-1859.

Ortiz, F. (2020). Coming Back from Disaster. *Public Roads, 83*(4).

Ozturk, D., & Uzel-Gunini, N. (2022). Investigation of the effects of hybrid modeling approaches, factor standardization, and categorical mapping on the performance of landslide susceptibility mapping in Van, Turkey. *Natural Hazards*. doi:10.1007/s11069-022-05480-y

Park, S., & Kim, J. (2019). Landslide Susceptibility Mapping Based on Random Forest and Boosted Regression Tree Models, and a Comparison of Their Performance. *Applied Sciences, 9*(5), 942. Retrieved from https://www.mdpi.com/2076-3417/9/5/942

Park, S. H., Goo, J. M., & Jo, C. H. (2004). Receiver operating characteristic (ROC) curve: practical review for radiologists. *Korean J Radiol, 5*(1), 11-18. doi:10.3348/kjr.2004.5.1.11

Pourghasemi, H. R., Teimoori Yansari, Z., Panagos, P., & Pradhan, B. (2018). Analysis and evaluation of landslide susceptibility: a review on articles published during 2005–2016 (periods of 2005–2012 and 2013–2016). *Arabian Journal of Geosciences, 11*(9), 193. doi:10.1007/s12517-018-3531-5

Quesada-Román, A. (2021). Landslide risk index map at the municipal scale for Costa Rica. *International Journal of Disaster Risk Reduction, 56*, 102144.

Regmi, N. R., Giardino, J. R., McDonald, E. V., & Vitek, J. D. (2014). A comparison of logistic regression-based models of susceptibility to landslides in western Colorado, USA. *Landslides, 11*(2), 247-262. doi:10.1007/s10346-012-0380-2

Schlögl, M., Richter, G., Avian, M., Thaler, T., Heiss, G., Lenz, G., & Fuchs, S. (2019). On the nexus between landslide susceptibility and transport infrastructure – an agent-based approach. *Nat. Hazards Earth Syst. Sci., 19*(1), 201-219. doi:10.5194/nhess-19-201-2019

State, N. C. S. o. (2024). Geography. Retrieved from https://www.sosnc.gov/divisions/publications/kids_page_geography

Sun, D., Wen, H., Zhang, Y., & Xue, M. (2021). An optimal sample selection-based logistic regression model of slope physical resistance against rainfall-induced landslide. *Natural Hazards, 105*(2), 1255-1279. doi:10.1007/s11069-020-04353-6

Taalab, K., Cheng, T., & Zhang, Y. (2018). Mapping landslide susceptibility and types using Random Forest. *Big Earth Data, 2*(2), 159-178. doi:10.1080/20964471.2018.1472392

USGS. (2023a). *1 Arc-second Digital Elevation Models (DEMs) - USGS National Map 3DEP Downloadable Data Collection: U.S. Geological Survey*. Retrieved from: https://www.sciencebase.gov/catalog/item/4f70aac4e4b058caae3f8de7

USGS. (2023b). Landslides 101. *Education.* Retrieved from https://www.usgs.gov/programs/landslide-hazards/landslides-101

USGS. (2023c). *USGS National Hydrography Dataset Best Resolution (NHD) - North Carolina (published 20230305) Shapefile: U.S. Geological Survey*. Retrieved from: https://www.sciencebase.gov/catalog/item/61f8b8aad34e622189c328b8

VanderWeele, T. J., & Knol, M. J. (2014). A tutorial on interaction. *Epidemiologic methods, 3*(1), 33-72.

Wubalem, A., & Meten, M. (2020). Landslide susceptibility mapping using information value and logistic regression models in Goncha Siso Eneses area, northwestern Ethiopia. *SN Applied Sciences, 2*(5), 807. doi:10.1007/s42452-020-2563-0

Zhang, Y., Lim, S., & Sharples, J. J. (2016). Modelling spatial patterns of wildfire occurrence in South-Eastern Australia. Geomatics, Natural Hazards and Risk, 7(6), 1800-1815. doi:10.1080/19475705.2016.1155501

Appendix A

No	Bridge ID	Longitude	Latitude	AFP	Our Assessment	Extra Observation	Probability of Landslide Occurrence
1	860024	-83.31964644	35.47677134	1.02	Valley Bridge	Valley Bridge	0.25
2	990034	-82.37624068	35.95286913	1.05	Valley Bridge	Valley Bridge	0.27
3	860020	-83.41412095	35.43162131	1.73	Valley Bridge	Valley Bridge	0.19
4	430010	-82.82258403	35.39932611	1.79	Valley Bridge	Valley Bridge	0.19
5	600084	-82.27706725	36.08360385	1.89	Valley Bridge	Valley Bridge	0.18
6	440161	-82.55773367	35.1673545	2.59	Valley Bridge	Valley Bridge	0.24
7	580017	-81.97599594	35.57528782	2.62	Valley Bridge	Valley Bridge	0.03
8	550229	-83.6553343	35.25717623	2.82	Valley Bridge	Valley Bridge	0.16
9	860137	-83.51710646	35.39425632	2.85	Valley Bridge	Valley Bridge	0.13
10	550228	-83.6690064	35.26770495	3.00	Valley Bridge	Valley Bridge	0.17
11	490080	-83.10854232	35.29399205	3.40	Valley Bridge	Valley Bridge	0.25
12	210057	-83.91391948	34.9993788	3.90	Valley Bridge	Valley Bridge	0.17
13	860104	-83.51851741	35.39461143	3.92	Valley Bridge	Valley Bridge	0.08
14	550230	-83.65351494	35.24695009	4.24	Valley Bridge	Valley Bridge	0.32
15	560138	-82.77026923	35.83929582	4.62	Valley Bridge	Valley Bridge	0.19
16	600026	-82.22878565	36.04036643	5.28	Valley Bridge	Valley Bridge	0.10
17	020021	-81.02105795	36.54282685	6.20	Valley Bridge	Not Valley Bridge	0.14
18	190159	-84.06817913	35.11164097	6.23	Valley Bridge	Valley Bridge	0.16
19	740002	-82.34673092	35.21555685	6.61	Valley Bridge	Valley Bridge	0.92
20	040045	-81.57578897	36.44914354	6.73	Valley Bridge	Valley Bridge	0.10
21	560122	-82.8361671	35.87993609	6.74	Valley Bridge	Valley Bridge	0.16
22	190271	-84.00223354	35.070788	7.94	Not Valley Bridge	Not Valley Bridge	0.03
23	100249	-82.62422335	35.71781996	9.14	Not Valley Bridge	Not Valley Bridge	0.13
24	040039	-81.3365605	36.47373934	10.74	Not Valley Bridge	Not Valley Bridge	0.08
25	040032	-81.49664884	36.55558414	11.18	Not Valley Bridge	Not Valley Bridge	0.40
26	370033	-83.93801605	35.44444511	11.37	Not Valley Bridge	Not Valley Bridge	0.08
27	190270	-84.02028287	35.07271993	11.42	Not Valley Bridge	Not Valley Bridge	0.19
28	050026	-82.01580245	35.98178364	11.91	Not Valley Bridge	Not Valley Bridge	0.06
29	100494	-82.30741992	35.61896287	12.44	Not Valley Bridge	Not Valley Bridge	0.16
30	560547	-82.55788273	35.91704369	12.55	Not Valley Bridge	Not Valley Bridge	0.40
31	600247	-82.08616795	35.9228022	15.85	Not Valley Bridge	Not Valley Bridge	0.07
32	430098	-82.94589996	35.58069908	16.11	Not Valley Bridge	Not Valley Bridge	0.11
33	580304	-82.21520267	35.63570163	22.58	Not Valley Bridge	Not Valley Bridge	0.13
34	980035	-80.43227182	36.21614972	23.48	Not Valley Bridge	Not Valley Bridge	0.00

35	430207	-82.9947526	35.66607999	24.49	Not Valley Bridge	Not Valley Bridge	0.43
36	850392	-80.86723297	36.25986437	24.55	Not Valley Bridge	Not Valley Bridge	0.02
37	850391	-80.867459	36.259959	25.31	Not Valley Bridge	Not Valley Bridge	0.00

Chapter 3: Nested Multi-Hazard Susceptibility for Bridges in North Carolina Mountain Ranges

3.1 Abstract

This research investigates the nested multi-hazard susceptibility of highways and roadway bridges in the mountainous western region of North Carolina. Nested multi-hazard (earthquake, wildfire, landslide and flooding) risks consider the causal-effect relations of different natural hazards, in this case, the consequences of forest fires are depletion of surface vegetation that reduces soil cohesion and leading to the risks of landslides and the potential flooding hazards to highway bridges. Earthquake-induced hazard can trigger landslides and is considered based on the distance to fault zone and the remote sensing data. Finally, bridges above water and situated in valleys can be exposed to heightened vulnerability of combined landslides and flooding events due to their proximity to the water surface and the potential for raised flood heights due to upstream landslides that caused constriction to waterways. To quantify flooding risks, the difference between bridge height and the lowest river elevation is established as an assumed flooding potential (AFP). To model the nested multi-hazard risks, both linear regression (LR) and random forest (RF) models have been constructed considering several parameters including forest fire, soil types, slopes, AFP, rainfall, etc. This paper is the first report evaluating the multi-hazard issue of bridges in valleys using nested multi-hazard susceptibility analysis. The results indicate that the digital elevation model (DEM) derived parameters have the most significant effect in the modeling strategies. Wildfire, while having some effects, is not the most significant factor for western North Carolina. The results further indicate that RF modeling performed slightly better than LR modeling. The

resulting high-fidelity risk map is important for proactive bridge maintenance and rehabilitation planning.

Keywords: Nested Multi-Hazards, Bridges, Flooding Potential, Random Forest Modeling

3.2 Introduction

Climate-related events can have significant adverse impacts on integrity and operation of civil infrastructure including freight routing, railroads and bridges (Caldwell et al.; Koetse & Rietveld, 2009; Rossetti, 2002). To include climate effects in risk modeling, several researchers suggested a downscale projection of Global Climate Models (GCM) to establish the potential hazards to infrastructure (Nasr et al., 2021; Palu & Mahmoud, 2019). However, due to many sources of uncertainties associated with GCM predictions, the disconnect between climate effect projections from GCMs and actual bridge hazard prediction can be quite substantial (Hurrell & Trenberth, 1999; Schulz et al., 2017).

This paper considers a more classical approach using a nested multi-hazard (NMH) modeling approach, which is defined as the combined multi-hazard modeling that considers four different natural hazards (landslide, forest fire, earthquake and flooding) that have the potential of increasing risks to highway bridges. Multi-hazard risk assessment have been an important topic for bridge infrastructure resilience (Banerjee et al., 2019; Kameshwar & Padgett, 2014), and quantifications of risks have been performed for different combinations of hazards including earthquake and scour, earthquake and corrosion, and earthquake and liquefaction (Banerjee et al., 2019).

As Lin et al. (2024) indicated, landslide occurrences can be severe in North Carolina, which poses critical risks to highway bridges in the western mountain ranges. In this study, we further investigate the risks of wildfire triggered landslides (Culler et al., 2023; DeBano et al.; He et al., 2021). Wildfires increase the susceptibility of landscapes to landslides due to the removal of surface vegetation, which reduces soil cohesion and increases the potential for runoff-generated debris flows (Culler et al., 2023). Rengers et

al. (2020) suggested that post-wildfire landslides might occur earlier in the wet season when the ground is less saturated, indicating greater susceptibility at these times. Burn severity, slope aspect, and smaller precipitation events in burned areas significantly increase the likelihood of landslides (Culler et al., 2023; DeBano et al., 1979).

Landslides are complex ground movements affected by several critical factors including site geology, geomorphology and hydrology, regional topography and hillslope morphology and anthropogenic activities (i.e. earthworks) (Highland & Bobrowsky, 2008; Kirschbaum et al., 2015; Regmi et al., 2014). With frequent forest wildfires, the landslide risks of a region can increase significantly. However, such risks are hard to establish due to the difficult differentiation between static factors (burn severity, vegetation and soil types) and dynamic factors (soil moisture, meteorology and the time gap to the latest fire (Culler et al., 2023). Many such factors are unfortunately not documented. To help establish landslide susceptivity, a machine learning approach has been attempted (Di Napoli et al., 2020).

Pourghasemi et al. (2023) used a machine learning to model multi-hazard risks (flood, landslides, forest fires and earthquake) for Khuzestan. In this case, several machine learning techniques including Support Vector Machine (SVM), Boosted Regression Tree (BRT), Random Forest (RF) and Maximum Entropy (MaxEnt) were attempted. RF was found to have the highest “Area Under the Curve” (AUC) values.

In this paper, we consider the multi-hazard risks that may occur to the highway bridges in the mountain regions of western North Carolina (NC). As one of the US southeastern coastal states, North Carolina is often impacted by the Atlantic hurricanes as well as drought-induced forest fires (Campbell et al., 2018). At the same time, the mountain

ranges are recognized for their landslide hazards (Pourghasemi et al., 2023). Because of the likelihood of exposure to different hazards, we are interested in studying the multi-hazard risks to highway bridges in North Carolina (Lin et al., 2024).

Although earthquakes are considered in current study, North Carolina has very limited earthquake history - Between 1735 and 2014, the state has only experienced 22 earthquakes that caused damage (B., 2014). The lack of seismographic data limited the capability to quantify risks due to seismicity. Hence, the earthquake risk is simplified to considering only the distance to fault lines and derived remote sensing data (elevation, slope and aspect parameters). For landslides due to recent and known seismic events, Wang et al. (2023) used the same parameters plus distance to epicenter and distance to seismogenic fault as triggering factors.

To assess the landslide risks due to multi-hazards in North Carolina, multiple databases have been collected and compiled and both Linear Regression (LR) and Random Forest (RF) have been used in current study. Because the focus of this study is the highway bridges in the mountain regions of North Carolina, the flooding risk is assumed using an assumed flooding potential (AFP), which will be explained in section 4. Because bridges are located at discrete locations, when compared to traditional flood risk values, the AFP, reported in elevation differences, is more straightforward and helps bridge engineers visualize the flood risk to a bridge (Lin et al., 2024). Since bridges may span over abutments of different elevations, digital elevation model (DEM) data is used to establish the AFP at the center of each bridge location, representing an average height to water level.

3.3 Study Area, Landslide Data and Wildfire Data

NC is divided into three main physiographic regions, each characterized by unique environmental and geological features: the eastern Coastal Plain, the central Piedmont, and the western Appalachian Mountains (from right to left, Figure 3-1a). The current study focuses on the western mountain region (Figure 3-1b), which encompasses an area of 26,572 km^2 as part of the Appalachian Mountains (State, 2024). River flow directions are divided by the Eastern Continental Divide (State, 2024).

U.S. Geological Survey (USGS) landslide database showed most landslides concentrated in the western NC region (Belair et al., 2022). Lin et al. (2024) confirms that the mountainous areas of NC experience the highest occurrence of landslides. The landslide data selection in our study is based on the confidence rule system by USGS (Belair et al., 2022). Following the confidence rule system used in the USGS landslide dataset (Belair et al., 2022) and Lin et al. (Lin et al., 2024) study, this paper uses susceptibility values ranging from 5, which indicates a confidence of a consequential landslide at a given location, and 8, which refers a high confidence in extent or nature of landslide (Mirus et al., 2020).

Wildfire is a common hazard due to fuel accumulation, seasonal precipitation variability, and frequent droughts (Li et al., 2019). Intini et al. (2019) described a wildfire as "an unplanned and uncontrolled fire spreading through vegetative fuels, including any structures or other improvements thereon." Figure 3-2 shows the number of wildfire events from 1928 to 2023 in NC, as collected by the North Carolina Forest Service (NCFS)(NCFS, 2024). Wildfire events have occurred every year during this period.

To establish the wildfire database, U.S. Department of Agriculture (USDA) wildfire data from 1995 to 2018 were collected (Short, 2021). USDA cause classification showed that the reasons why the fire occurred are man-made, natural causes or

undetermined. Hence, the USDA database differentiated the wildfire causes as human - induced, nature-induced and missing data/not specified/undetermined. For our research purposes, we focused on both human-induced and natural wildfire events and undetermined wildfire events were not considered in this study. The wildfire database represents point features and includes 112,454 events in NC. The biggest natural wildfire event in NC was the Pains Bay fire in 2011 (Short, 2021).

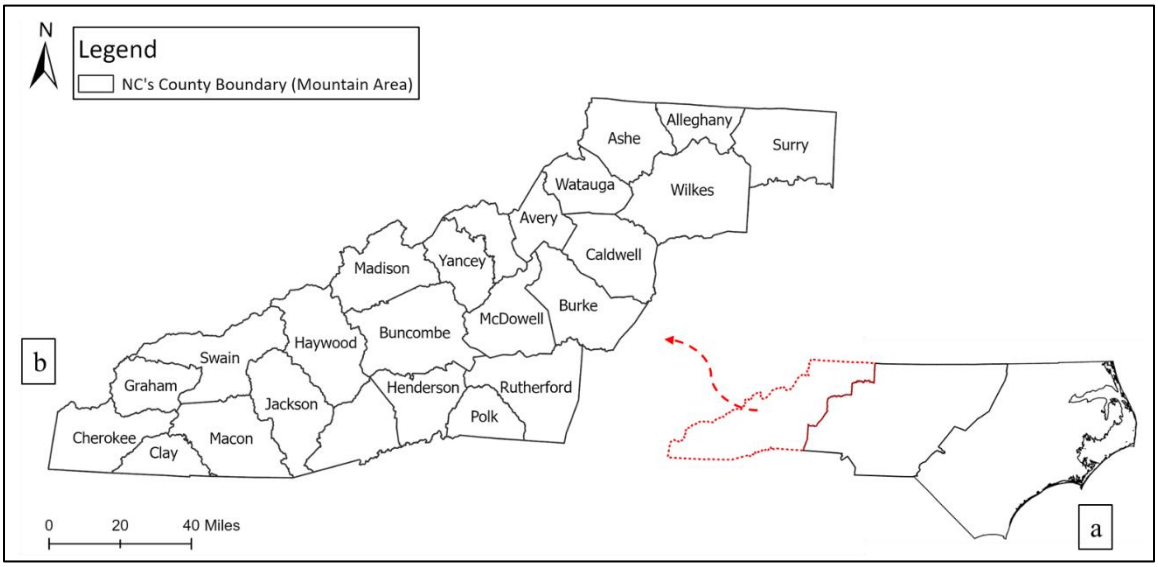

Figure 3-1 Study area with location map illustrating North Carolina's Mountain area. a. North Carolina distinct physiographic regions distribution, b. Blue Ridge Mountain area.

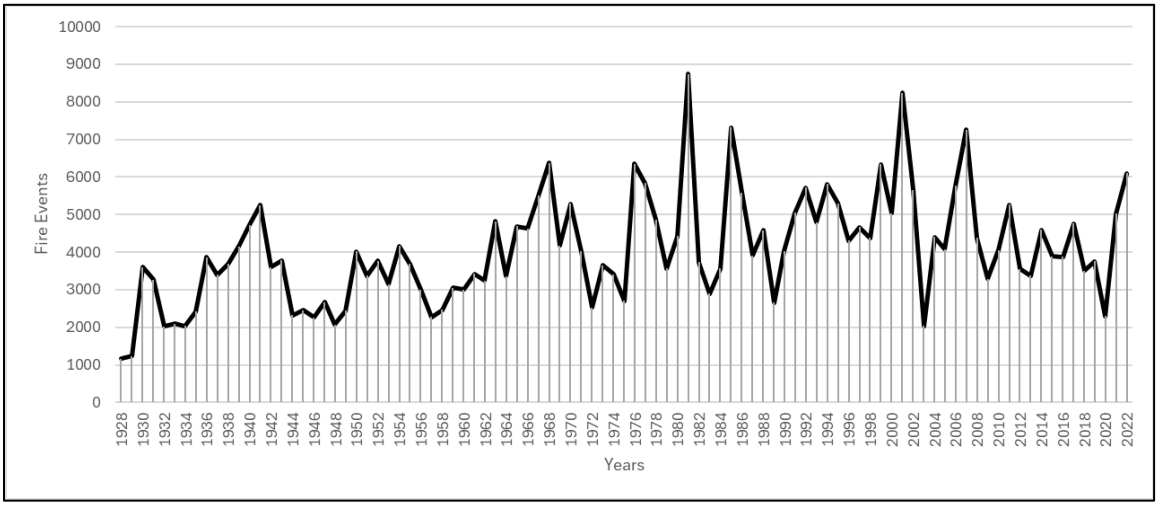

Figure 3-2 Number of wildfire events from 1928 to 2023 in North Carolina (collected from North Carolina Forest Service).

3.4 Materials and Methods

3.4.1 Wildfire, Landslide and Bridge Inventory

The compiled landslide database contains 4,794 landslides and 6,653 polygons (Belair et al., 2022). Figure 3-3 shows the landslides considered in the western mountain region. Figure 3-4 shows the wildfire point features from 1995 to 2018 with 24,738 events (Short, 2021).

Highway bridge inventory is compiled from data provided by the North Carolina Department of Transportation (NCDOT) and the Federal Highway Administration (FHWA). Bridge ID is used to combine the two datasets (up to 2023) containing 22,812 bridges statewide (Figure 3-5). Out of which only 3,084 bridges were considered for the western mountain range.

3.4.2 Conditioning Factors

3.4.2.1 Landslide

Landslide susceptibility variables considered include aspect, slope, elevation, distance to faults, distance to rivers, rainfall, soil type, etc. (Chang et al., 2023; Huang et al., 2024; Liu et al., 2023; Sengupta & Nath, 2024). Of which, remote sensing information such as elevation and derived factors such as slope have been recognized to affect landslide occurrences (Chang et al., 2023; Huang et al., 2024; Liu et al., 2023). Using DEM data from the USGS (USGS, 2023a) at a 1 arc-second resolution (Figure 3-6a) , a DEM layer with 30m × 30m cell dimensions was generated based on contour lines containing elevation values (USGS, 2023a).

Slopes were determined from DEM using slope tool (Figure 3-6b) and the aspect variable with the aspect tool (Figure 3-6c) in ArcGIS Pro. The aspect variables were defined according to Ayalew and Yamagishi (Sengupta & Nath, 2024) and were divided

into nine classes including west (292.5–337.5°), northwest (247.5–292.5°), southwest (202.5–247.5°), south (157.5–202.5°), southeast (112.5–157.5°), east (67.5–112.5°), northeast (22.5–67.5°), north (0–22.5° and 337.5–360°), and flat (−1°), which is indicate 9 to 1 values.

Figure 3-6d shows different soil types which can contribute to landslides after severe wildfires (Culler et al., 2023; Rengers et al., 2020). Soil type also significantly influences slope instability and landslide occurrence based on the properties of the rocks and soils (Wubalem & Meten, 2020). Burned soils may lose organic content during the combustion process, reducing their water-holding capacity and increasing the risk of erosion (Wubalem & Meten, 2020). We classified the soil types into four groups: Most critical (4), medium critical (3), less critical (2), and least critical (1). The most critical group includes residuum weathered soil and organic matter found in clayey, sandy clay loam, and complex soils. The medium critical group does not include organic matter or residuum weathered soil in clayey, sandy clay loam, and complex soils. The less critical group consists of other soils or rocks that may include some organic matter or residuum weathered soil. The least critical group consists of all remaining soil types. The soil type data were collected from the USDA soil survey database (Staff, 2003).

Rainfall observation data from the National Oceanic and Atmospheric Administration (NOAA) was analyzed in ArcGIS Pro. Using Inverse Distance Weighted (IDW) tool (Sengupta & Nath, 2024). Finally, Euclidean distances tool were used for the distance to river and distance to faults calculation using USGS National Hydrography Dataset (NHD) (Figure 3-6h) and North Carolina Environmental Quality (NCDEQ) database (Figure 3-6i) (NCDEQ, 2022; USGS, 2023c). Seismicity and distance to rivers

are another key factor in triggering landslides that warrants explicit investigation (Liu et al., 2023).

3.4.2.2 Wildfire

To further elaborate on the effects of wildfire on the occurrence of landslides (Culler et al., 2023; Rengers et al., 2020; Staley et al., 2016), several variables were used to define wildfire areas including elevation, slope, forest cover, rainfall, temperature, distance to high population intensity, distance to rivers, and distance to roads (Busico et al., 2019; Jain et al., 2020; Milanović et al., 2021; Nhongo et al., 2019; Zhang et al., 2016). The justifications of the selected factors are as follows.

Elevation (Figure 3-6a) and slope (Figure 3-6b) play critical roles in wildfire (Iban & Sekertekin, 2022; Leuenberger et al., 2018; Moayedi & Khasmakhi, 2023). Meteorological factors like temperature and precipitation may be influenced by these topographic features (Leuenberger et al., 2018). The slope can influence both airflow and the local microclimate, which in turn impacts the spread of fire (Chang et al., 2022; Kumi-Boateng et al., 2021).

Rainfall (Figure 3-6e) and temperature (Figure 3-6f) are also critical as higher temperature and less precipitation can generate more favorable conditions for triggering forest fire (Chang et al., 2022; Chuvieco & Salas, 1996). Dry leaves, grass, twigs, branches, and other debris on the forest floor, as well as the trees themselves increase the fuel load feeding forest fire (Kumari & Pandey, 2020). Therefore, certain forest types (Figure 3-6g) are identified as more flammable than others, leading to a higher risk of fire occurrence (Kumari & Pandey, 2020; Taylor et al., 2005).

In distance to rivers (Figure 3-6h), the presence of water courses and springs is considered a deterring factor to forest fire (Busico et al.). The majority of wildfires originate from human activities, whether intentional or accidental, suggesting a potential link between fire occurrence and socioeconomic factors, such as distance to roads (Figure 3-6j) and distance to high population zones (Figure 3-6k) (Chuvieco & Salas, 1996; Nhongo et al., 2019; Zhang et al., 2016).

3.4.3 Logistic Regression Model

Our workflow schematic for models and calculations is illustrated in Figure 3-7. Here, logistic regression (LR) is used to estimate the relationship between a variable and its influential factors (Bai et al., 2010; Milanović et al., 2021) and to calculate the probability of an event occurrence (Bai et al., 2010; Milanović et al., 2021), which is described as:

$$p = \frac{e^z}{1+e^z} = \frac{1}{1+e^{-z}} \tag{3.1}$$

where p is the probability of the occurrence of an event (1: occurrence; 0: no occurrence). Logit z, defined as a linear combination of the independent variables, is expressed as:

$$z = \beta_0 + \beta_1 x_1 + \beta_2 x_2 + \ldots + \beta_i x_i \tag{3.2}$$

β_0 is the intercept of the model, x_i is the ith variable, and β_i is the coefficient of the variable x_i. The statistical package in RStudio 2021.09.2+382 was used for the LR modeling and the probability map of event occurrence was generated. The maps were then presented using ArcGIS Pro 3.1.2.

The performance of a binary classification model is represented by the Receiver Operating Characteristic (ROC) curve (Iban & Sekertekin, 2022). Variable significance has been

widely applied for variable selection in numerous studies on extreme weather events (Milanović et al., 2021). The importance of individual variables selected through the LR procedure is assessed using the Wald statistical test (Martínez-Fernández et al., 2013; Milanović et al., 2021). The Wald statistic tests whether each variable contributes to the model and helps identify which predictors are most influential (Martínez-Fernández et al., 2013).

We used R to generate the models, producing the LR results, such as variable importance, variable significant, ROC curve, and AUC values.

3.4.4 Random Forest Model

Alzubi et al. (2018), defined Machine Learning (ML) as a subset of artificial intelligence allowing computers to learn from repetitions and has been used in geospatial modeling for extreme event predictions. It has been utilized in geospatial modeling for predicting extreme events (Jain et al., 2020; Liu et al., 2023). Random Forest (RF) is a well-known machine learning method that combines multiple binary decision trees, each built on random vector values, to model the spatial distribution of extreme weather events (Breiman, 2001; Sengupta & Nath, 2024). Extreme weather events have been analyzed using various methods, including hazard susceptibility mapping, remote sensing data modeling, and spatial information analysis (Iban & Sekertekin, 2022; Liu et al., 2023). RF has been applied in spatial regression analyses for risk modeling, where it is used to predict the likelihood of extreme events (Iban & Sekertekin, 2022; Milanović et al., 2021; Sengupta & Nath, 2024).

RF modeling requires data representing both occurrence and non-occurrence sets (Milanović et al., 2021). In our study's dataset, landslide occurrence points were labeled

with a value of 1, while non-occurrence points were labeled as 0 (Milanović et al., 2021). RF modeling and analysis performed using RStudio 2021.09.2+382, which produced outputs such as out-of-bag (OOB) errors, accuracy metrics, ROC curves, AUC values, and a probability map illustrating landslide occurrence in North Carolina.

In the RF modeling, variable importance is assessed using the Gini impurity function (Milanović et al., 2021; Sengupta & Nath, 2024), which is calculated across all decision trees and is then scaled with a higher value means that helps to make cleaner splits, thus improving the model's performance (Milanović et al., 2021).

3.4.5 North Carolina Highway Bridges

For our study, we focused on bridges over water with a length exceeding 6 meters, excluding those designated as ramps or over pipes and culverts. Using ArcGIS Pro, we calculated the bridge's flooding potential (AFP) from DEM data by utilizing various tools, including the split line to points tool, extract multi-values to points tool, bearing distance to line tool, buffer tool, and zonal statistics tool. These tools provided elevation data for both the riverbanks and the river itself. The elevation data were then incorporated into the calculation of the bridge's AFP, which is defined as follows:

$$B_i = \frac{E_{1i}+E_{2i}}{2} - E_{Li} \tag{3.3}$$

where B_i denotes the bridge's AFP, i represents the bridge's ID, E_{1i} and E_{2i} represent the elevations on the two sides of the bridge, while E_{Li} denotes the elevation of the river. Unlike bridge clearance, AFP is determined by subtracting the river elevation from the DEM at the bridge location from the average height of the bridge, calculated from the elevations of both banks.

We used several criteria, such as landforms, elevation differences, and slope to identify bridges situated within valleys (Lin et al., 2024). The landform factor was analyzed using the Geomorphon Landforms tool in ArcGIS Pro (ESRI, 2023). In our study, slope values were determined by calculating the maximum slope degree within a 30-meter radius surrounding each bridge.

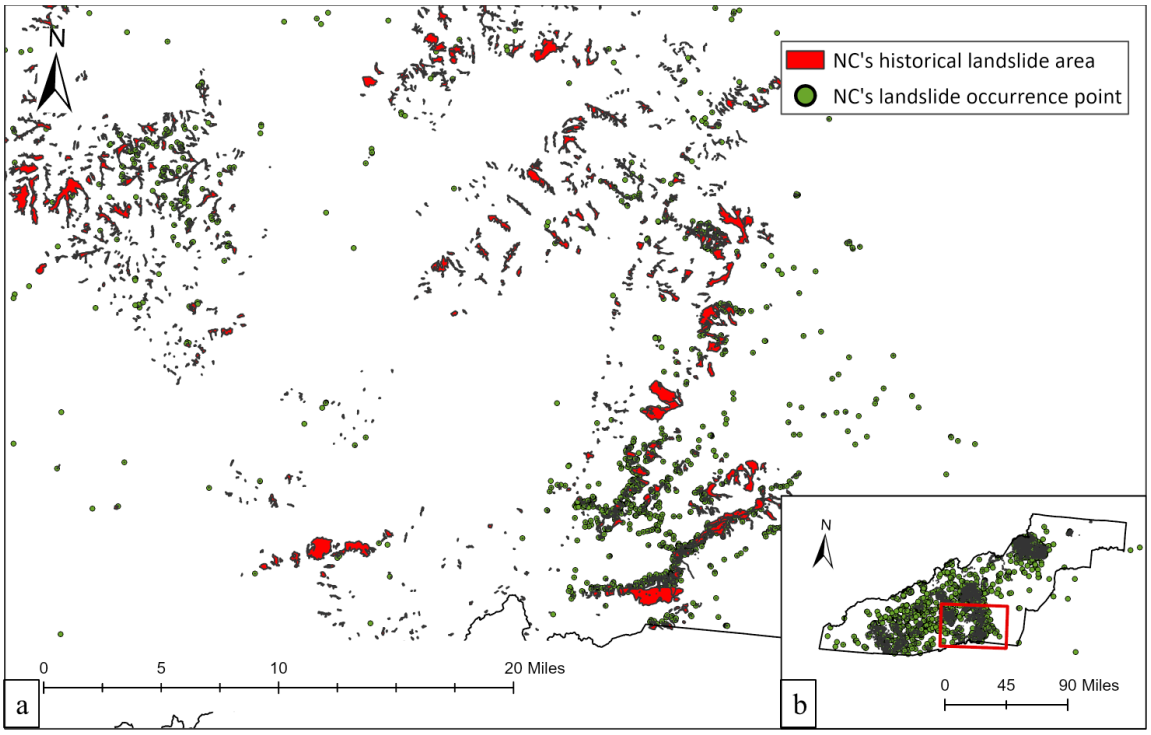

Figure 3-3 Location of landslide points and polygons within the study area. a. Showing closer version in Buncombe County, Henderson County, Polk County, Rutherford County, and Transylvania County. b. Showing NC's Mountain areas.

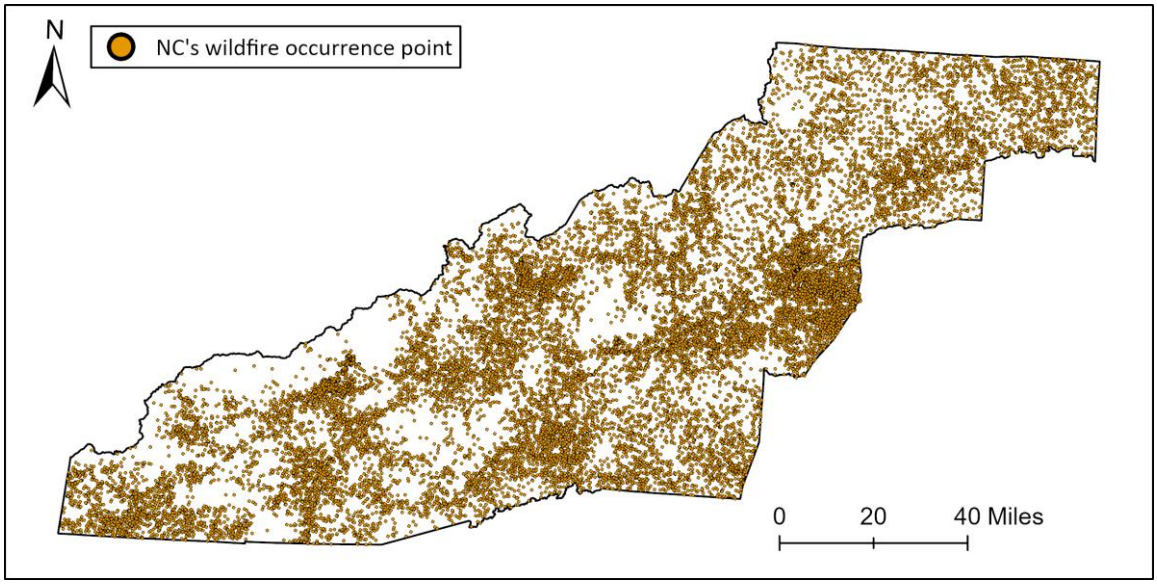

Figure 3-4 Location of wildfire points within the study area.

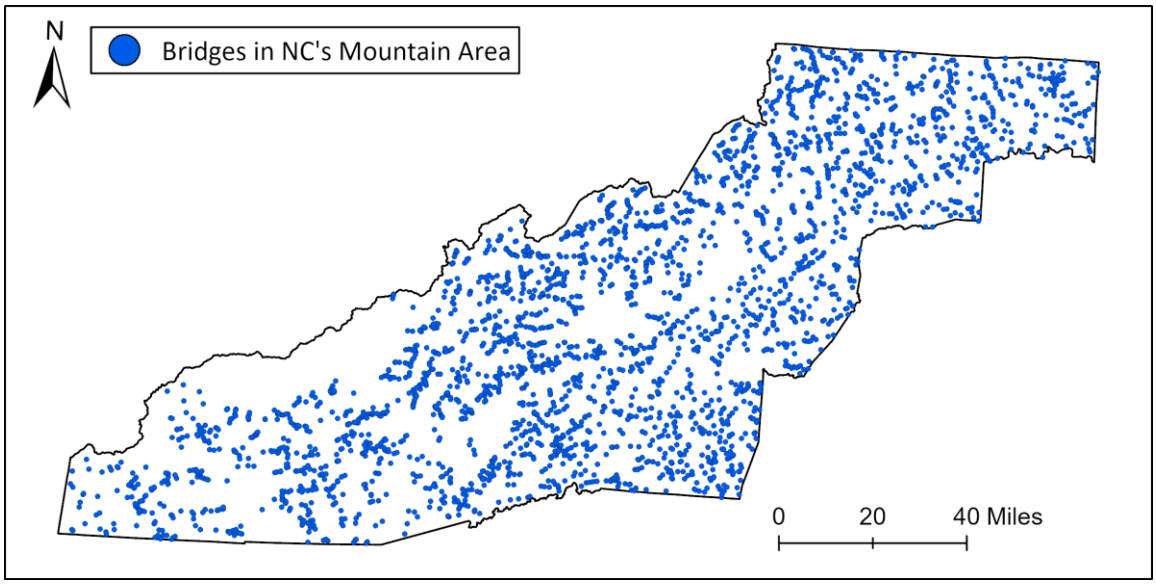

Figure 3-5 Location of bridges within the study area.

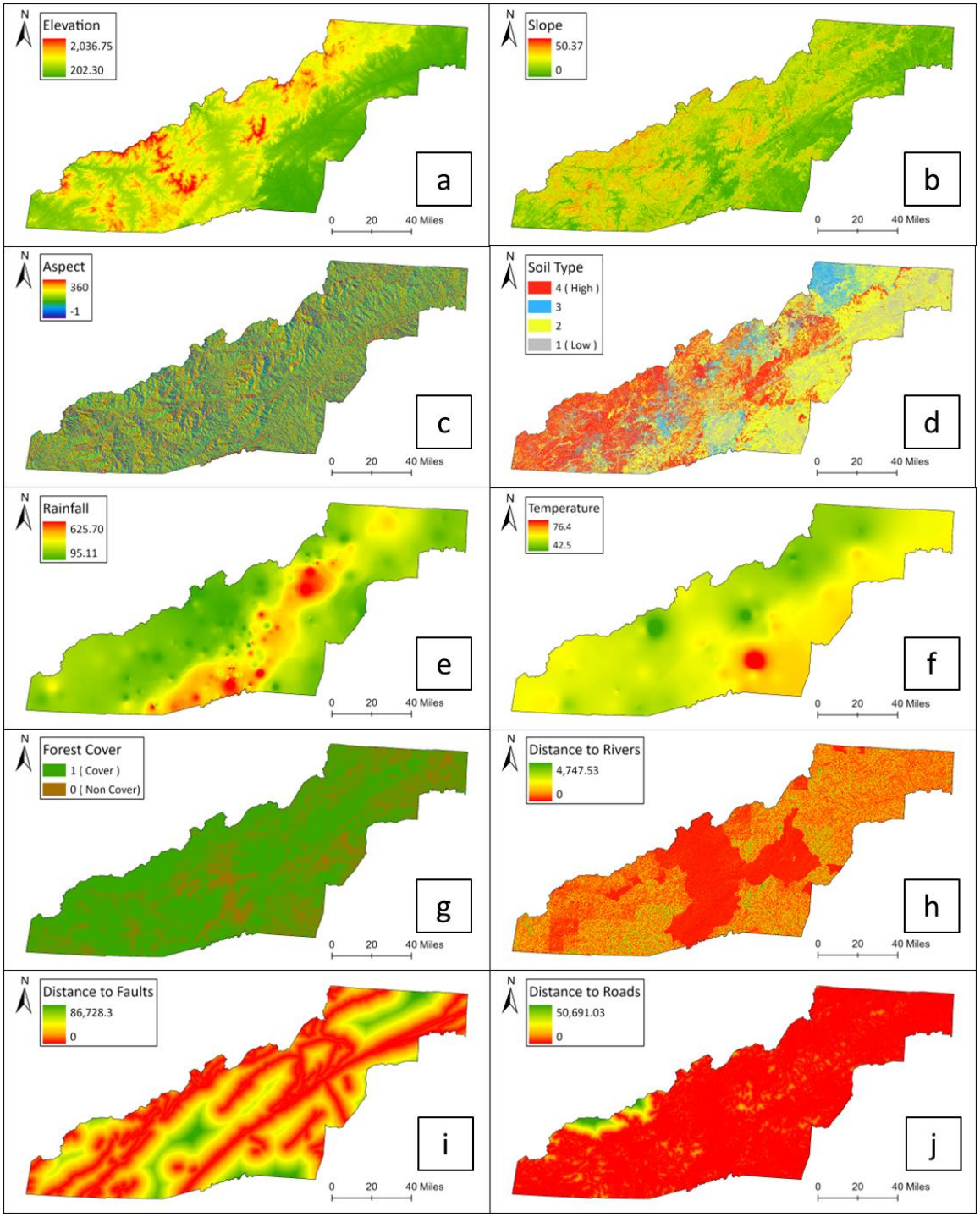

Figure 3-6 Conditioning factors used in this study: a. Elevation, b. Slope, c. Aspect, d. Soil type, e. Rainfall, f. Temperature, g. Forest cover, h. Distance to rivers, i. Distance to faults, j. Distance to roads, k. Distance to high population intensity, l. probability of wildfire occurrence.

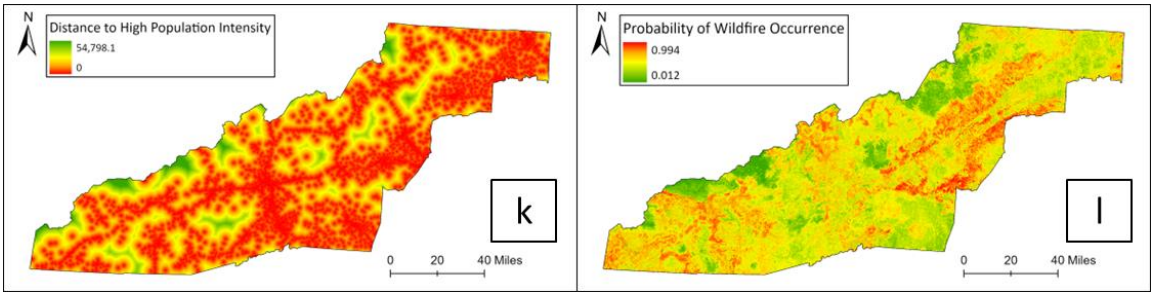

Figure 3-6 (continued)

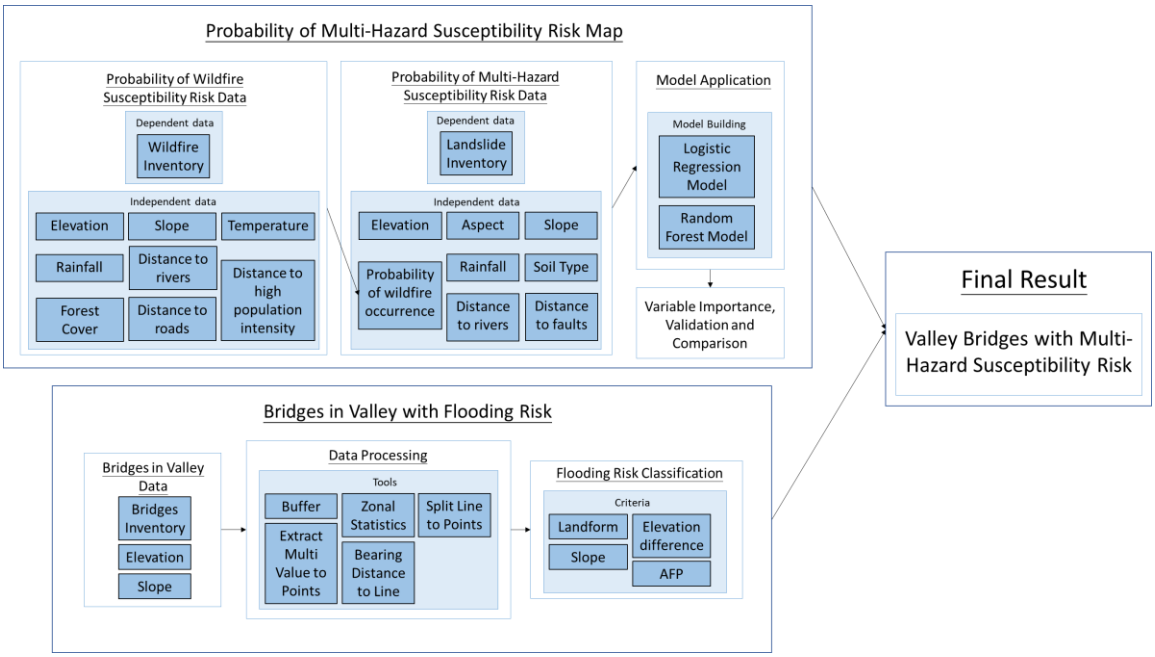

Figure 3-7 A schematic of the calculation workflow for the probability of multi-hazard (wildfire, landslide, earthquake and flooding) occurrence map, the probability of wildfire occurrence map, and bridges in the valley.

3.5 Results and Discussions

For landslide modeling, we utilized a total of 9,794 sample points of which 4,794 represent landslide occurrences and 5,000 non-landslide occurrences. For the wildfire events, we used 24,738 points for historical landslide occurrences and a total of 25,000 for non-wildfire occurrence for conducting the LR and RF modeling.

3.5.1 Statistical Results

Table 3-1 shows that most predictive variables are negative (except intercept) and significant indicating that the wildfire events are critical for areas with lower elevations, flatter slope, lower amounts of rainfall, lower temperature, closer to the roads, not covered by forest, or closer to areas with a higher population density (e.g., urban). The distance to rivers resulted in a negative correlation and was not significant, which implies that the factor is not reliable as a predictor.

Table 3-1 Correlation coefficient values for LR predictor variable in wildfire occurrence.

Variable	Unit	Coefficient	Significance	Source
Elevation	m	-6.637e-04	***	DEM
Slope	Degree	-2.119e-02	***	
Rainfall	mm/year	-6.016e-03	***	Weather Station
Temperature	°F/year	-2.101e-02	***	Weather Station
Distance to roads	m	-6.926e-04	***	Road
Distance to rivers	m	-4.432e-05	.	Stream
Forest cover	0/1	-3.262e-01	***	Forest Cover
Distance to areas of high population density	m	-4.523e-05	***	Land Cover
Intercept		3.510e+00	***	

* Significance codes: 0‘***’ 0.001 ‘**’ 0.01 ‘*’ 0.05 ‘.’ 0.1 ‘ ’ 1.

Table 3-2 presents the variables used in the analysis and the results for the LR model for landslide occurrence. The results show that several variables are positively correlated and statistically significant, suggesting that landslides are more likely to occur

in areas characterized by higher elevations, steeper slopes, heavier rainfall, greater distances to rivers, and slopes with northeast (aspect 3), east (aspect 4), southeast (aspect 5), south (aspect 6), or southwest (aspect 7) orientations.

In contrast, distance to faults, soil type, wildfire and the interaction between slope and elevation are negative correlated and statistically significant. This indicates that landslides tend to occur closer to the least critical of soil type, closer to less wildfire occurrence area, closer to fault lines, and the interaction effect suggests that higher slopes correspond to lower elevations in these areas. Additionally, aspects 2, 8 and 9 (northward-facing, northwestward-facing and westward-facing slopes) are identified as a negative factor, with aspects 2 and 8 being more statistically significant. This implies that landslides are less likely on west-facing slopes, especially for aspect 9. Finally, the model does not provide conclusive evidence regarding landslide frequency on flat (aspect 1) slopes, as the mountainous region lacks flat or level surfaces without an incline.

Table 3-2 Coefficient values for LR in the case of each predictor variable in landslide.

Variable	Unit	Coefficient	Significance	Derive
Elevation	m	2.111e-03	***	DEM
Slope	Degree	6.869e-01	***	
Aspect2		-6.261e-01	***	
Aspect3		6.261e-01	***	
Aspect4		1.165e+00	***	
Aspect5		1.356e+00	***	
Aspect6		9.098e-01	***	
Aspect7		5.151e-01	***	
Aspect8		-3.836e-01	**	
Aspect9		-2.955e-01	*	
Rainfall	mm/year	3.811e-03	***	Weather Station
Distance to faults	m	-1.045e-05	***	Fault
Distance to rivers	m	1.415e-04	*	Stream
Soil Type		-1.313e-01	***	
Wildfire		-1.101e+00	***	
Slope: Elevation		-3.785e-04	***	
Intercept		-4.989e+00	***	

* Significance codes: 0 ‘***’ 0.001 ‘**’ 0.01 ‘*’ 0.05 ‘.’ 0.1 ‘ ’ 1.

3.5.2 Importance of Variables

Table 3-3 displays the importance of each variable for both the LR and RF modeling approaches for the prediction of wildfire occurrence and the LR result shows that distance to rivers is the most important variable followed by temperature and slope (Table 3-3). However, distance to rivers does not display significant effects on the RF model (Table 1). In the RF model, distance to roads is the most important explanatory variable, followed by elevation and distance to high population density areas (Table 3-3). It is intriguing is that distance to roads has the lowest impact in the LR model, while distance to rivers has the second lowest impact in the RF model.

Table 3-3 Wildfire risk modeling variable importance evaluation (Wald statistics for LR model and Gini impurity measures for RF model).

Logistic Regression		**Random Forest**	
Variable	Wald Statistics	Variable	Gini Impurity
Distance to rivers	-1.79	Distance to roads	3748.30
Temperature	-3.82	Elevation	3117.71
Slope	-4.68	Distance to high population intensity	3072.96
Rainfall	-9.08	Temperature	2732.57
Elevation	-11.06	Rainfall	2605.56
Forest cover	-12.99	Slope	2544.97
Distance to high population intensity	-21.91	Distance to rivers	1705.21
Distance to roads	-40.84	Forest cover	264.12

In the landslide modeling, the LR results indicate that slope is the most important variable for landslide occurrences, followed by rainfall and elevation (Table 3-4). Slope has a highly significant effect on the model (Table 3-2). Similarly, in the RF model, slope is also the most important variable, followed by rainfall and elevation (Table 3-4). In the LR model, the variable with the lowest impact is distance to faults, while soil type has the lowest impact in the RF model. Comparing the LR and RF models, slope, rainfall, and

elevation are consistently the most important variables and have significant effects on landslide susceptibility.

Table 3-4 Variable importance evaluation based on Wald statistics for LR model and Gini impurity for RF model for landside risks.

Logistic Regression		**Random Forest**	
Variable	Wald Statistics	Variable	Gini impurity
Slope	24.40	Slope	1160.17
Rainfall	10.48	Rainfall	630.71
Elevation	9.94	Elevation	548.39
Aspect	4.76	Distance to faults	481.95
Distance to river	2.41	Wildfire	365.57
Soil Type	-4.57	Aspect	353.40
Wildfire	-5.52	Distance to rivers	263.52
Distance to faults	-6.32	Soil Type	96.13

3.5.3 Validation and Comparison of Models

Table 3-5 demonstrates that the LR model achieves an overall accuracy of 68.5%, indicating how effectively it predicts the correct outcomes. In terms of sensitivity, the model correctly identifies 58.2% of true positive cases. LR model also shows a low Akaike Information Criterion (AIC) value indicating a good model fit and a high AUC value with an accuracy of 74.6% for distinguishing between positive and negative cases.

An OOB error estimate signifies improved model performance, indicating that the model has a strong capacity for generalization of new data. The goal of this optimization process is to minimize the OOB error while achieving robust predictive performance (Chowdhury et al., 2024). To enhance model performance, users must optimize two key hyperparameters namely, the number of trees in the forest (ntree) and the number of variables considered at each node (mtry)(Chowdhury et al., 2024).

In the results from the RF model in wildfire, the performance of our study area surpasses that from the LR model. For accuracy, the correct predictions increased by 4.4% when compared to the LR model. Furthermore, the AUC for the RF model is 81.4%,

demonstrating superior model performance when compared to the LR model. The OOB error rate was 27.0%, achieved with optimized values of 500 for ntree and 3 for mtry.

For the landslide analysis, Table 3-5 shows that the LR model has an accuracy of 76.3%. Additionally, the sensitivity analysis shows a prediction accuracy of 77.4%, reflecting model's ability to correctly identify positive instances. Regarding the Akaike Information Criterion (AIC), lower values typically indicate a better model fit. However, in our case, the AIC value is relatively high at 8,116.8. For reference, AIC values commonly range from 200 to 1,000,000 (Nowicki Jessee et al., 2018; Quesada-Román, 2021). As highlighted in Section 3.4.3, the ROC curve (Figure 3-8) and AUC are widely accepted metrics for evaluating the performance of both RF and LR models (Chen et al., 2019). In this study, the LR model achieved an AUC of 74.7%, indicating an acceptable level of model performance.

In the RF landslide prediction, the OOB error was 15.98%. The model demonstrated an overall prediction accuracy of 83.9%. In sensitivity analysis, the RF model correctly identified 86.7% of the positive instances. Additionally, the model achieved an AUC value of 91.5%, indicating exceptional performance and a strong ability to distinguish between positive and negative cases.

Table 3-5 Summary of model performances for LR model and RF model for wildfires and landslides.

Models	Evaluation	Value of Wildfire	Value of Landslide
Logistic Regression	AIC[1]	46,860	7805.9
	Accuracy	0.685	0.7567
	Sensitivity	0.5820	0.7505
	AUC	0.7464	0.8211
Random Forest	OOB	26.96%	15.98%
	Accuracy	0.7287	0.8386
	Sensitivity	0.7051	0.8671
	AUC	0.8104	0.9153

[1] AIC: Akaike information criterion.

In summary, as illustrated in Table 3-3, for the landslide modeling, the results from the landslide's LR modeling indicate that slope is the most influential variable for predicting landslide occurrences, with rainfall and elevation following closely behind. (Table 3-4). Slope has a highly significant effect on the model (Table 3-2). Similarly, for the RF model, slope is also the most important variable, followed by rainfall and elevation (Table 3-4). In the LR model, the variable with the lowest impact is distance to faults, while soil type has the lowest impact in the RF model. Comparing the LR and RF models, slope, rainfall, and elevation are consistently the most important variables and have significant effects on landslide susceptibility.

As shown in Table 3-4, Table 3-5, and Figure 3-8, the RF model outperformed the LR model in predicting both wildfire and landslide occurrences. Hence, the RF model was used to generate probability maps for wildfire and landslide occurrences.

3.5.4 Predicted Probabilities and Susceptibility Map

RStudio was used in the generation of probability maps for wildfire and multi-hazard (wildfire + earthquake + landslide) susceptibilities and the results are presented separately in Figure 3-9 and Figure 3-10. Figure 3-9 displays the wildfire-only risk susceptibility map, where different colors are used to classify varying levels of susceptibility: red indicates a high probability of wildfire occurrence, yellow signifies a medium probability, and green represents a low probability. Figure 3-10 presents the combined hazard (wildfire + earthquake + landslide) susceptibility map where the color classification follows the same scheme as the wildfire susceptibility map.

Using a landslide probability of 50% or greater, Figure 3-11 shows bridges that are most susceptible to the multi-hazard risks. Previous results without consideration of wildfire (Lin et al., 2024) were also presented for comparison. The present study identifies

26 bridges located in areas with a probability of multi-hazard risks exceeding 50%, a reduction from the 47 bridges identified in Lin et al. (2024) study. In terms of significant findings, the landslide susceptibility map, which includes wildfire and earthquake data, reveals that four new bridges not identified in the Lin et al. (2024) study, while 25 bridges from the previous study no longer appear in high-probability zones. The differing results are due to the inclusion of wildfire risks and soil type variables.

The bridges located in areas with over a 70% probability of multi-hazard occurrence are situated around Henderson County, Polk County, and Rutherford County. The highest probability, 87.4%, is found in Henderson County (Figure 3-1).

3.5.5 Bridge in a Valley and Flooding Risk

In the current study, 21 bridges were identified as being in valley settings (Figure 3-12). To combine the multi-hazard risks with flooding risks, Lin et al. (2024) first identified bridges in a valley, which implied additional search criteria including slope (e.g., above 9 degrees), elevation difference (e.g., above 15 m), AFP value (e.g., under 7 m) and landform (e.g., valley and pit) data.

Field observations (Lin et al., 2024) conducted to assess the classification of bridges based on AFP indicate that bridges with AFP between 7 m and 30 m are not all located in a valley and may be situated at mid-valley height or on a ridgetop. Hence, AFP less than 7 m were used to identify bridges in valley and with flooding risks.

The bridge-in-valley data with the probability of multi-hazard risks are presented in Figure 3-12 and Appendix B. According to Appendix B, the results indicate that four bridges have a landslide occurrence probability of less than 10%; 11 bridges have a probability between 10% and 20%; two bridges have a probability between 24% and 30%;

and four bridges have a probability between 31% and 78%.Additional analysis (Figure 3-12) showed that over 31% of the areas surrounding Henderson, Jackson, Macon, and Polk Counties are predicted to experience landslides. The highest landslide probability is 77.8%, located in Polk County.

Landslides can be exacerbated by factors such as seismic activity and rainstorms intensified by global warming, leading to an increasing frequency of landslide events (Huang et al., 2024). Hurricane Helene provides evidence of this, as it brought heavy rainfall and high wind gusts that caused significant damage to the Western North Carolina and Eastern Tennessee regions (Pourghasemi et al., 2018). Figure 3-13 shows state highway bridge (ID: 100239) over Swannanoa River with damaged approaches during Hurricane Helene because of the heightened flooding (estimated over 3 m at bridge approach). The heightened flood level was due to debris from both downed trees and rock falls from upstream. The current study examines the impacts of landslides on highways and bridges, where debris and blockages can lead to collisions, unsafe conditions, and even fatalities (Ozturk & Uzel-Gunini, 2022). Large landslides can collapse bridges and overpasses, highlighting the need for improved monitoring and resilience strategies to protect transportation infrastructure (Ozturk & Uzel-Gunini, 2022). Therefore, it would be beneficial for regional departments of transportation to provide an accurate multi-hazard sustainability risk map to strengthen routing decision-making, optimize future site preparation, and improve planning for weather-related damage assessments.

3.6 Conclusion

To avoid multi-hazards associated with highway bridges in North Carolia, a risk susceptibility analysis is performed to identify vulnerable bridges in the western

mountainous region. Following the recent tragic hurricane event in western North Carolina (September 2024 Hurricane Helene), where numerous road closures and bridge damage led to injuries and fatalities due to flooding and landslides (NCDHHS, 2024; NCDOT, 2008), it has become increasingly important to investigate such risks.

The risk modeling focuses on landslide and flooding risks with inclusion of earthquake and wildfire risks forming a nested multi-hazard risk analysis strategy. Logistic Regression (LR) and Random Forest (RF) models were employed to generate wildfire and landslide susceptibility maps. In this study, the wildfire susceptibility map was used as an independent factor to predict landslide occurrences. The LR and RF models yielded wildfire prediction accuracy rates of 68.5% and 72.9%, respectively. Landslide prediction accuracy rates were 75.7% for the LR model and 83.9% for the RF model, respectively. As shown in the ROC curves (Figure 3-8), the RF model demonstrated higher sensitivity when compared to the LR model for both wildfire and landslide predictions. Bridges at high risk of landslide exposure were identified by integrating highway and roadway bridge data into the landslide risk data.

Upon further examination of the variables in both events, the wildfire-related variables: distance to roads, elevation, and distance to high population density are identified as the most important in the Random Forest (RF) model. This suggests that remote sensing data, including elevation, slope and aspect, plays a significant role in predicting extreme weather events. We included soil type variable in the landslide model. However, it did not significantly increase the accuracy of the modeling. It might be caused by the soil type classification method and future studies should consider more complex soil types and smaller regions.

Further analysis of bridges located in valleys, in relation to the probability of multi-hazard risks, reveals a decrease in both the probability values and the number of bridges with a multi-hazard risk probability exceeding 50%. Specifically, the number of such bridges decreased from 47 to 26 (Figure 3-11). Our study utilizes the bridge's Assumed Flooding Potential (AFP) as an indicator of combined risks from multi-hazard events, such as landslides, wildfire, earthquake and flooding. If flood levels reach the AFP, uplift forces from rapid channel flow may lift the bridge deck, leading to a washout. Twenty-five bridges identified in the previous study no longer appear in high-probability zones, while four new bridges are now located in areas with over a 50% probability of multi-hazard risk. This shift can be attributed to the inclusion of additional factors, such as wildfire susceptibility and soil type, which enhanced the accuracy and precision of the predictions. The reduction in bridges with over a 50% probability of multi-hazard risk is reasonable, as the focus is on areas where landslide events are likely to be triggered by wildfire activity. The increase in probability for some bridges indicates that these structures may be more vulnerable to wildfire-triggered landslides. This observation provides crucial insights for managers and decision-makers, allowing them to implement proactive strategies aimed at mitigating potential future bridge damage.

The development of a landslide risk prediction model poses a challenge if we take into consideration the complex nature of geo-environments, encompassing factors such as geology, hydrology, topography, and human activities (land use) (Palu & Mahmoud, 2019). The current study covered a large area and only considered the aspect variable and seismicity; hence, future work aiming for increased precision that can delve into additional factors such as geology and lithology.

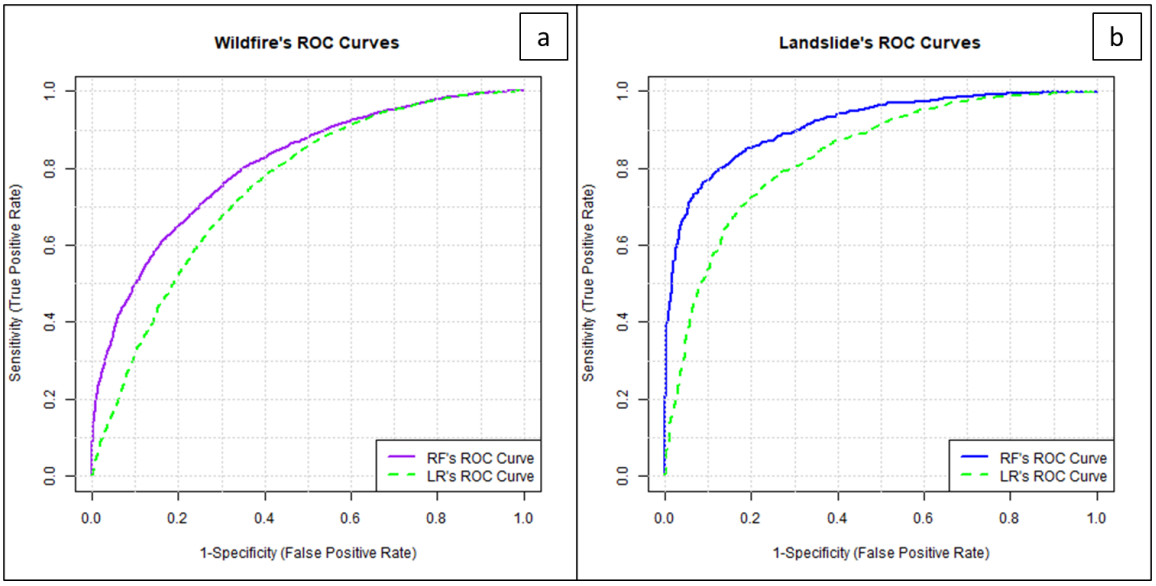

Figure 3-8 ROC curves of the LR model and RF model : a. Wildfire only, b. Landslide with earthquake risks.

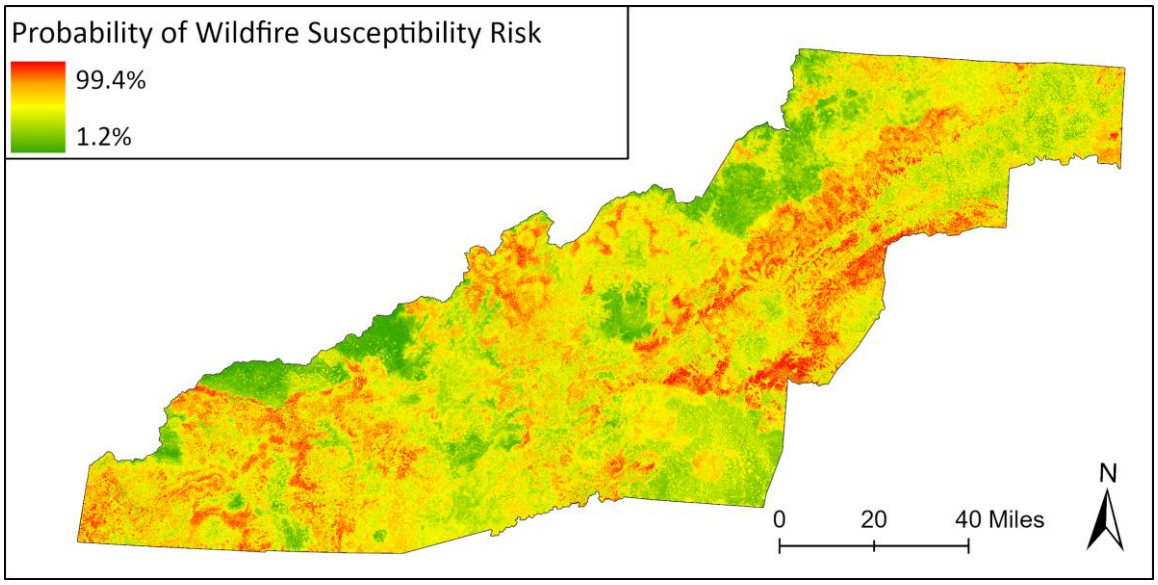

Figure 3-9 Wildfire susceptibility map in North Carolina.

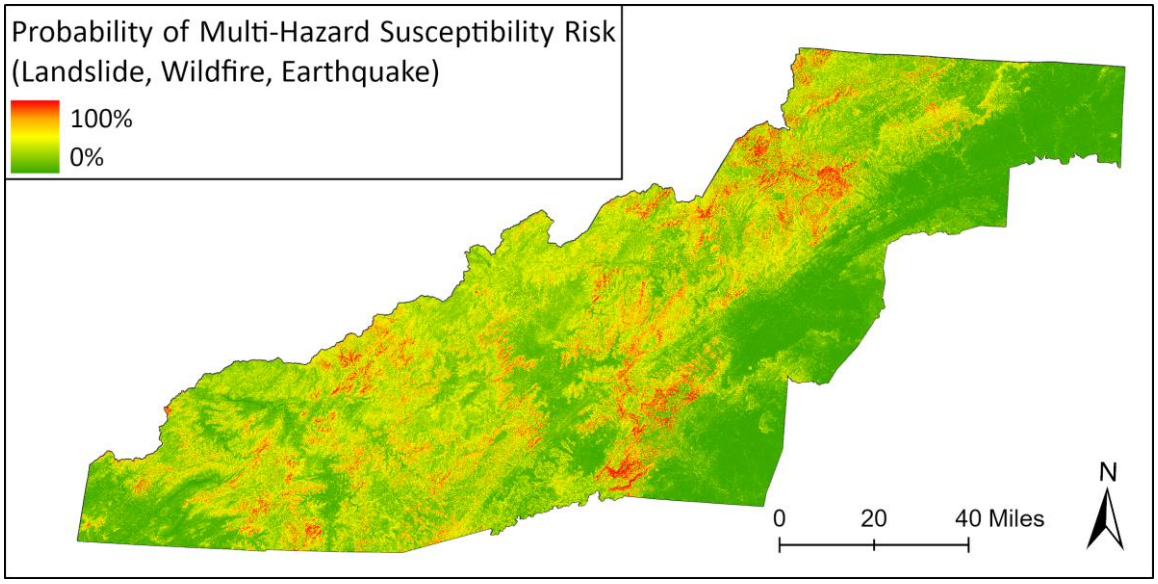

Figure 3-10 Multi-hazard (Wildfire, landslide and earthquake) susceptibility map in North Carolina.

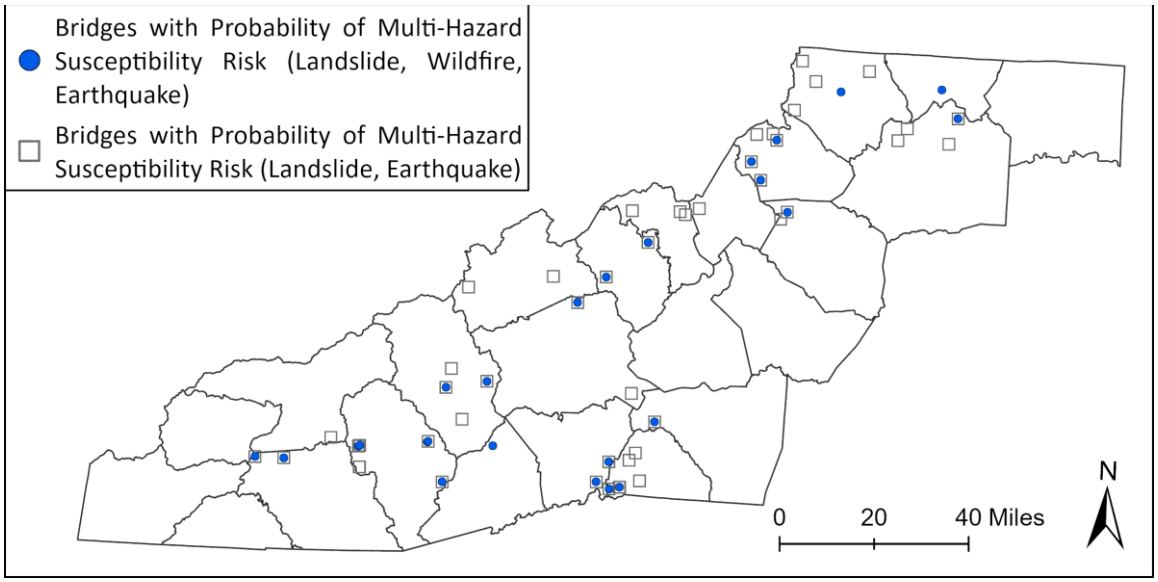

Figure 3-11 Bridges with 50% or greater probabilities of multi-hazard risks (not considering flooding) in NC's mountain area.

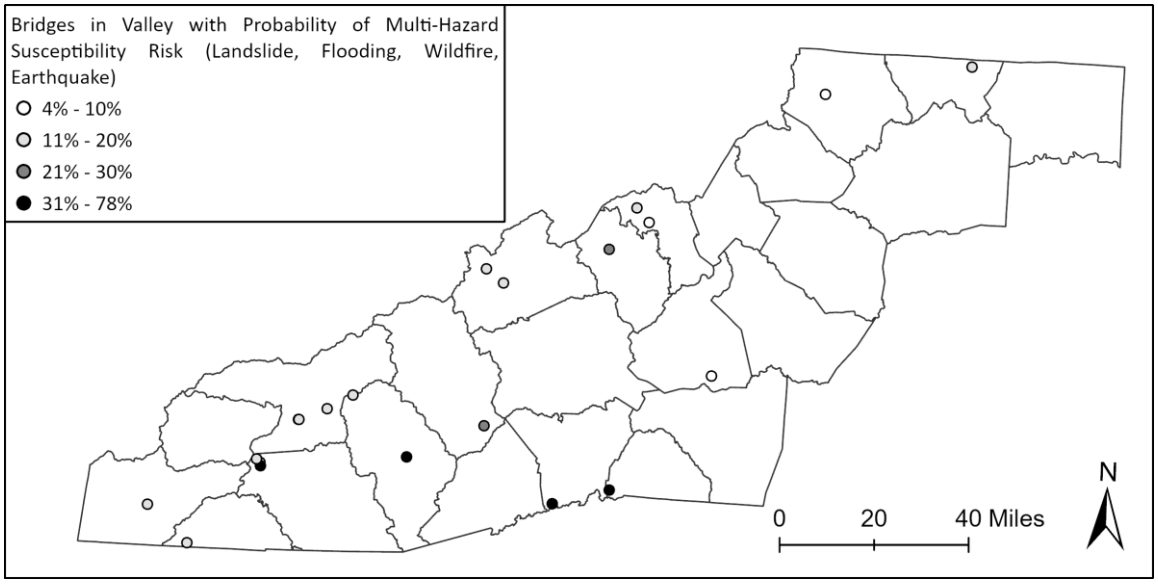

Figure 3-12 Bridges in valley under 7m above stream elevation assuming flooding potential (AFP) in NC's mountain area, indicating the potential of exposing to multi-hazard (landslide, flooding, wildfire and earthquake) dangers.

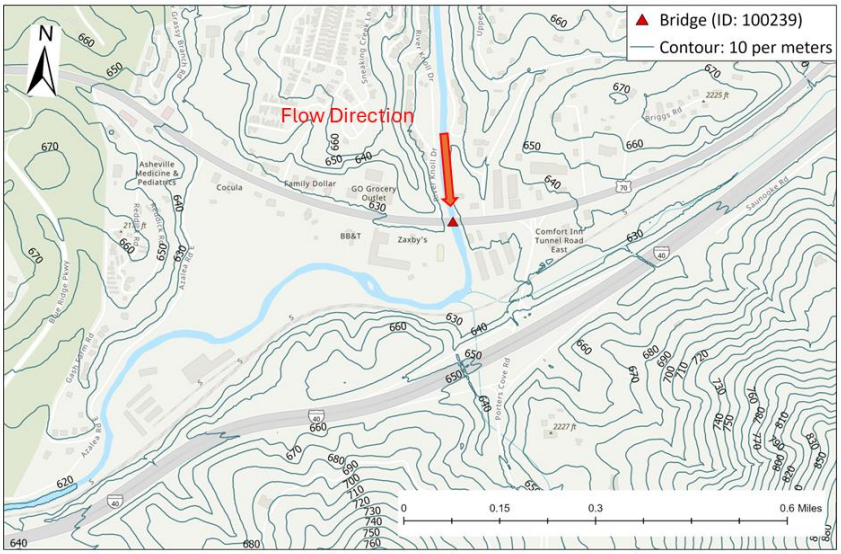

(a)

(b)

Figure 3-13 Damaged Bridge (ID:100239) after unprecedented flooding from Hurricane Helene above the Swannanoa River, Black Mountain, NC: a) Site Contour and Bridge ID100239 Location; b) Bridge (ID: 100239) showing one approach scoured from flooding and the upstream debris fall and congested river scene.

Reference

Alzubi, J., Nayyar, A., & Kumar, A. (2018). Machine Learning from Theory to Algorithms: An Overview. *Journal of Physics: Conference Series, 1142*(1), 012012. doi:10.1088/1742-6596/1142/1/012012

B., T. K. (2014). *Earthquake History of North Carolina*. Retrieved from Charlotte, Candler, and Winston-Salem, North Carolina, United States.: https://wlos.com/resources/pdf/13dbc52b-261e-4570-995f-6ebe0f745bd4-EarthquakeHistoryofNorthCarolina.pdf

Bai, S.-B., Wang, J., Lü, G.-N., Zhou, P.-G., Hou, S.-S., & Xu, S.-N. (2010). GIS-based logistic regression for landslide susceptibility mapping of the Zhongxian segment in the Three Gorges area, China. *Geomorphology, 115*(1), 23-31. doi:https://doi.org/10.1016/j.geomorph.2009.09.025

Banerjee, S., Vishwanath, B. S., & Devendiran, D. K. (2019). Multihazard resilience of highway bridges and bridge networks: A review. *Structure and Infrastructure Engineering, 15*(12), 1694-1714.

Belair, G. M., Jones, E. S., Slaughter, S. L., & Mirus, B. B. (2022). *Landslide Inventories across the United States version 2: U.S. Geological Survey data release*.

Breiman, L. (2001). Random Forests. *Machine Learning, 45*(1), 5-32. doi:10.1023/A:1010933404324

Busico, G., Giuditta, E., Kazakis, N., & Colombani, N. (2019). A Hybrid GIS and AHP Approach for Modelling Actual and Future Forest Fire Risk Under Climate Change Accounting Water Resources Attenuation Role. *Sustainability, 11*(24), 7166. Retrieved from https://www.mdpi.com/2071-1050/11/24/7166

Caldwell, H., Quinn, K. H., Meunier, J., Suhrbier, J., & Grenzeback, L. (2002). Potential impacts of climate change on freight transport. *US DOT*, 1-2.

Campbell, J. W., Vigueira, P. A., Viguiera, C. C., & Greenberg, C. H. (2018). The effects of repeated prescribed fire and thinning on bees, wasps, and other flower visitors in the understory and midstory of a temperate forest in North Carolina. *Forest Science, 64*(3), 299-306.

Chang, C., Chang, Y., Xiong, Z., Ping, X., Zhang, H., Guo, M., & Hu, Y. (2022). Model Comparisons for Predicting Grassland Fire Occurrence Probability in Inner

Mongolia Autonomous Region, China. *Natural Hazards and Earth System Sciences Discussions*, 1-25. Retrieved from https://nhess.copernicus.org/preprints/nhess-2022-72/

Chang, Z., Huang, F., Huang, J., Jiang, S.-H., Liu, Y., Meena, S. R., & Catani, F. (2023). An updating of landslide susceptibility prediction from the perspective of space and time. *Geoscience Frontiers, 14*(5), 101619. doi:https://doi.org/10.1016/j.gsf.2023.101619

Chen, W., Sun, Z., & Han, J. (2019). Landslide Susceptibility Modeling Using Integrated Ensemble Weights of Evidence with Logistic Regression and Random Forest Models. *Applied Sciences, 9*(1), 171. Retrieved from https://www.mdpi.com/2076-3417/9/1/171

Chowdhury, M. S., Rahman, M. N., Sheikh, M. S., Sayeid, M. A., Mahmud, K. H., & Hafsa, B. (2024). GIS-based landslide susceptibility mapping using logistic regression, random forest and decision and regression tree models in Chattogram District, Bangladesh. *Heliyon, 10*(1). doi:10.1016/j.heliyon.2023.e23424

Chuvieco, E., & Salas, J. (1996). Mapping the spatial distribution of forest fire danger using GIS. *International Journal of Geographical Information Systems, 10*(3), 333-345. doi:10.1080/02693799608902082

Culler, E. S., Livneh, B., Rajagopalan, B., & Tiampo, K. F. (2023). A data-driven evaluation of post-fire landslide susceptibility. *Nat. Hazards Earth Syst. Sci., 23*(4), 1631-1652. doi:10.5194/nhess-23-1631-2023

DeBano, L. F., Rice, R. M., & Conrad, C. E. (1979). Soil heating in chaparral fires: effects on soil properties, plant nutrients, erosion, and runoff. *Berkeley, CA: U.S. Department of Agriculture, Forest Service, Pacific Southwest Forest and Range Experiment Station, Res. Paper PSW-RP-145*, 21 p.

Di Napoli, M., Marsiglia, P., Di Martire, D., Ramondini, M., Ullo, S. L., & Calcaterra, D. (2020). Landslide Susceptibility Assessment of Wildfire Burnt Areas through Earth-Observation Techniques and a Machine Learning-Based Approach. *Remote Sensing, 12*(15), 2505. Retrieved from https://www.mdpi.com/2072-4292/12/15/2505

ESRI. Geomorphon Landforms (Spatial Analyst).

He, Q., Jiang, Z., Wang, M., & Liu, K. (2021). Landslide and Wildfire Susceptibility Assessment in Southeast Asia Using Ensemble Machine Learning Methods. *Remote Sensing, 13*(8), 1572. Retrieved from https://www.mdpi.com/2072-4292/13/8/1572

Highland, L. M., & Bobrowsky, P. (2008). *The landslide handbook-A guide to understanding landslides*: US Geological Survey.

Huang, F., Xiong, H., Jiang, S.-H., Yao, C., Fan, X., Catani, F., . . . Liu, K. (2024). Modelling landslide susceptibility prediction: A review and construction of semi-supervised imbalanced theory. *Earth-Science Reviews, 250*, 104700. doi:https://doi.org/10.1016/j.earscirev.2024.104700

Hurrell, J. W., & Trenberth, K. E. (1999). Global sea surface temperature analyses: Multiple problems and their implications for climate analysis, modeling, and reanalysis. *Bulletin of the American Meteorological Society, 80*(12), 2661-2678.

Iban, M. C., & Sekertekin, A. (2022). Machine learning based wildfire susceptibility mapping using remotely sensed fire data and GIS: A case study of Adana and Mersin provinces, Turkey. *Ecological Informatics, 69*, 101647. doi:https://doi.org/10.1016/j.ecoinf.2022.101647

Intini, P., Ronchi, E., Gwynne, S., & Pel, A. (2019). Traffic Modeling for Wildland–Urban Interface Fire Evacuation. *Journal of Transportation Engineering, Part A: Systems, 145*(3), 04019002. doi:doi:10.1061/JTEPBS.0000221

Jain, P., Coogan, S. C. P., Subramanian, S. G., Crowley, M., Taylor, S., & Flannigan, M. D. (2020). A review of machine learning applications in wildfire science and management. *Environmental Reviews, 28*(4), 478-505. doi:10.1139/er-2020-0019

Kameshwar, S., & Padgett, J. E. (2014). Multi-hazard risk assessment of highway bridges subjected to earthquake and hurricane hazards. *Engineering Structures, 78*, 154-166.

Kirschbaum, D., Stanley, T., & Zhou, Y. (2015). Spatial and temporal analysis of a global landslide catalog. *Geomorphology, 249*, 4-15.

Koetse, M. J., & Rietveld, P. (2009). The impact of climate change and weather on transport: An overview of empirical findings. *Transportation Research Part D: Transport and Environment, 14*(3), 205-221.

Kumari, B., & Pandey, A. C. (2020). Geo-informatics based multi-criteria decision analysis (MCDA) through analytic hierarchy process (AHP) for forest fire risk mapping in Palamau Tiger Reserve, Jharkhand state, India. *Journal of Earth System Science, 129*(1), 204. doi:10.1007/s12040-020-01461-6

Kumi-Boateng, B., Peprah, M. S., & Larbi, E. K. (2021). Prioritization of forest fire hazard risk simulation using Hybrid Grey Relativity Analysis (HGRA) and Fuzzy Analytical Hierarchy Process (FAHP) coupled with multicriteria decision analysis (MCDA) techniques–a comparative study analysis. *Geodesy and Cartography, 47*(3), 147-161.

Leuenberger, M., Parente, J., Tonini, M., Pereira, M. G., & Kanevski, M. (2018). Wildfire susceptibility mapping: Deterministic vs. stochastic approaches. *Environmental Modelling & Software, 101*, 194-203. doi:https://doi.org/10.1016/j.envsoft.2017.12.019

Li, D., Cova, T. J., & Dennison, P. E. (2019). Setting Wildfire Evacuation Triggers by Coupling Fire and Traffic Simulation Models: A Spatiotemporal GIS Approach. *Fire Technology, 55*(2), 617-642. doi:10.1007/s10694-018-0771-6

Lin, S., Chen, S.-E., Tang, W., Chavan, V., Shanmugam, N., Allan, C., & Diemer, J. (2024). Landslide Risks to Bridges in Valleys in North Carolina. *GeoHazards, 5*(1), 286-309. Retrieved from https://www.mdpi.com/2624-795X/5/1/15

Liu, S., Wang, L., Zhang, W., He, Y., & Pijush, S. (2023). A comprehensive review of machine learning-based methods in landslide susceptibility mapping. *Geological Journal, 58*(6), 2283-2301. doi:https://doi.org/10.1002/gj.4666

Martínez-Fernández, J., Chuvieco, E., & Koutsias, N. (2013). Modelling long-term fire occurrence factors in Spain by accounting for local variations with geographically weighted regression. *Nat. Hazards Earth Syst. Sci., 13*(2), 311-327. doi:10.5194/nhess-13-311-2013

Milanović, S., Marković, N., Pamučar, D., Gigović, L., Kostić, P., & Milanović, S. D. (2021). Forest Fire Probability Mapping in Eastern Serbia: Logistic Regression

versus Random Forest Method. *Forests, 12*(1), 5. Retrieved from https://www.mdpi.com/1999-4907/12/1/5

Mirus, B. B., Jones, E. S., Baum, R. L., Godt, J. W., Slaughter, S., Crawford, M. M., . . . McCoy, K. M. (2020). Landslides across the USA: occurrence, susceptibility, and data limitations. *Landslides, 17*(10), 2271-2285. doi:10.1007/s10346-020-01424-4

Moayedi, H., & Khasmakhi, M. A. S. A. (2023). Wildfire susceptibility mapping using two empowered machine learning algorithms. *Stochastic Environmental Research and Risk Assessment, 37*(1), 49-72. doi:10.1007/s00477-022-02273-4

Nasr, A., Björnsson, I., Honfi, D., Larsson Ivanov, O., Johansson, J., & Kjellström, E. (2021). A review of the potential impacts of climate change on the safety and performance of bridges. *Sustainable and Resilient Infrastructure, 6*(3-4), 192-212. doi:10.1080/23789689.2019.1593003

NCDEQ. (2022). *Geologic Faults*. Retrieved from: https://data-nconemap.opendata.arcgis.com/datasets/nconemap::geologic-faults/explore?location=35.380206%2C-80.335448%2C7.97

NCDHHS. (2024). Hurricane Helene Storm Related Fatalities. *Hurricane Helene Recovery Resources.* Retrieved from https://www.ncdhhs.gov/assistance/hurricane-helene-recovery-resources/hurricane-helene-storm-related-fatalities

NCDOT. (2008). DriveNC/TIMS Incidents data. Retrieved from https://drivenc.gov/?ref=share&type=state&layers=congestion&pins=incidents_planned-road-work,incidents_other-incidents,roads_interstate,roads_us,roads_nc

NCFS. (2024). *Historical Wildfire Information*. Retrieved from: https://www.ncforestservice.gov/fire_control/wildfire_statistics.htm

Nhongo, E. J. S., Fontana, D. C., Guasselli, L. A., & Bremm, C. (2019). Probabilistic modelling of wildfire occurrence based on logistic regression, Niassa Reserve, Mozambique. *Geomatics, Natural Hazards and Risk, 10*(1), 1772-1792. doi:10.1080/19475705.2019.1615559

Nowicki Jessee, M., Hamburger, M. W., Allstadt, K., Wald, D. J., Robeson, S. M., Tanyas, H., . . . Thompson, E. M. (2018). A global empirical model for near-real-time assessment of seismically induced landslides. *Journal of Geophysical Research: Earth Surface, 123*(8), 1835-1859.

Ozturk, D., & Uzel-Gunini, N. (2022). Investigation of the effects of hybrid modeling approaches, factor standardization, and categorical mapping on the performance of landslide susceptibility mapping in Van, Turkey. *Natural Hazards*. doi:10.1007/s11069-022-05480-y

Palu, S., & Mahmoud, H. (2019). Impact of climate change on the integrity of the superstructure of deteriorated US bridges. *Plos one, 14*(10), e0223307.

Pourghasemi, H. R., Pouyan, S., Bordbar, M., Golkar, F., & Clague, J. J. (2023). Flood, landslides, forest fire, and earthquake susceptibility maps using machine learning techniques and their combination. *Natural Hazards, 116*(3), 3797-3816.

Pourghasemi, H. R., Teimoori Yansari, Z., Panagos, P., & Pradhan, B. (2018). Analysis and evaluation of landslide susceptibility: a review on articles published during 2005–2016 (periods of 2005–2012 and 2013–2016). *Arabian Journal of Geosciences, 11*(9), 193. doi:10.1007/s12517-018-3531-5

Quesada-Román, A. (2021). Landslide risk index map at the municipal scale for Costa Rica. *International Journal of Disaster Risk Reduction, 56*, 102144.

Regmi, N. R., Giardino, J. R., McDonald, E. V., & Vitek, J. D. (2014). A comparison of logistic regression-based models of susceptibility to landslides in western Colorado, USA. *Landslides, 11*(2), 247-262. doi:10.1007/s10346-012-0380-2

Rengers, F. K., McGuire, L. A., Oakley, N. S., Kean, J. W., Staley, D. M., & Tang, H. (2020). Landslides after wildfire: initiation, magnitude, and mobility. *Landslides, 17*(11), 2631-2641. doi:10.1007/s10346-020-01506-3

Rossetti, M. A. (2002). *Potential impacts of climate change on railroads.* Paper presented at the The Potential Impacts of Climate Change on Transportation: Workshop Summary.

Schulz, A., Zia, A., & Koliba, C. (2017). Adapting bridge infrastructure to climate change: institutionalizing resilience in intergovernmental transportation planning processes in the Northeastern USA. *Mitigation and Adaptation Strategies for Global Change, 22*(1), 175-198. doi:10.1007/s11027-015-9672-x

Sengupta, A., & Nath, S. K. (2024). Landslide Susceptibility and Risk Mapping in the Tectonic Ensemble Comprising of Eastern Himalayan Zone, Northeast India and

Bhutan using Logistic Regression and Random Forest Techniques. *Journal of the Geological Society of India, 100*(2), 168-180. doi:10.17491/jgsi/2024/173817

Short, K. C. (2021). Spatial wildfire occurrence data for the United States, 1992-2018 [FPA_FOD_20210617]. 5th Edition (Publication no. https://doi.org/10.2737/RDS-2013-0009.5). Retrieved 07/05/2022

Staff, S. S. (2003). *Soil Survey Geographic (SSURGO) Database for Soil Survey Area, State*. Retrieved from: https://websoilsurvey.nrcs.usda.gov/app/WebSoilSurvey.aspx

Staley, D. M., Negri, J. A., Kean, J. W., Laber, J. L., Tillery, A. C., & Youberg, A. M. (2016). *Updated logistic regression equations for the calculation of post-fire debris-flow likelihood in the western United States* (2016-1106). Retrieved from Reston, VA: https://pubs.usgs.gov/publication/ofr20161106

State, N. C. S. o. (2024). Geography. Retrieved from https://www.sosnc.gov/divisions/publications/kids_page_geography

Taylor, S., Parminter, J., & Thandi, G. (2005). Logistic regression models of wildfire probability in British Columbia. *Natural Resources Canada, Canadian Forest Service, Pacific Forestry Centre, Victoria, BC Annual Technical Report Supplement, 2*. Retrieved from https://www.for.gov.bc.ca/hfd/library/fia/2005/FSP_Y051233c.pdf

USGS. (2023a). *1 Arc-second Digital Elevation Models (DEMs) - USGS National Map 3DEP Downloadable Data Collection: U.S. Geological Survey*. Retrieved from: https://www.sciencebase.gov/catalog/item/4f70aac4e4b058caae3f8de7

USGS. (2023b). *USGS National Hydrography Dataset Best Resolution (NHD) - North Carolina (published 20230305) Shapefile: U.S. Geological Survey*. Retrieved from: https://www.sciencebase.gov/catalog/item/61f8b8aad34e622189c328b8

Wang, X., Wang, X., Zhang, X., Wang, L., Guo, H., & Li, D. (2023). Near real-time spatial prediction of earthquake-induced landslides: A novel interpretable self-supervised learning method. *International Journal of Digital Earth, 16*(1), 1885-1906. doi:10.1080/17538947.2023.2216029

Wubalem, A., & Meten, M. (2020). Landslide susceptibility mapping using information value and logistic regression models in Goncha Siso Eneses area, northwestern Ethiopia. *SN Applied Sciences, 2*(5), 807. doi:10.1007/s42452-020-2563-0

Zhang, Y., Lim, S., & Sharples, J. J. (2016). Modelling spatial patterns of wildfire occurrence in South-Eastern Australia. *Geomatics, Natural Hazards and Risk, 7*(6), 1800-1815. doi:10.1080/19475705.2016.1155501

Appendix B

No	Bridge ID	Longitude	Latitude	AFP	Probability of Landslide Occurrence (Earthquake)	Probability of Landslide Occurrence (Wildfire and Earthquake)
1	550228	-83.6690064	35.26770495	0.67	0.17	0.19
2	860024	-83.31964644	35.47677134	1.02	0.25	0.12
3	990034	-82.37624068	35.95286913	1.05	0.27	0.22
4	860020	-83.41412095	35.43162131	1.73	0.19	0.14
5	430010	-82.82258403	35.39932611	1.79	0.19	0.29
6	600084	-82.27706725	36.08360385	1.89	0.18	0.12
7	440161	-82.55773367	35.1673545	2.59	0.24	0.35
8	580017	-81.97599594	35.57528782	2.62	0.03	0.07
9	550229	-83.6553343	35.25717623	2.82	0.16	0.15
10	860137	-83.51710646	35.39425632	2.85	0.13	0.16
11	490080	-83.10854232	35.29399205	3.40	0.25	0.34
12	210057	-83.91391948	34.9993788	3.90	0.17	0.20
13	860104	-83.51851741	35.39461143	3.92	0.08	0.04
14	550230	-83.65351494	35.24695009	4.24	0.32	0.43
15	560138	-82.77026923	35.83929582	4.62	0.19	0.15
16	600026	-82.22878565	36.04036643	5.28	0.10	0.08
17	020021	-81.02105795	36.54282685	6.20	0.14	0.11
18	190159	-84.06817913	35.11164097	6.23	0.16	0.15
19	740002	-82.34673092	35.21555685	6.61	0.92	0.78
20	040045	-81.57578897	36.44914354	6.73	0.10	0.09
21	560122	-82.8361671	35.87993609	6.74	0.16	0.19

Chapter 4: Landslides and Bridge Damages in Western North Carolina After Hurricane Helene

4.1 Abstract

Hurricane Helene, a Category 4 storm at landfall in 2024, caused extensive damage across the Southeastern United States, with sustained winds reaching 220 km/h. Helene resulted in over $9.8 billion in economic losses and claimed more than 200 lives, making it one of the most destructive hurricanes in recent history. Hurricane Helene was unique in its rapid intensification and its sustained strength as it reached the western Carolina mountains, bringing prolonged heavy rainfall that triggered multiple hazards, including widespread bridge failures. This paper reports ground observations and lessons learned from the structural damage associated with the hurricane event, highlighting the need to evaluate bridge approach designs for overtopped bridges and debris flows during extreme flooding.

KEYWORDS: Hurricane Maria, Puerto Rico, Power Grid, Physical Resilience, Spatial Correlation Analysis

4.2 Introduction

Atlantic tropical storms often develop within the North Atlantic basin near the Caribbean Sea, where limited open water and environmental conditions can hinder their intensification to hurricane strength. As a result, the eventual upgrading to hurricane classification is not as frequent as the Pacific tropical storms. Occasionally, intense storms that become name-bearing hurricanes form in the open Atlantic Ocean starting from near the western coast of Africa. Figure 4-1 shows the historical tropical storms and their paths over a 40-year period. Hurricane Helene, which occurred from September 25-28, 2024, is unique among storms originating in the Caribbean Sea because of its short period to intensify to a Category 4 hurricane. As a result, the storm impacted a significant portion of the continental US and became one of the most severe hurricanes in recent US history. As a contrast, both Hurricanes Irma and Maria of 2017 had their genesis from the west African coast (August 21 for Irma and September 12 for Maria) and they became a major storm several days later (11 days for Irma and 6 days for Maria).

Helene started on September 22, 2024, as a tropical low-pressure disturbance within the western Caribbean Sea (Reinhardt 2024). The low-pressure zone started around September 17, 2024 (Blake 2024) and by September 23 it became a tropical depression and was named Helene. By September 24th, Helene had an increased wind speed of 130 km/h and was officially named a hurricane. The hurricane traveled within the Gulf on a north-bound path and within two days had become a category 4 hurricane with a maximum sustained wind speed of 220 km/h and a minimum barometric pressure of 938 millibars (Hagan 2024). On September 26, Helene made landfall southwest of Perry, Florida (from Apalachee Bay to Waccasassa Bay). Helene was downgraded to a post-tropical cyclone

after it travelled deeper inland traversing through Georgia and eventually reaching the western mountain region of North Carolina. In western North Carolina alone, Helene resulted in more than 100 deaths, caused historic flooding, landslides, and destroyed infrastructure, including numerous bridges and roads throughout western North Carolina.

Specific to landslides, past tropical storm impacts including Hurricanes Opal (1995), Frances (2004), and Ivan (2004), have triggered similar landslides to western North Carolina but to smaller extents. Fuhrmann et al. (2008) reported that synoptic and cyclonic rainfalls for the Appalachian Mountain region can be as much as 593 mm for a two-day event and can continue to trigger landslides 4 to 90 days after the event. Lyons et al. (2014) and Wooten et al. (2016) stated that debris flows, which are often caused by intense periods of rainfall, are the most prevalent landslide type in the southern Appalachians. In the southern Appalachian Highlands, rainfall from cyclonic storms has triggered hundreds to thousands of debris flows on at least six separate occasions over the past century (Wooten et al. 2016).

Post-hurricane disaster structural assessments are critical for hazard characterizations and lessons learned can help improve regional resilience via improved structural designs (Chen et al. 2016). However, not all hurricanes resulted in the same hazard risks: Some brought in torrential rains, while others resulted in significant storm surges and wind forces (Peraza et al. 2014, Joyce et al. 2019). The goal of this paper is to identify critical landslide and flooding hazards brought about by Hurricane Helene in western North Carolina and report preliminary observations regarding damage to infrastructure, in particular, bridge structures.

4.3 Hurricane Helene: Genesis and History

Figure 4-2 depicts the path of Hurricane Helene (Category 1, September 12 to 14, 2024) showing both wind intensity and central pressure (in mb). The genesis of Helene is very similar to Hurricane Humberto (2007), both were formed as local depressions in the Gulf of Mexico and migrated northward into continental inland. Humberto of 2007 was a Category 1 storm and was formed quickly and dissipated quickly (Blake 2007). To explain the rapid intensification of Humberto, Sippel and Zhang (2010) combined ensemble Kalman filter analyses and short-range ensemble forecasts. Their results suggested that the heavy moisture laden tropical depression along with a relatively unstable convection may cause the rapid intensification of the hurricane. Emanuel (1986) and Rontunno and Emanuel (1987) stressed that a genesis environment with a deep layer of moisture with relative humidity exceeding 85% is a critical ingredient for tropical cyclones. Similarly, it took Helene three days from the low-pressure trough intensification to making landfall in the Big Bend area of Florida as a powerful Category 4 storm on Wednesday, September 25, 2024 (at 8:15 UTC). Once making landfall, Helene traveled rapidly through Florida, Georgia and reached Tennessee and Carolinas before dissipating in Virginia. Other than torrential rain (some parts in North Carolina received more than 62 cm rain, (US Department of Commerce 2024)), Helene also traveled with sustained gusts of 110 km/h.

The impact of Hurricane Helene in North Carolina was most evident in the western mountain region including Buncombe, Henderson, Yancey, Haywood, Rutherford and Madison counties, and municipals including Asheville, Chimney Rock and Black Mountain, etc. Examples of the types of damage observed after Helene are shown in Figure

4-3 to Figure 4-6. Observations on the damages to the built environment in the mountains can be summarized as:

1) With a recorded maximum wind speed of 70 km/h, a significant number of trees were down. Figure 4-3 shows several trees were blown down by strong wind.
2) With heavy rains, significant surficial erosions including landslides occurred. Figure 4-4 shows different size landslides triggered by the hurricane.
3) Some parts of the valley regions such as Asheville valley experienced flooding resulting in mud flows and accumulation of debris. Figure 4-5 shows example of severe mud and debris flows that entrapped vehicles and damaged buildings.
4) Due to unprecedented river flooding, several bridges were damaged. Figure 4-6 shows scouring damaged buildings and bridges.

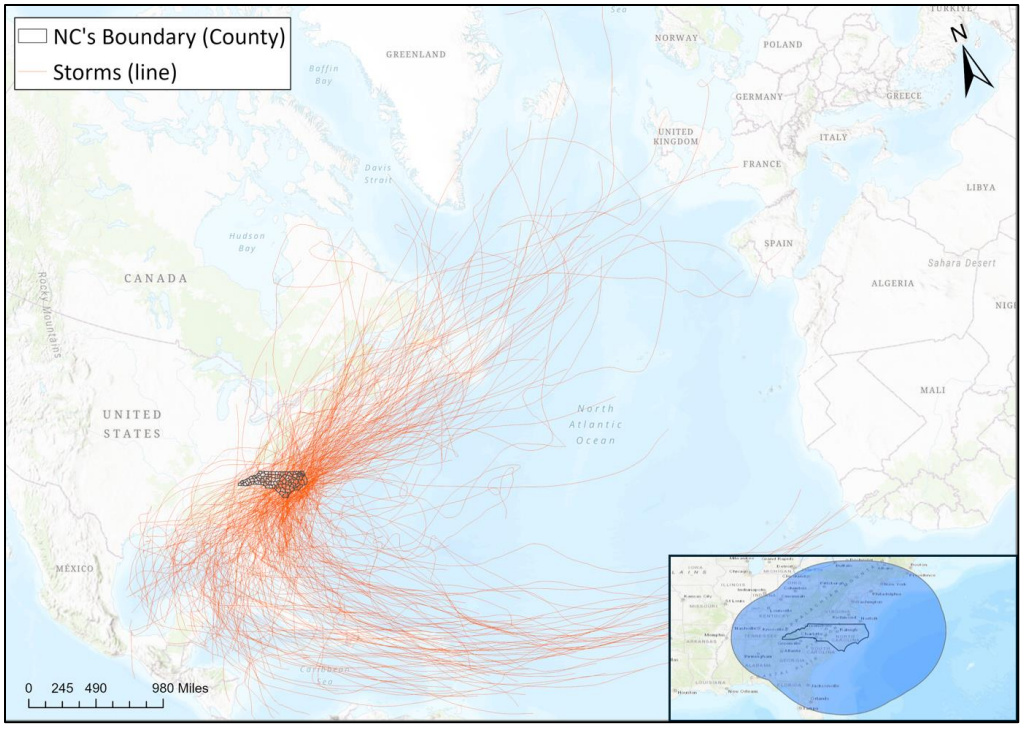

Figure 4-1 Seasonal hurricanes that either entered North Carolina or reached within 400 miles of the state boundary during the period of 1981-2021.

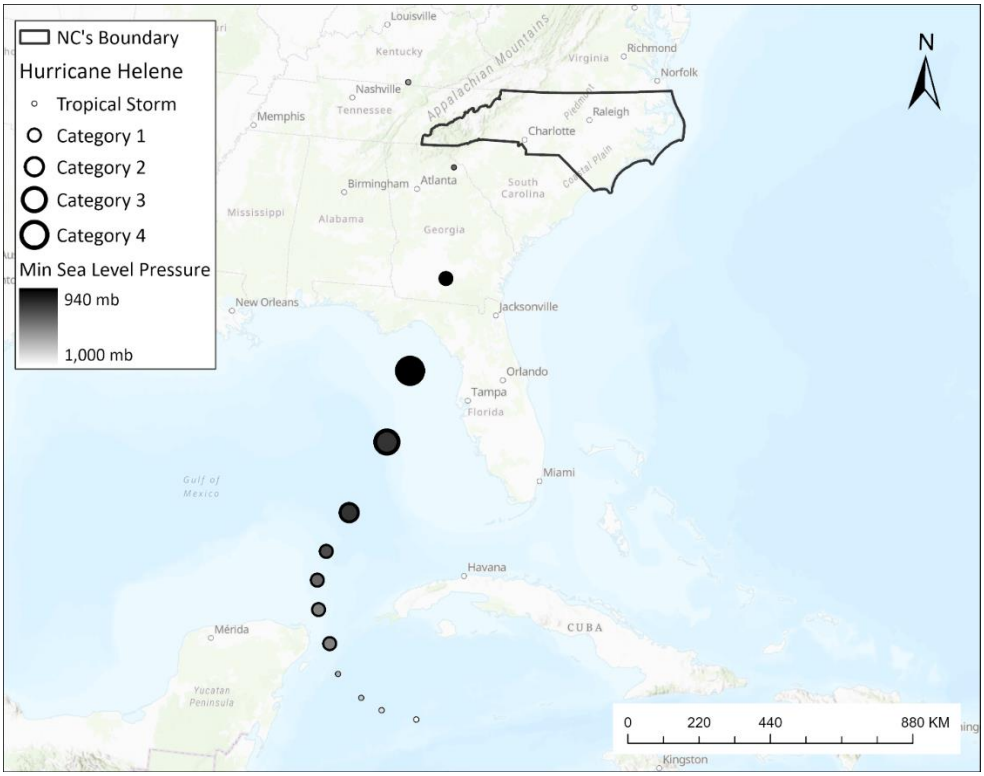

Figure 4-2 Path of Hurricane Helene (the hurricane reached Category 4 upon landfall near Perry, Florida).

Figure 4-3 Fallen trees indicate strong wind forces from Hurricane Helene. (Photo credits: Shenen Chen and Sophia Lin)

Figure 4-4 Landslides of varied sizes triggered by Hurricane Helene. (Photo Credit: Shenen Chen, Sophia Lin)

Figure 4-5 Evidence of sustained flooding and rapid mud flows at the Asheville basin including Asheville watershed. (Photo Credits: Shenen Chen and Sophia Lin)

Figure 4-6 Scour (red circle) of building and bridge foundations in Asheville region. (Photo Credits: Shenen Chen and Sophia Lin)

4.4 Observations on Landslides

Landslides pose significant hazards in mountainous areas impacted by hurricanes. Debris flows are the most common form of landsliding in western North Carolina (Wooten et al. 2016). Debris flows are fast-moving mixtures of water, saturated soil, rock, and organic material that rapidly traverse downslope, often triggered by intense rainfall. Further, debris flows, and other forms of landslides, can block river basins and lowlands, which can lead to severe flooding and mudflows (Bessette-Kirton et al. 2019). For example, Ramos-Scharron et al. (2021) reported more than 436,330 megagrams of sediments were deposited at a watershed in Puerto Rico during Hurricane Maria. Such mass transport plus the downing of large trees resulted in unprecedented flooding in the mountain regions.

Debris flows are influenced by a combination of geologic, geomorphic, and meteorological conditions and are prone to develop in high-relief regions such as the mountains of western North Carolina. High-relief landscapes, especially those with intersecting bedrock discontinuities and differential weathering, often create convergent landforms such as colluvial hollows where debris flows are likely to initiate (Wooten et al., 2016). These colluvial hollows often consist of loose unconsolidated sediments deposited via mass wasting. Underlying these colluvial soils, the site geology in the western mountain region is described as "*metasedimentary slate, phyllite, marble, schist, and gneiss, and metaigneous amphibolite and greenstone (metabasalt), granitic gneiss, and relatively unmetamorphosed granitic rock*" (Wooten et al. 2016 page 210). Many of these geologies (e.g., phyllite, slate, gneiss, schist) exhibit foliation and discontinuity planes, which serve as not only planes of weakness, but also preferential pathways for water migration to increase saturation in soils. Because debris flows are shallow failures, forest cover also

plays an important role in stabilizing hillslopes. Debris flows often occur where there is reduced hillside reinforcement from plant roots, whether due to lack of vegetation, anthropogenic changes, weakened root systems, or lack of connection between roots and underlying bedrock. Debris flows initiate when the forces acting downslope surpass the slope material's ability to resist movement (i.e., shear strength), a capacity determined by the friction and cohesion within the soil, rock fragments, and roots present. Numerous geological factors – such as slope, landform characteristics (which affect rainfall distribution, runoff, and water absorption in convergent areas), bedrock structure, soil properties, and vegetation/landcover – interact with meteorological factors, particularly rainfall, to initiate debris flows. Excessive rainfall is the primary trigger as it increases the driving force due to its weight while also reducing resistance by raising pore water pressure, which reduces the soil's shear strength.

Heavy rainfall in western North Carolina is typically the result of airmass moving and cooling over the high relief area, producing excess precipitation. Prior to Hurricane Helene, heavy rainfall events have caused significant flooding and landslides in western North Carolina and the surrounding region in the past, including 10 times from 1924 to 2013, giving an average frequency of about 9 years (Wooten et al. 2016). A common factor amongst the worst of these past storms was heavy rainfall from a hurricane in addition to multiple storms occurring within a short period of time. In 1916, 1940, and 2004, multiple storms, at least one of which was a hurricane, occurred within days to weeks of each other causing significant rainfall on already saturated soil, generating widespread flooding and hundreds to thousands of landslides. Hurricane Helene was similar to these past events. Helene hit western North Carolina days after a low-pressure system dropped up to 25.4 cm

of rain in some locations of western North Carolina (e.g., Asheville Regional Airport). The already waterlogged region experienced devastation as significant additional rainfall occurred during Helene where some areas like Asheville, North Carolina received an additional 35.6 cm of rain (National Weather Service, 2024). Like the past multi-storm events to impact western North Carolina, Hurricane Helene and its preceding storm produced thousands of landslides. At the time of writing this article, the USGS Helene landslide dashboard (2024) reports 1,984 landslides (including landslides reported in Tennessee) that are initially identified as debris flows, landslides, and unknowns. Of the 1,984 landslides, 1,060 have currently been flagged as impacting rivers, roads, and structures, indicating the vast impact of the event. The following describes the landslide observations and their impacts on bridges made by the authors in the weeks following hurricane Helene.

Figure 4-7 shows a large-scale mud (debris) slide with a base as wide as 33 m in Saluda, NC. The debris slide occurred along a cut-slope along Pearson Falls Road where the previously vegetated slope failed without visible surface of rupture. Several similar localized debris slides were identified in the area with some extending into Joels Creek, which is on the downhill side of the road. These slides mobilized a significant amount of sediment. For example, Figure 4-8 shows the before and after images of Pearson Falls Road leading up to a resident building. After hurricane Helene, landslide debris completely covered Pearson Falls Road for approximately 50 meters. Figure 4-9 shows landslide debris surrounding the Saluda wastewater treatment plant along Joels Creek after Helene compared to what it looked like in September 2023. In addition to landslides, scours were also observed in the road to the wastewater treatment plant.

Figure 4-10 shows a large debris flow on highway 176 near Saluda Bear Creek originating from a slope with an incline of approximately 75^{o}. The 40 m tall slide caused debris to cover the highway, deformed the highway's guardrails (some portions dangling mid-air above the slope below), and emptied into the creek below. A mile upstream from the debris flow in Figure 4-10, near Melrose Falls, a large debris flow occurred between Highway 176 (slope top) and the Pearson Falls Road (Slope bottom) (Figure 4-11). Notably, Figure 4-11 shows the debris flow caused a portion of Highway 176 to be undermined while also covering Pearson Falls Road on its way to emptying into the stream below. The debris flow resulted in multiple circular slip surfaces that can be identified.

Figure 4-12 shows multiple slope failures occurring along both sides of a small stream. It is unclear whether these failures originated due to erosion from highwater flooding, landsliding, or a combination of both. The narrow passageway between the two banks and the large amount of rainfall that occurred over a short period of time indicates highwater flooding may have occurred in this area. The failure in the foreground of Figure 4-12 appears to be a road embankment that has been eroded away by high flood waters while the failure on the other side of the stream appears to be a debris flow, potentially made less stable by erosion at the toe of the slope near the riverbed. This dual phenomenon of scour and landsliding results in complex slope movements. Several failure modes are closely associated with colluvial movements caused by river erosion, as described by Cebulski (2022). Cebulski referred to these debris movements as 'near-channel landslides,' which can be triggered by both fluvial erosion and high flood flows. Yuan et al. (2018) studied loess landslides induced by river erosion and found that erosion along the riverbank can alter the internal stresses within the slope, potentially leading to destabilization.

Figure 4-13 and Figure 4-14 show a landslide occurring at a previously repaired road embankment along Pearson Falls Road, which runs parallel to Joels Creek below. The embankment was stabilized in 2023 using a soil nail wall (Lin et al. 2024). However, after Hurricane Helene, landslides still occurred at this repaired embankment. In some areas, the concrete grout and the soil it held was eroded away and defeated the original slope reinforcement. For example, Figure 4-13 shows scouring behind a nearly vertical wall and Figure 4-14 shows another wall with a section scoured away.

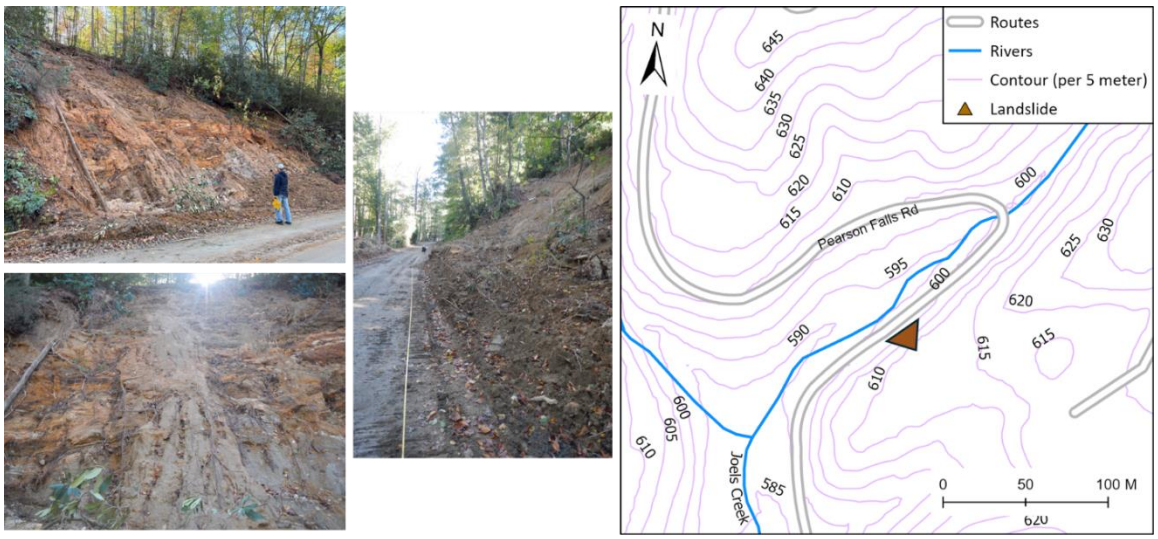

Figure 4-7 A large mud slide with a base width of 33 m in Saluda, NC. (Photo Credits: Sophia Lin and Shenen Chen)

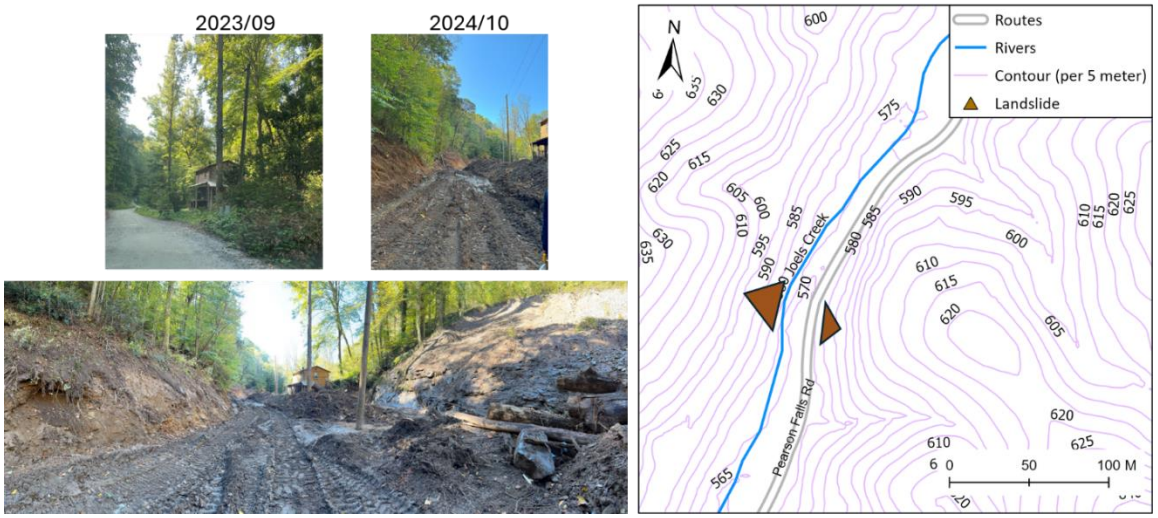

Figure 4-8 Transformation of a roadway due to massive landslide and mudflow along Pearson's Fall Road in Saluda, NC. (Photo Credits: Sophia Lin and Shenen Chen)

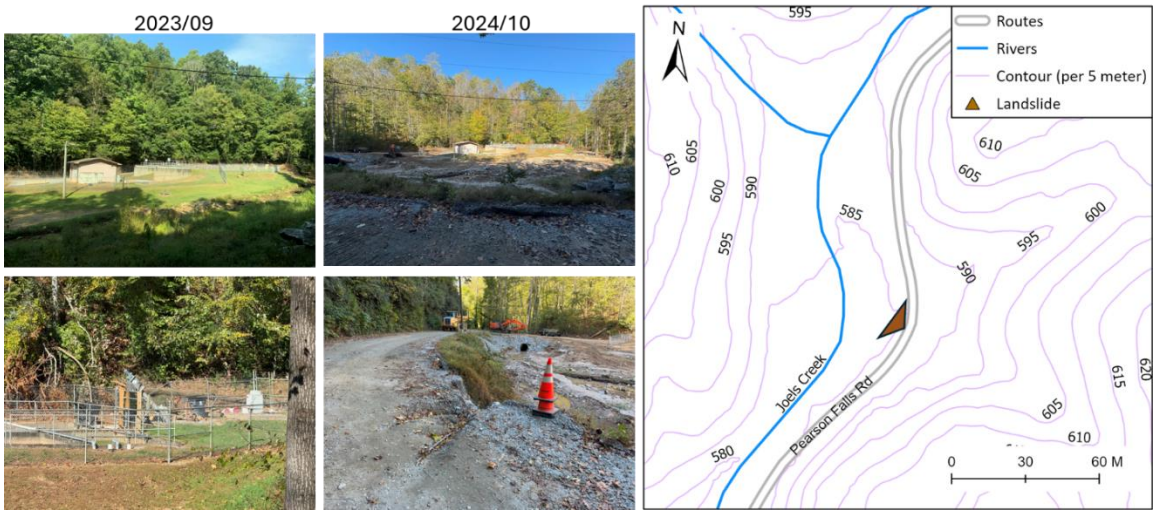

Figure 4-9 Landslide and scour damage to the Saluda wastewater treatment plant in Saluda, NC. (Photo Credits: Sophia Lin and Shenen Chen)

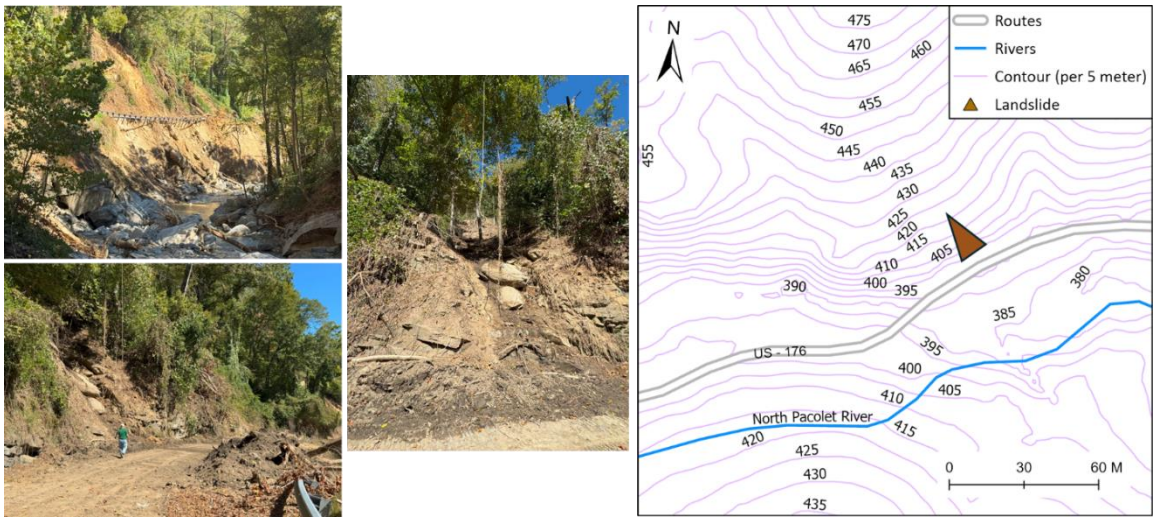

Figure 4-10 A large debris flow consisting of water, soil, rocks, and trees crossing Highway 176. (Photo Credits: Sophia Lin and Shenen Chen)

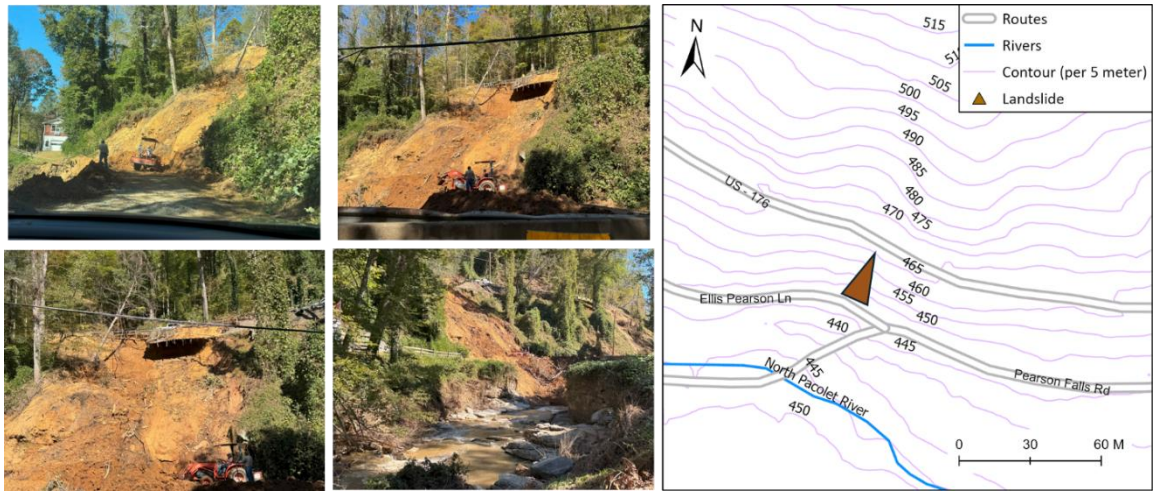

Figure 4-11 Large debris flows between Highway 176 (road above) and the Pearson Falls Road (road below) next to the North Pacolet River, Melrose Falls, NC. (Photo Credits: Sophia Lin and Shenen Chen)

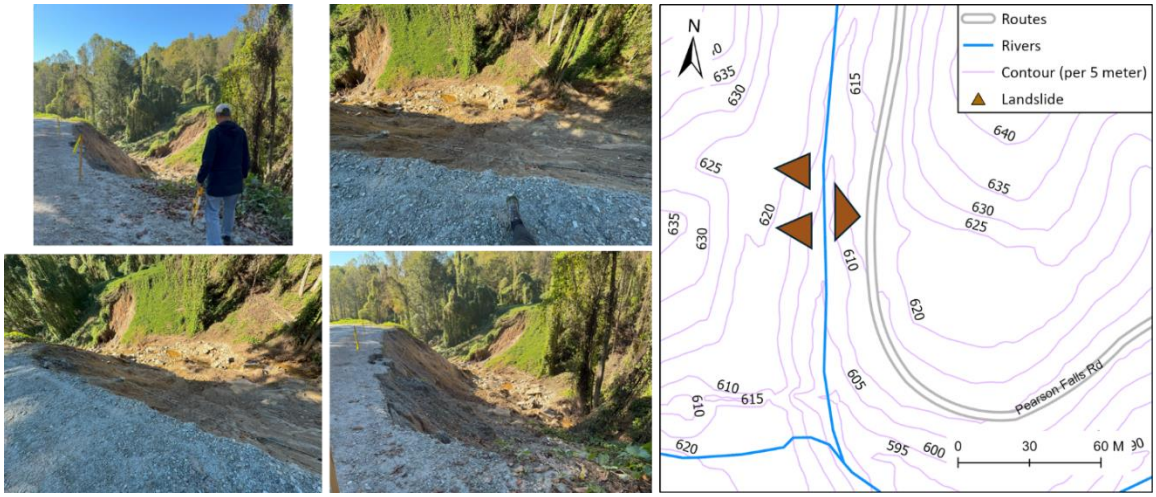

Figure 4-12 Multiple slope failures on both sides of a small stream. (Photo Credits: Sophia Lin and Shenen Chen)

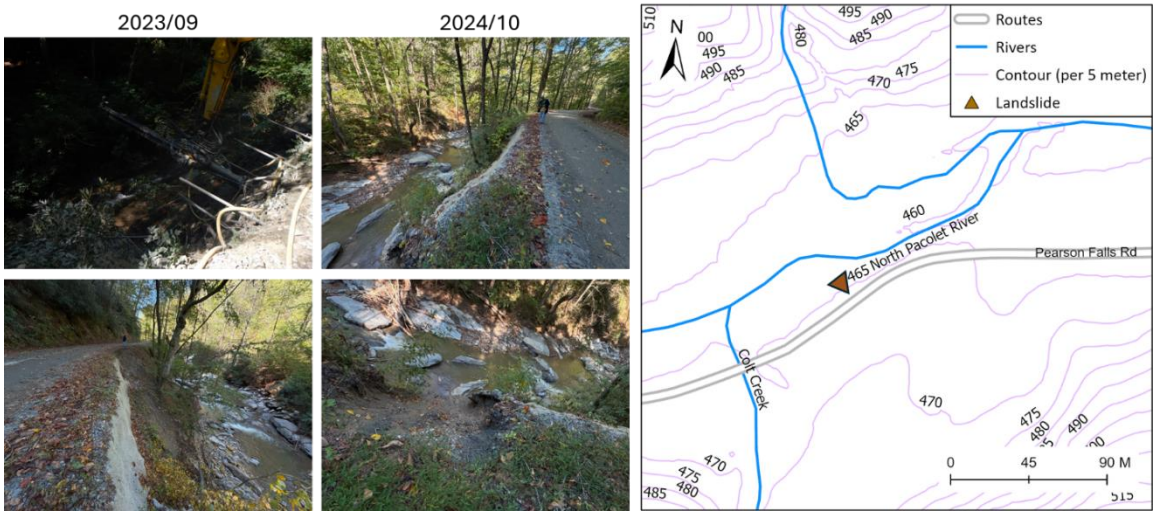

Figure 4-13 Landslide at a previously grouted and repaired slope. (Photo Credits: Sophia Lin and Shenen Chen)

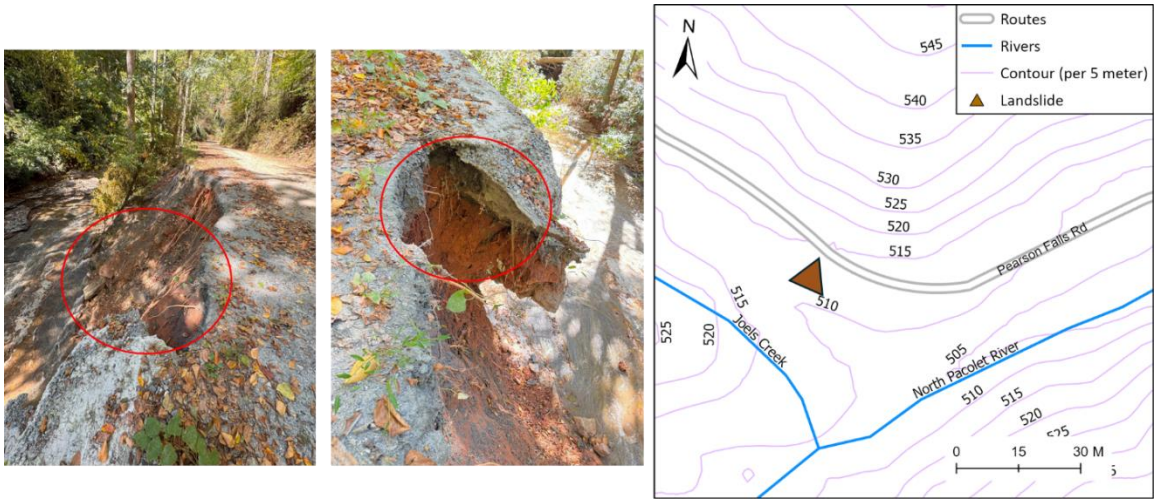

Figure 4-14 Mass loss behind the grout wall after landslide. (Photo Credits: Sophia Lin and Shenen Chen)

4.5 Observations on Bridge Structure Damages

The debris flow resulted in unprecedented highwater flooding and damaged several bridges in the mountain regions – North Carolina Department of Transportation (NCDOT) reported more than 654 bridges that are either washed-out, damaged, or closed due to debris accumulation (NCDOT 2024). Figure 4-15 shows bridge ID: 740037 on Highway 176 (over a branch of the North Pacolet River) before and after Hurricane Helene. The bridge experienced loss of bridge approach support materials due to localized debris flow, despite no damage to the bridge piers. Lin et al. (2024) predicted that the steel girder bridge has only a 10% to 20% chance of experiencing landslides. But the landslides (at least two from upstream within 30 m from the bridge) in the surrounding resulted in significant debris such as tree trunks and loose rocks that raised the river water. The high and rapid floodwater from the hurricane event, as indicated by the loss of graffiti between the before and after pictures, appear to have caused scouring of the bridge approach embankment slopes in addition to mass loss of the bridge approach itself, but landslides do not appear prevalent at the bridge location. While no major landslides seem to have occurred at this site, some shallow slides or slope erosion due to rainfall may have contributed to the damage to the approach. The primary cause, however, appears to be scour from the high floodwaters. Additionally, debris carried by floodwater from upstream likely worsened flooding around the bridge by blocking water flow. Although the bridge remains safe for crossing, repairing the approach is both necessary and critical.

Figure 4-16 shows bridge ID: 100239 on Highway 70 (also identified as Tunnel Road), which sustained significant damage in Asheville, NC. The four-lane highway bridge resides spans the Swannanoa River and experienced severe mud flows and flooding as

shown in Figure 4-17. Figure 4-17 also depicts several damaged residences, including some downstream residential structures completely buried in mud. Similar to bridge ID: 740037 shown in Figure 4-15, the main body of the bridge remained intact, however, one of the bridge approaches suffered substantial scouring. This scouring resulted in more than 5 meters of mass loss beneath the concrete approach slab. In some areas, sections of the slabs have broken off from the approach, leaving a ½ meter wide gap between the approach and the bridge deck. Mud and debris on the bridge deck indicate that floodwaters likely reached the bridge deck.

Several bridges experienced similar damage modes as shown in Figure 4-15 and Figure 4-16, with bridge approaches and wingwalls affected by highwater flooding and mud and debris flows. For example, scouring is the most likely cause of mass loss at the abutment of the Tunnel Road bridge (Figure 4-16).

However, scouring is not the only failure mode observed. Figure 4-18 shows the approach of a bridge ID: 740005 on I-176 (Main Street) in downtown Saluda, which failed due to a landslide occurring in the road embankment. The bridge is not over water but over a railroad track. The landslide did not impact the railroad tracks passing beneath the bridge, but there are multiple rail transportation networks that were affected by hurricane Helene in western North Carolina. In the case of bridge ID: 740005, the embankment failure led to significant soil loss behind the bridge's wing wall, compromising the road embankments support. Although the bridge remains drivable, it requires repairs, as additional soil loss behind the wingwall is likely if no action is taken.

Figure 4-15 Bridge (ID:740027) on highway 176 experienced support mass loss at the bridge approach after Hurricane Helene. (Photo Credits: Sophia Lin and Shenen Chen)

Figure 4-16 The Tunnel Road Bridge (ID:100239) over Swannanoa River in Asheville, NC, experienced support mass loss at the bridge approach after Hurricane Helene. (Photo Credits: Sophia Lin and Shenen Chen)

Figure 4-17 Massive debris filled floodwater resulted in mud caked cars and lots and damaged buildings and constricted the Swannanoa River, Asheville, NC. (Photo Credits: Sophia Lin and Shenen Chen)

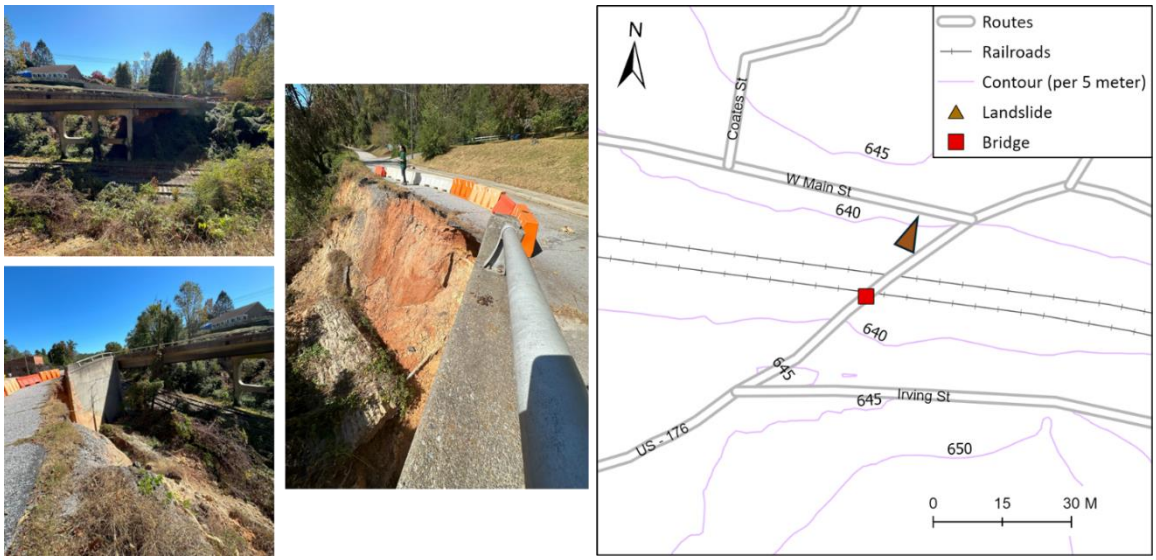

Figure 4-18 Damaged I-176 Bridge on Main Street, Saluda, North Carolina (The damage to the bridge abutment is due to a debris slide around the wing wall). (Photo Credits: Sophia Lin and Shenen Chen).

4.6 Discussion

The 2024 Hurricane Helene is an extraordinary storm event for the western North Carolina mountain areas. The storm triggered numerous landslides with a majority classified as debris slides. Figure 4-19 shows a compilation of damaged bridges and landslides data from state agencies (USGS 2024 and NCDOT 2024). The data includes 1,792 reported landslides and 79 reported damaged bridges. The geospatial data presentation is displayed over a landslide susceptibility map considering multiple trigger mechanisms (earthquake, rainfall, flooding) that was developed prior to current study (Lin et al. 2024). It is shown that most of the damaged bridges are in close vicinities of the landslide areas and most of them are in the predicted high susceptibility zones. At the time of this manuscript preparation, the state is still actively collecting data on both landslides and damaged bridges.

Two critical issues raised by the observations made in this study both related to the design of bridges in the mountain areas include: 1) the differentiation between landslides and river scours and 2) the importance of bridge abutment design to avoid mass extraction underneath the bridge approaches.

Because of the high elevations and landforms of the mountains, bridge and roadway safety can be critical during highwater floodings. The highwater flooding may be a result of upstream debris slides and downed trees that constricted the waterways at the bridge sites. This is a phenomenon that has been observed in prior disasters (Bessette-Kirton et al. 2019). It is important to point out that the current scour depth estimation methods are largely based on clear water or live bed scenarios and not for debris-laden water scenarios (Ettema et al. 2010). Also, most of the abutment scour considerations do not include

scouring behind the abutments and water level close to or exceeding the bridge deck or roadway surface (Ettema et al. 2013). To illustrate Helene flooding to a bridge, Figure 4-20 shows current considerations of bridge abutment scour and slope failure due to waterway erosion. The hypothetical water level due to Hurricane Helene is highlighted as a dashed line. As a result of bridge submerging under the floodwater, scours can be initiated behind the bridge embankment. Considering the failure modes of these bridges, it is critical that bridge design approaches should consider extending the continuity of bridge deck beyond the clear span of the river channel below the bridge, so that when excessive flooding occurs, there will not be the separation of bridge and roadway and hinder evacuation efforts or post-disaster support transports. However, this recommendation would need to be further developed because of the potential of limiting bridge deck thermal expansions and the potential of elevating costs of bridge construction. Similar bridge failures were observed in other significant storms in mountainous regions such as Puerto Rico after Hurricane Maria where several bridges were washed out by flood water (Lin et al. 2024).

The above failure mode consideration is also critical to bridges without pier supports. Figure 4-21 shows a collapsed bridge (ID: 100041) over Blue Ridge Road in Black Mountain, NC, washed out by Hurricane Helene flooding. The river channel width is about 6 m and bridge clearance is not more than 1.7 m above river water. Significant scouring around the bridge approaches has resulted in the bridge completely collapsing into the river. To quantify the tractive force (shear stress) of the flooding water, Chow (1959) used assumed clear water and sediment filled fluid unit weights of 9.8 kN/m^3 and 18 kN/m^3, and the computed shear stresses are in the range from 0.00784 kN/m^2 to 0.05 kN/m^2. These

values are critical for silt or clay particles of erodible sediments typical in the mountain region and may result in the scour (Arneson et al. 2012, HEC-18).

Because of the site geology, debris flows will always happen in the Appalachian Mountains. However, existing bridges may not have the extra measures to address the excessive flooding and debris flow. The geo-risk may be further amplified by climate extremities such as extremely strong hurricanes, which can bring about multi-hazards that were not considered in current bridge designs (Schulz et al. 2017, Palu et al. 2019, and Nasr et al. 2021). Even though bridge pier scour was not observed in current study, post-disaster investigation should include detailed investigation of the bridge foundation conditions and should also include mass loss around piers on banks that may be exposed to local scours (Chaven et al. 2022a and b).

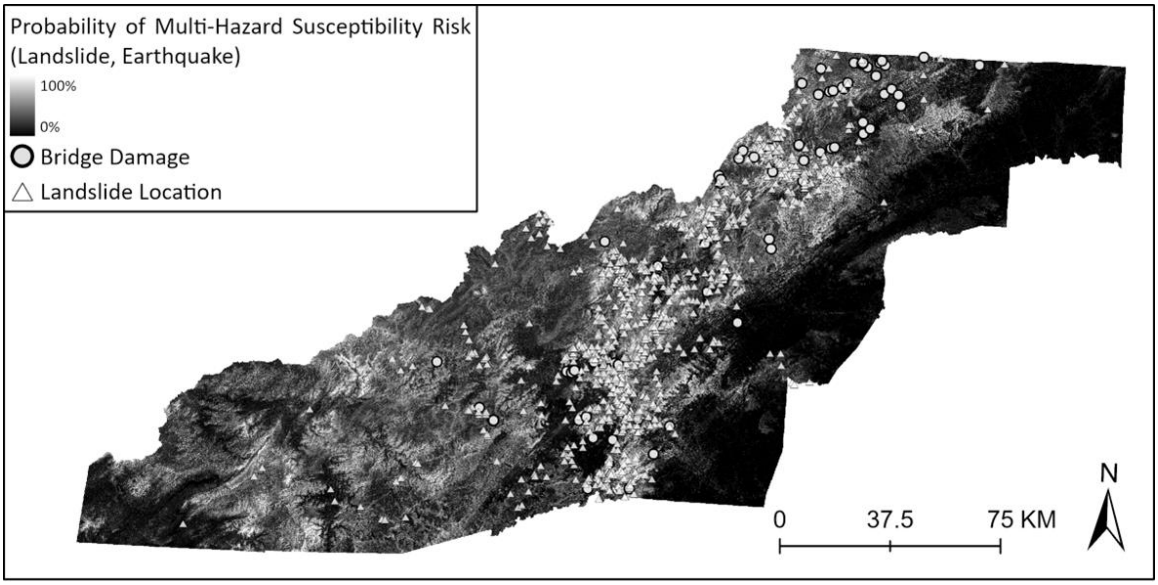

Figure 4-19 A composite representation of damaged bridges and landslide locations after Hurricane Helene superimposing over the landslide susceptibility map for western North Carolina mountain regions.

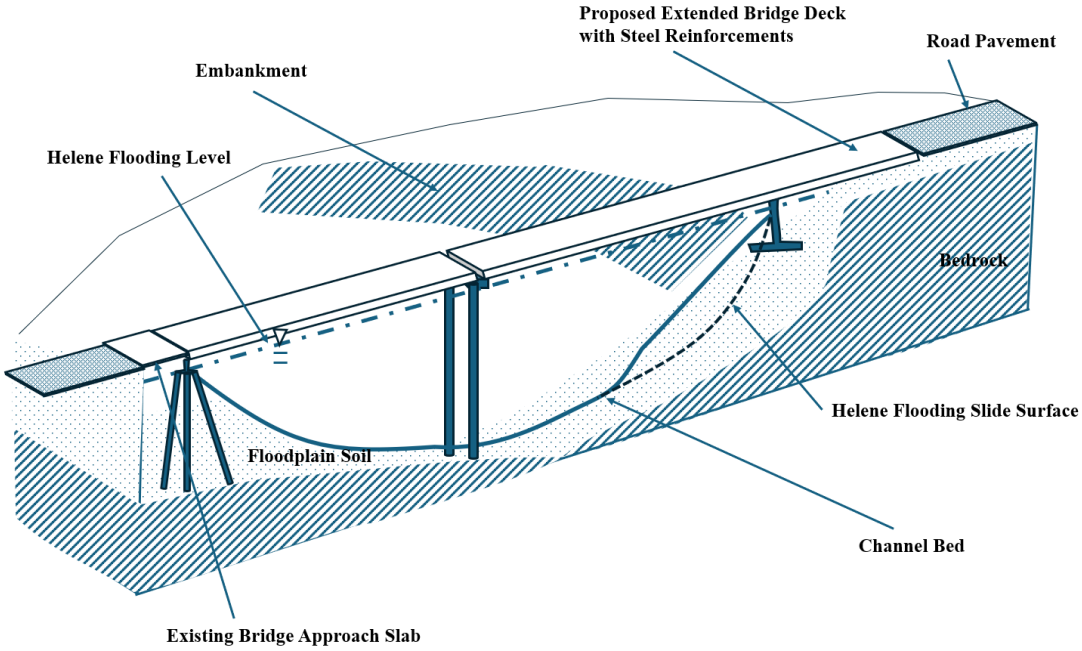

Figure 4-20 Helene flooding level and current abutment scour design considerations which do not include landslide behind the abutment walls. Left-side abutment represents conventional bridge design and right-side abutment represents the proposed extended bridge deck design.

Figure 4-21 Collapsed bridge (ID: 100041) washed out by Hurricane Helene flooding. (Photo Credits: Sophia Lin and Shenen Chen)

4.7 Conclusion

The 2024 hurricane season has brought about two unprecedented hurricanes (Helene and Milton) that lead to severe damage to infrastructure and loss of human lives. Hurricane Helene was a Category 4 hurricane and traveled inland to Tennessee, Virginia, and Western Carolinas. This paper reported observations of landslides and bridge damage in the Appalachian Mountains and confirmed several debris slides due to the unprecedent level of rainfall brought by Hurricane Helene. More than 1,900 landslides, reported by USGS, were triggered and more than 600 bridges were damaged at the time of reporting.

Detailed studies of the bridge failures indicated that scouring and slides at bridge approaches are a critical issue attributed to the damages of many bridges in the region, which eventually become a hindrance to the safety of the local population including inhibiting the transportation of sustenance and daily necessities to the trapped residents. Hence, to keep the bridges functional after the storm, there is a need to ensure the bridge approaches remain intact. One suggestion is to extend the bridge deck to reasonable length into the roadway section, so that the travelable bridge surface will not be significantly impacted by the scour or land slide at the bridge approach. However, further studies are needed to justify such measures to ensure safe designs.

Reference

Arneson, L.A., Zevenbergen, L.W., Lagasse, P.F. and Clopper, P.E. (2012) Evaluating Scour at Bridges, Fifth Edition, FHWA-HIF-12-003, HEC-18, US Department of Transportation, Washington, DC.

Bessette-Kirton, E.K., Cerovski-Darriau, C., Schulz, W.H., Coe, J.A., Kean, J.W., Godt, J.W., Thomas, M.A. and Hughes, K.S. (2019) "Landslides Triggered by Hurricane Maria: Assessment of an Extreme Event in Puerto Rico." GSA Today Archive, 29(6), 4-10.

Blake, E. (2007). "Tropical Cyclone Report: Hurricane Humberto 12-14 September 2007," Report AL092007, National Hurricane Center.

Blake, E. (2024). "Seven-Day Graphical Tropical Outlook," Miami, Florida: National Hurricane Center. Archived from the original on September 22, 2024. Retrieved September 23, 2024.

Cebulski, J. (2022) "Impact of river erosion on variances in colluvial movement and type for landslides in the Polish Outer Carpathians," Catena, 217, 106415.

Chavan, V.S., S.E. Chen, N.S. Shanmugam, W. Tang, J. Diemer, C. Allan, N. Braxtan, T. Shukla and T. Chen, (2022a) "Modeling of Progressive Scouring of a Pier-on-Bank," CivilEng, 3, 365-384.

Chavan, V.S., S.E. Chen, N.S. Shanmugam, W. Tang, J. Diemer, C. Allan, N. Braxtan, T. Shukla and T. Chen, (2022b) "Analysis of Local and Combined (Global) Scours on Bridge Piers-on-Bank," CivilEng, 3, doi.org/10.3390/civileng301001.

Chen, S.E., Leeman, M.E., English, J.B., Kennedy, A.B., Masters, F.J., Pinelli, J.P., Pang, W.C., Rullan-Rodriguez, J.A., Satyanarayana, P., Calvo, J., Murugan, B. and Natarajan,

C. (2016) “Basic Structure System Rating of Post-Hurricane Haiyan Structures in Tacloban and East Guiuan,” ASCE Journal of Performance of Constructed Facilities, 30(5), DOI:10.1061/(ASCE)CF.1943-5509.0000872.

Chow, V.T. (1959) Open-Channel Hydraulics, McGraw-Hill, New York.

Emanuel, K. (1986) “An air-sea interaction theory for tropical cyclones, Part 1: Steady-state maintenance,” Journal of Atmospheric Science, 43, 585-605.

Ettema, R., Nakato, T. and Muste, M. (2010) Estimation of Scour Depth at Bridge Abutments, NCHRP 24-20, Transportation Research Board, Washington DC.

Ettema, R. and Fuller, J. (2013), “Abutment failure during bridge waterway scour,” Proceedings, 2013 IAHR World Congress, International Association for Hydro-Environment Engineering and Research, Chengdu, China, 7 pages.

Fuhrmann, C.M., Konrad, C.E. and Band, L.E. (2008) “Climatological Perspectives on the Rainfall Characteristics Associated with Landslides in Western North Carolina,” Physical Geography, 29(4). 289-305.

Hagan, E. (2024). “Seven-Day Graphical Tropical Outlook,” Miami, Florida: National Hurricane Center. Archived from the original on September 22, 2024. Retrieved September 23, 2024.

Hall, J., Muscarella, R., Quebbeman, A., Arellano, G., Thmpson, J., Zimmerman, J.K. and Uriarte, M. (2020) “Hurricane-Induced Rainfall is a Stronger Predictor of Tropical Forest Damage in Puerto Rico than Maximum Wind Speeds,” Scientific Reports, Nature, 10:4318, doi.org/10.1038/s41598-020-61164-2.

Joyce, B.R., Gonzalez-Lopez, J., Van der Westhuysen, A.J., Yang, D., Pringle, W.J., Westerink, J.J. and Cox, A.T. (2019) “US IOOS Coastal and Ocean Modeling Testbed:

Hurricane-Induced Winds, Waves, and Surge for Deep Ocean, Reef-Fringed Islands in the Caribbean," Journal of Geophysical Research: Oceans, 124, 2876-2907.

Lin, S., Chen, S.E., Tang, W., Chavan, V., Shanmugam, N., Allan, C. and Diemer, J. (2024) "Landslide Risks to Bridges-in-Valley in North Carolina," Geohazards, 5, 289-309.

Lyons, N.J., Mitasova, H. and Wegmann, K.W. (2014) "Improving mass-wasting inventories by incorporating debris flow topographic signatures," Landslides, 11, 385-397.

Nasr, A., et al., (2021) "A review of the potential impacts of climate change on the safety and performance of bridges." Sustainable and Resilient Infrastructure, 6(3-4), 192-212.

NCDOT (2024) DriveNC/TIMS Incidents data. Available from: https://drivenc.gov/?ref=share&type=state&layers=congestion&pins=incidents_planned-road-work,incidents_other-incidents,roads_interstate,roads_us,roads_nc. Last access: 10/11/2024.

Palu, S. and Mahmoud, H. (2019) "Impact of climate change on the integrity of the superstructure of deteriorated US bridges." Plos One. 14(10), e0223307.

Peraza, D.B., Coulbourne, W.L. and Griffith, M. (2014) Engineering Investigation of Hurricane Damage: Wind versus Water, ASCE, Reston, VA.

Ramos-Scharrón, C.E., Arima, E.Y., Guidry, A., Ruffe, D. and Vest, B. (2021) "Sediment mobilization by hurricane-driven shallow landsliding in a wet subtropical watershed," Journal of Geophysical Research: Earth Surface, 126, e2020JF006054.

Reinhart, B. (2024). "Seven-Day Graphical Tropical Outlook." Miami, Florida: National Hurricane Center. Archived from the original on September 23, 2024. Retrieved September 23, 2024.

Rotunno, R. and Emanuel, K.A. (1987) “An air-sea interaction theory for tropical cyclones. Part II: Evolutionary study using a nonhydrostatic axisymmetric numerical model,” Journal of Atmospheric Science, 44, 542-561.

Schulz, A., Zia, A. and Koliba, C. (2017) “Adapting bridge infrastructure to climate change: institutionalizing resilience in intergovernmental transportation planning processes in the Northeastern USA.” Mitigation and Adaptation Strategies for Global Change, 22(1), 175-198.

Sippel, J. and Zhang, F. (2010) “Factors affecting the predictability of Hurricane Humberto (2007),” Journal of the Atmospheric Sciences, 67, 1759-1778.

US Department of Commerce, NOAA. "Post Hurricane Helene Report for the Western Carolinas and Northeast Georgia". www.weather.gov. Retrieved 2024-10-03.

USGS (2024a). “Preliminary data for the 2024 Hurricane Helene Landslide Emergency Response: 2024 USGS Provisional Data Release.” Geologic Hazards Science Center, USGS (https://doi.org/10.5066/P1G6Y6HP).

USGS (2024b), Hurricane Helene Observation Dashboard, Geologic Hazards Science Center, USGS.; Available from: https://usgs.maps.arcgis.com/apps/dashboards/01b4f51fc0b64002bf7722a9acfc181d. Last accessed; 10/21/2024.

Yuan, X.Q., Duan, Z. and Zhao, F.S., (2018) “The formation mechanism of river erosion-induced loess landslide,” IOP Conference Series: Earth and Environmental Science, 186, 012045.

Wooten, R.M., Witt, A.C., Miniat, C.F., Hales, T.C., and Aldred, J.L. (2016) “Frequency and magnitude of selected historical landslide events in the Southern Appalachian

highlands of North Carolina and Virginia: Relationships to rainfall, geological and ecohydrological controls, and effects." Chapter 9. C.H. Greenberg and B.S. Collins eds., Natural Disturbances and Historical Range of Variation, Managing Forest Ecosystems, 32, 203-262.

Wooten, Richard & Cattanach, Bart & Bozdog, G. & Isard, Sierra. (2024). The September 18, 2018, Debris Slide in Warrensville, NC: A Landslide Response Case Study. Environmental & Engineering Geoscience. 30. 59-76. 10.21663/EEG-D-23-00069.

Chapter 5: Landslide Prediction Validation in Western North Carolina after Hurricane Helene

5.1 Abstract

Hurricane Helene triggered 1,792 landslides across western North Carolina and has caused damage to 79 damaged bridges to date. Helene hit western North Carolina days after a low-pressure system dropped up to 10 inches of rain in some locations of western North Carolina (e.g., Asheville Regional Airport). The already waterlogged region experienced devastation as significant additional rainfall occurred during Helene where some areas like Asheville, North Carolina received an additional 14 inches of rain (National Weather Service, 2024). In this study, machine learning (ML)-generated multi-hazard landslide susceptibility maps are compared to the documented landslides from Helene. The landslide models use the North Carolina landslide database, soil survey, rainfall, USGS digital elevation model (DEM), and distance to rivers to create the landslide variables. From the DEM, aspect factors and slope are computed. Because recent research in western North Carolina suggest fault movement is destabilizing slopes, distance to fault was also incorporated as a predictor variable. Finally, soil types were used as a wildfire predictor variable. In total, 4,794 landslides were used for model training. Random forest and logistic regression machine learning algorithms were used to develop the landslide susceptibility map. Furthermore, landslide susceptibility was also examined with and without consideration of wildfires. Ultimately, this study indicates heavy rainfall and debris-laden floodwaters were critical in triggering both landslides and scour, posing a dual threat to bridge stability. Field investigations from Hurricane Helene revealed that bridge damage was concentrated at bridge abutments, with scour and sediment deposition

exacerbating structural vulnerability. We evaluated the assumed flooding potential (AFP) of damaged bridges in the study area, finding that bridges with lower AFP values were particularly vulnerable to scour and submersion during flood events. Differentiating between landslide induced and scour induced damage is essential for accurately assessing risks to infrastructure. The findings emphasize the importance of comprehensive hazard mapping to guide infrastructure resilience planning in mountainous regions.

Keywords: landslides, bridge failures, hurricane Helene, Random Forest

5.2 Introduction

Western North Carolina is part of the Appalachian Mountain range that stretches from northern Maine to southern Alabama. The Appalachian orogeny started during the forming of the supercontinent Rodina where continental plate collisions resulted in the mountain-building process (Hatcher et al., 2010; Li et al., 2008). The upward process continued until 200 million years ago when North America and African continents started to drift away. Because of the Appalachian Wilson cycle process, three orogenies created the Appalachian Mountain chain. Figure 5-1 shows the western mountain region in North Carolina. A 3D land forming sketch is included to illustrate the forming of the mountain range. The region's distinctive landscape of valleys and ridges, combined with its climate, creates ideal conditions for landslides due to continuous weathering and erosion (Wooten et al., 2008; Wooten et al., 2016). Landslides are particularly common in western North Carolina, especially following periods of heavy rainfall. However, landslides are not the only natural hazard frequently affecting the state—hurricanes also pose a significant threat. When these hazards occur together, their combined impact intensifies the overall damage. Therefore, landslides pose significant hazards in mountainous areas impacted by hurricanes.

September 25-28, 2024, Hurricane Helene traveled through the western mountain regions of North Carolina and triggered thousands of landslides. Hurricane Helene, which originated in the Caribbean Sea, started on September 22 as a tropical low-pressure disturbance and within a short period intensified to a Category 4 hurricane (September 26th). By the time Helene arrived in Georgia, it was downgraded to a post-tropical cyclone and eventually reached the western mountain region of North Carolina following the path

shown in Figure 5-1. In western North Carolina alone, Helene resulted in 102 deaths, caused excessive flooding and landslides, and destroyed infrastructures, including numerous bridges and roadways throughout western North Carolina (NCDHHS, 2024). The storm impacted a significant portion of the southeastern continental US and became one of the most severe hurricanes in recent US history (Reinhart, 2024).

Prior to Hurricane Helene, heavy rainfall events have caused significant flooding and landslides in western North Carolina and the surrounding region in the past, including 10 times from 1924 to 2013, giving an average frequency of about 9 years (Wooten et al. 2016). A common factor amongst the worst of these past storms was heavy rainfall from a hurricane in addition to multiple storms occurring within a short period of time. In 1916, 1940, and 2004, multiple storms, at least one of which was a hurricane, occurred within days to weeks of each other causing significant rainfall on already saturated soil, generating widespread flooding and hundreds to thousands of landslides. Hurricane Helene was similar to these past events. Helene hit western North Carolina days after a low-pressure system dropped up to 25 cm of rain in some locations of western North Carolina (e.g., Asheville Regional Airport). The already waterlogged region experienced devastation as significant additional rainfall occurred during Helene where some areas like Asheville and Bat Cave received an additional over 35 cm of rain (NWS, 2024). Like the past multi-storm events to impact western North Carolina, Hurricane Helene and its preceding storm produced thousands of landslides, a majority of which are classified as debris flows. Debris flows, which are the most common form of landsliding in western North Carolina (Wooten et al., 2016)., are fast-moving mixtures of water, saturated soil, rock, and organic material that rapidly traverse downslope, often triggered by intense rainfall. At the time of writing

this article, the USGS Helene landslide dashboard (2024) reports 1,792 landslides are initially identified as debris flows, landslides, and unknowns (USGS, 2024).

To assess the landslide susceptibility in the region, we used machine learning (ML) and parameters that may trigger a landslide to generate a landslide risk map (Lin, 2024; Lin et al., 2024). The risk map considers multi-hazard scenarios including landslide, earthquake, wildfire and flooding. Figure 5-2 shows the different counties that are considered in the study. Wildfire is included in the study because it can result in soil losing moisture retention capability and make the slopes more susceptible to sliding (Culler et al., 2023; DeBano et al., 1979; He et al., 2021; Rengers et al., 2020). The affecting variables included distance to rivers, digital elevation model (DEM) and its derivatives (different aspect parameters such as slopes and orientation of slopes), soil types, rainfall, forest cover, distance to faults, distance to high population density areas, and annual temperature. Two algorithms were considered: Random Forest (RF) and Logistic Regression (LR), where RF is a machine learning technique that uses supervised learning from a set of decision trees created from a bootstrap sampling approach (Breiman, 2001; Ho, 1998). RF has been used previously in landslide susceptibility analysis (Catani et al., 2013; Chen, Zhang, et al., 2018; Pourghasemi et al., 2018). LR is a machine learning algorithm and has been used by several researchers for landslide susceptibility analysis including Regmi et al. (Regmi et al., 2014), Sun et al. (Sun et al., 2021), and Rasanen and Maurer (2022).

These landslide susceptibility models for the western North Carolina mountains are also used to determine the flooding risks to the highway bridges, since landslides can result in significantly raised water and cause flooding damages to the bridges (Lin et al., 2024). To quantify flooding potential, bridge to water clearance is defined as an assumed flooding

potential (AFP), which is the computed mid-span height of a bridge structure. AFP is used to determine if a bridge is in a valley and if it has high flooding potential.

This paper compares the currently documented landslides in western North Carolina with the landslide susceptibility models (Lin et al., 2024). Furthermore, these landslide susceptibility models were modelled both with and without wildfire predictor variables. The results are further compared to field observations made by the authors after Hurricane Helene. This is the first validation report of the landslide susceptibility mapping based on newly documented landslides that the model was not trained upon. Additionally, this paper reports the damage to the bridge structures from the landslides and flooding caused by Hurricane Helene. We further discuss the issue of differentiating landslide versus scour in the valley regions.

.

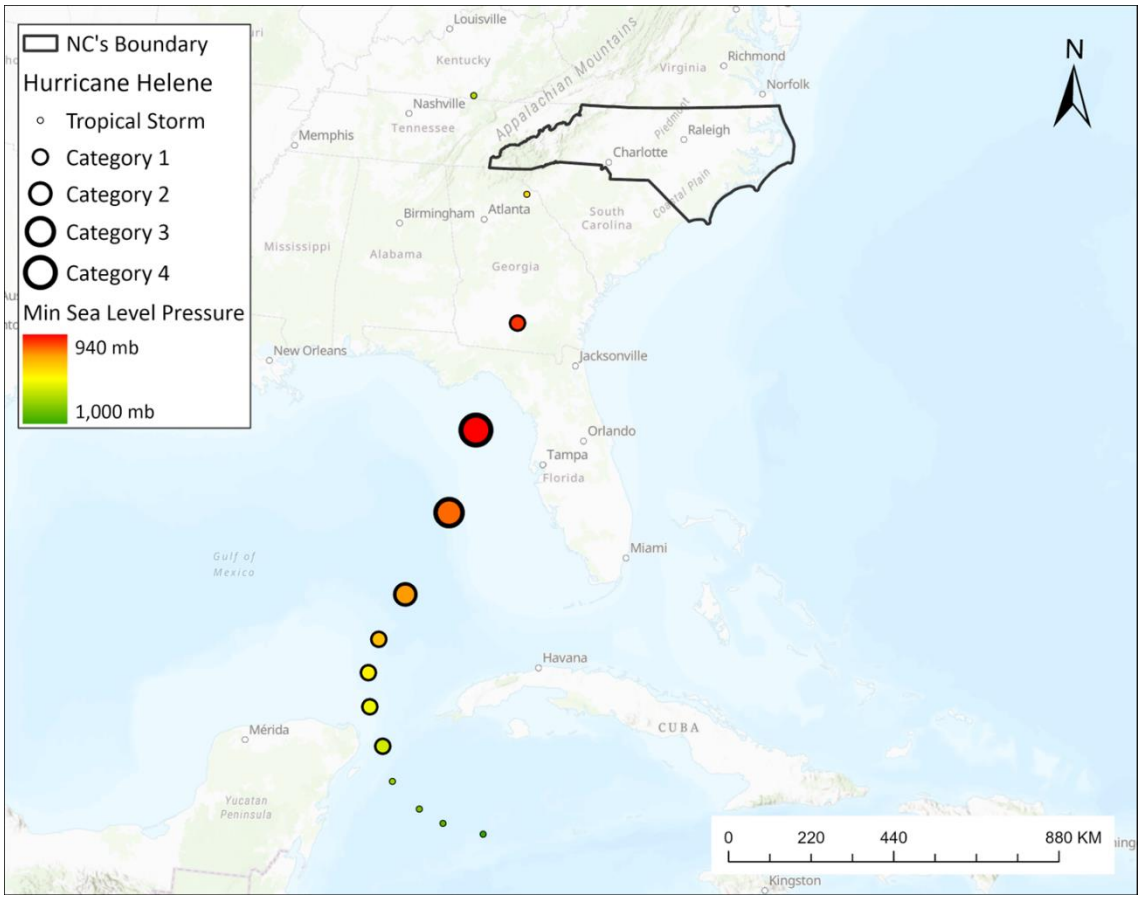

Figure 5-1 Path of Hurricane Helene moving through the Gulf of Mexico and landed near Perry, Florida as a Category 4 storm.

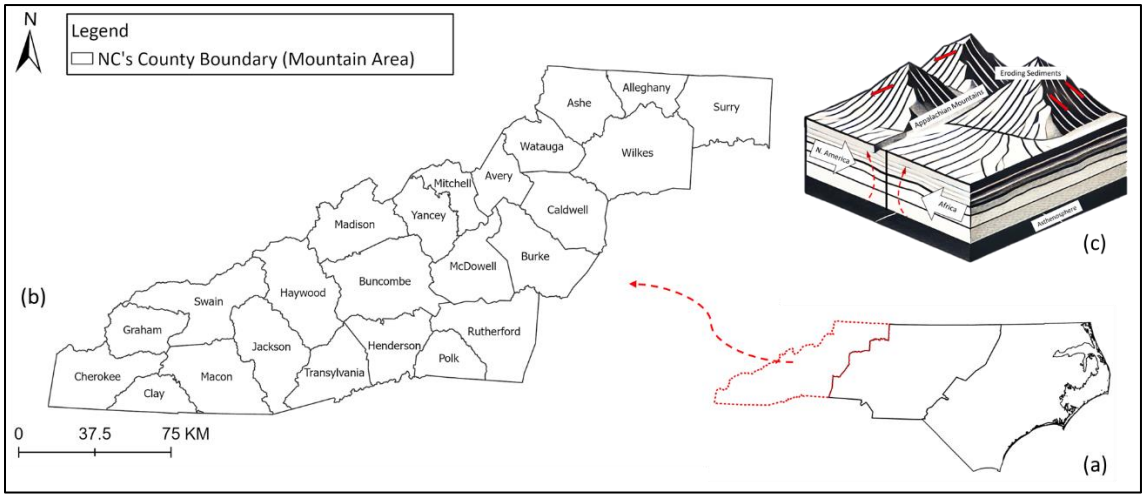

Figure 5-2 Study area with location map illustrating North Carolina's mountain area. a) North Carolina distinct physiographic regions distrbution, b) Blue Ridge Mountain area and c) hypothetical Appalachian mountain formation.

5.3 Study Area and Methods

5.3.1 Study Area and Effects from Helene

Figure 5-3 shows the study regions covering an area of 26,572 $km^{2,}$ in the Appalachian Uplands (State). Also shown in Figure 5-3 are the state reported landslide locations and damaged bridges after Hurricane Helene (NCDOT, 2008; USGS, 2024). Highlighted boundaries in Figure 5-3 are the ground truthing regions covered by the research team. Figure 5-4 shows some typical landslides from Hurricane Helene with size description using NASA's slide identification technique (NASA, 2024). It should be noted that the disaster caused by Helene extended beyond North Carolina and included Tennessee, Georgia, Florida, South Carolina, and Southern Virginia. However, the scope of study reported in this paper only considers the mountain region of western North Carolina.

5.3.2 Landslide Susceptibility Modeling

Historical landslide data was retrieved from the US national database and the landslide susceptibility modeling followed the confidence rule system and used susceptibility values ranging from 5 (a confidence of a consequential landslide at a given location) and 8 (high confidence in extent or nature of landslide)(Belair et al., 2022). The resulting landslide database included 4,794 landslides and 6,653 polygons.

For the multi-hazard modeling, a nested approach is used: We assume that the risk of landslide is the critical risk-of-interest and consider other hazards including earthquake, rainfall and forest fire as contributing factors.

For the multi-hazard modeling, wildfire database from U.S. Department of Agriculture (USDA) wildfire data were collected (NCFS, 2024): Considering, only human-induced and natural wildfire events, our wildfire database consists of 112,454 events in NC.

The other wildfire-related variables include annual temperature (°F/yr), rainfall, forest cover, distance to roads, distance to high population density, elevation and slope. Forest cover only considers cover and non-cover types and is extracted from NC OneMap 2016 dataset (Services, 2016).

Some soil types are more receptive to loss of moisture and can increase the susceptibility of landslides (Short, 2021). Our approach for wildfire risk in the landslide modeling first included modeling wildfire susceptibility and then used the computed risk factor as a variable in the landslide susceptibility modeling (Lin, 2024). Due to limited available data, our wildfire susceptibility modeling is not as comprehensive as some other modeling reports (Abdollahi et al., 2024; Leuenberger et al., 2018). However, our wildfire susceptibility model has an accuracy of 72%, which is reasonably close to other more accurate (including more variables such as wind speed, surface roughness, fire history, minimum and maximum annual temperatures) models such as the 85.46% using convolution neural network (CNN) by Bjånes et al. (Bjånes et al., 2021).

During model development, the multi-hazard landslide susceptibility model also included earthquake hazard via a distance to faults metric because the global landslide database the landslide susceptibility model was trained upon included both seismic and aseismic landslides (Belair et al., 2022). While the landslides caused by Hurricane Helene were aseismic, recent research (Langille et al., 2023)in the western North Carolina suggests that fault movement is currently destabilizing slopes. Therefore, some slopes in western North Carolina – those closer in distance to faults – Also, it looks like Figure 5-15i seems to indicate some correlation between distance to fault and landslides. However, this could just be because faults are located at locations where the mountains are at a greater elevation.

Furthermore, it is important for a multi-hazard landslide susceptibility model to also include earthquake hazard, especially considering seismic activity has drawn increased attention to the Carolina region. Notable examples include the 2011 moment magnitude (M_w) 5.8 Mineral, Virginia, and 2020 M_w5.1 Sparta, North Carolina earthquakes, which garnered national attention due to their damage and the significant population across the eastern U.S. exposed. The 2020 Sparta earthquake, for example, triggered rockfalls and slope bulge (pre-slide land deformation) in the Little River Valley region (Figueiredo et al., 2022). In addition to these recent events, paleoseismic evidence indicates that the region has experienced significant seismic activity in the past, such as the ~M_w7-7.5 1886 Charleston, South Carolina earthquake (Rasanen & Maurer, 2023). Moreover, the introduction of anthropogenic activities, such as increased natural gas production in Virginia, raises concerns about the potential for fracking-induced earthquakes in the future. Thus, while the effects of including an earthquake prediction variable in a landslide susceptibility model is important in North Carolina, it currently has a relatively small influence on the predictions for aseismic landslides and may indirectly serve as a predictor for them given fault movements link to slope destabilization.

Both LR and RF modeling were conducted using RStudio and 9,794 sample points were used for the RF and LR modelling (4,794 for historical landslide occurrences and 5,000 for no landslide occurrences). In our dataset, we used random points tool in ArcGIS Pro.

Furthermore, to automate the computation of flooding potentials of bridges over water, ArcGIS Pro was used. A bridge's flooding potential is defined as the Assumed Flooding Potential (AFP), which is computed as:

$$B_i = \frac{E_{1i}+E_{2i}}{2} - E_{Li} \quad (5.1)$$

where B_i denotes the bridge's AFP, i represents the bridge's ID, E_{1i} and E_{2i} represent the elevations on the two sides of the bridge, while E_{Li} denotes the elevation of the river. AFP is in essence the averaged clearance of the bridge from the river level. State DEM data were used to quantify the bridge embankment heights using a 30 m radius around a bridge. Several ArcGIS tools, including the split line to points tool, extract multi-values to points tool, bearing distance to line tool, buffer tool, and zonal statistics tool, were used in the calculation of the bridge's AFP.

The modeling workflow is shown in Figure 5-5, where the results (landslide susceptibility maps) are shown in Figure 5-6 and Figure 5-7 for landslides due to are shown in Figures 6 and 7 for landslides not considering wildfire effects and considering wildfire effects, respectively The comparison between LR and RF modeling has been published by Lin et al. (Lin et al., 2024) where RF results are shown to be more accurate than LR results. Hence, hereafter, only the RF results will be used for Helene landslide validation.

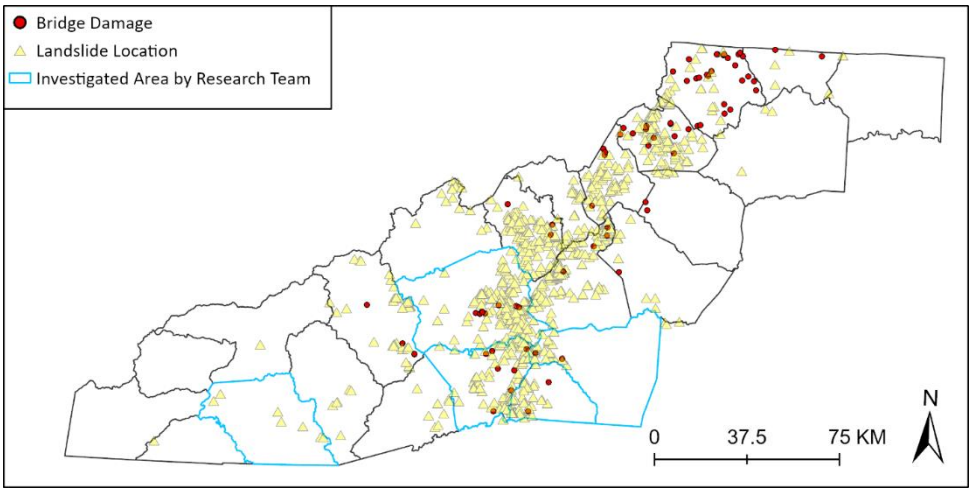

Figure 5-3 A composite representation of damaged bridges and landslide locations after Hurricane Helene.

Figure 5-4 The locations after Hurricane Helene. (Photo credit: Shen-En Chen, Sophia Lin, and Qifan Zhao)

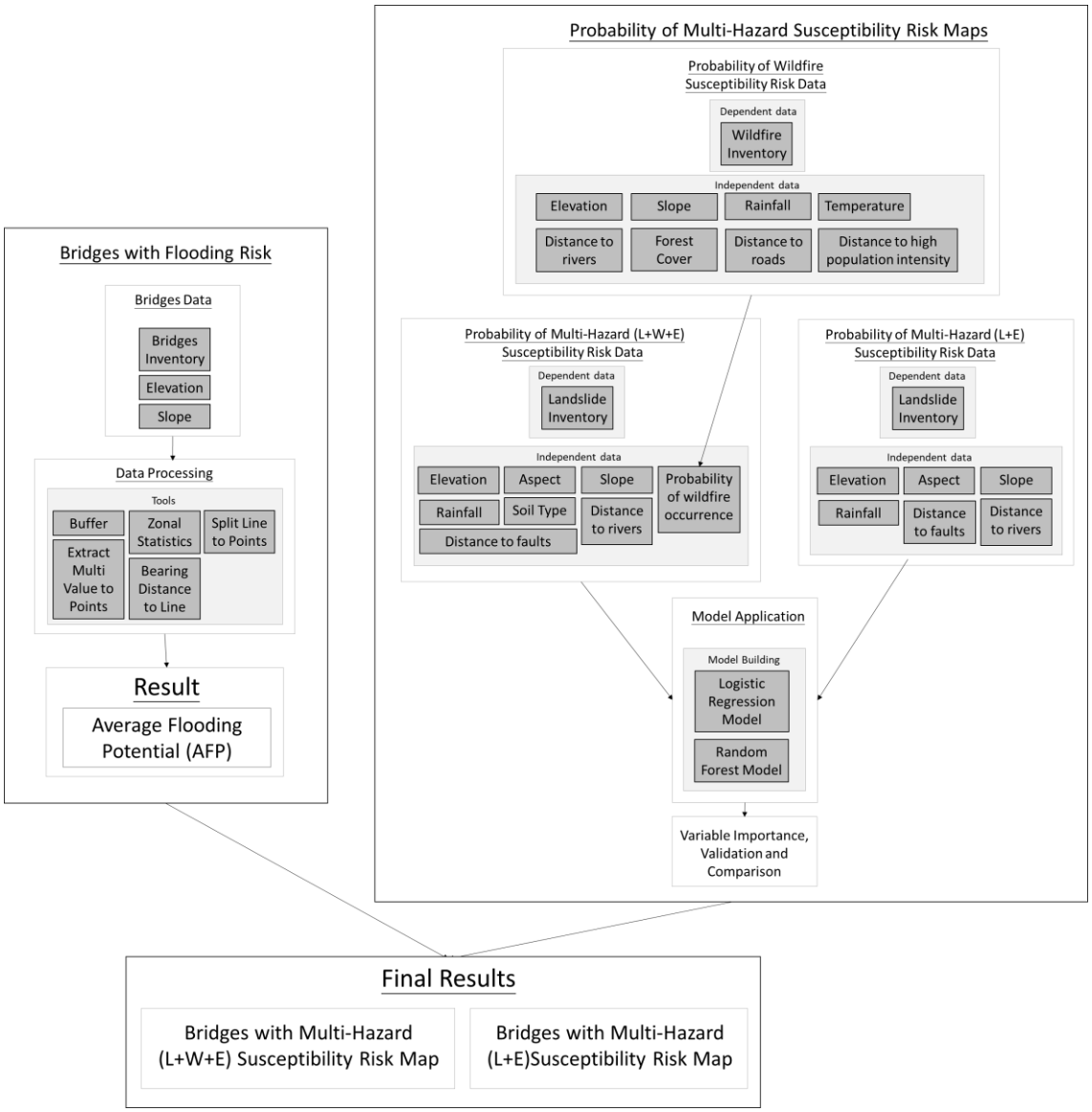

Figure 5-5 A schematic of the calculation workflow for the probability of multi-hazard (wildfire, landslide, earthquake and flooding) occurrence map, the probability of wildfire occurrence map, and bridges of average flooding potential (AFP).

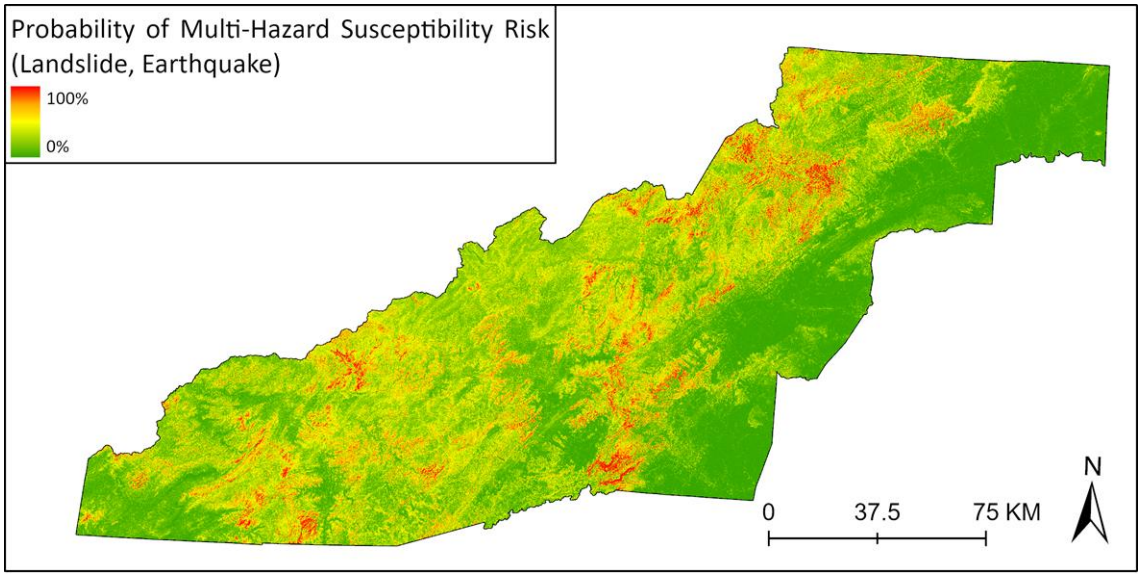

Figure 5-6 Multi-hazard (Landslide and earthquake) risk map in North Carolina.

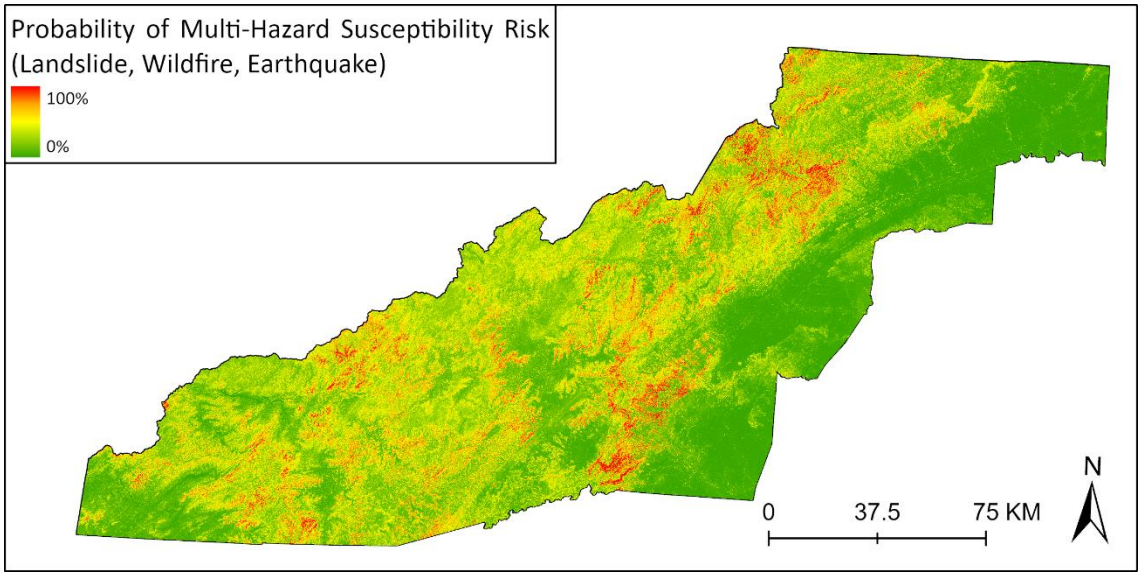

Figure 5-7 Multi-hazard (Wildfire, landslide and earthquake) susceptibility map in North Carolina.

5.4 Results

In the following, we will first discuss the state reported landslide locations and the comparisons to the two multi-hazard susceptibility maps. We then discuss detailed observations from field investigations.

5.4.1 Model and Helene landslide comparisons

Figure 5-8 shows the locations for the 1,792 landslides reported by the state superimposed on the multi-hazard susceptibility maps for a) not considering wildfire effects; and b) considering wildfire effects, respectively. The figures show that the landslide sites are clustered mostly in the central portion of western North Carolina and overlap several of the highly probable landslide susceptibility sites. The clustering of the landslides is probably due to the mountain range trapping the storm and forcing moisture dump in the region. Unfortunately, the meteorological record of Hurricane Helene did not have sufficient information to indicate the precise storm path through the mountain range. To better represent the prediction for each landslide site, the results are reversely presented using color coding of the landslide susceptibility at the location of each slide as shown in Figure 5-9. This helps in processing the quantitative analysis of the landslide validation.

Figure 5-9a and Figure 5-9b show the landslide with different susceptibility probabilities for the multi-hazard scenarios landslide, with and without wildfire effects, respectively. The susceptibilities are reported in 10% intervals, such as 0–10%, 10–20%, and so on. In both L+E and L+W+E cases, the landslides of different susceptibilities are shown to be uniformly distributed throughout the middle region of the study area. Critical counties with significant number of landslides are Allegheny, Ashe, Watauga, Avery,

Mitchell, Yancey, McDowell, Rutherford, Madison, Buncombe, Henderson, Polk and Haywood.

The difference between the models with and without wildfire effects is presented in Figure 5-9c indicating that it is difficult to conclude if one case is more frequent than the other case. Both cases seem to be distributed at the same locations. This observation indicates that wildfire is currently not a significant landslide factor for western North Carolina.

To show a better contrast between the number of slides of the two scenarios, a bar chart is presented in Figure 5-9d, which shows that the biggest differences between the two scenarios are in the probability ranges of 0 to 10% and 60 to 70%. Figure 5-9d also shows that Helene landslides occurred with all the susceptibility ranges with the most cases in the probability range of 60% to 70%.

5.4.2 Ground Observations of Landslides and Damages to Transportation Infrastructures

Field investigation of the landslides shows a mixture of different extents of landslides from small roadside runoffs to large sections of mountain slope with rolling rocks and debris flows (Figure 5-4). Several of the landslides resulted in damage to roadways and parking facilities (Figure 5-10) and endangered bridge structures (Figure 5-11). Markings in Figure 5-10 and Figure 5-11 are added to show the likely boundary of the landslide.

Damages to bridge structures showed a critical issue differentiating landsliding versus river water scouring. Landslides, specifically debris slides in the western North Carolina mountain case, are typically described as the ground movement due to an increase in soil moisture, which reduces the soil strength and resulted in land mass flow

(Easterbrook, 1999), whereas scour is described as “Erosion of streambed or bank material due to flowing water”(Arneson et al., 2012). Due to the rapid accumulation of rainwater during Helene, many of the roadway embankments experienced rapid runoff of rainwater that travelled downslope into the river, forming first gullies and eventually triggered slides that converged with the rapid river flow. As a result of the significant number of landslides in the mountains, severe debris flows emptied into rivers and streams and resulted in massive erosion of riverbanks, such as in the case of Chimney Rock, NC.

Figure 5-12 shows a section of the Broad River (near Chimney Rock Village) that was washed away by the massive flooding during Hurricane Helene. Figure 5-12a shows the site of the washed-away bridge on Chimney Rock Scenic Road over the Broad River, and Figure 5-12b, Figure 5-12c, and Figure 5-12d show different views of the eroded riverbanks and basin of the Broad River. The entire Broad River basin from Bat Cave, Chimney Rock Village to Lake Lure experienced severe riverbank erosions.

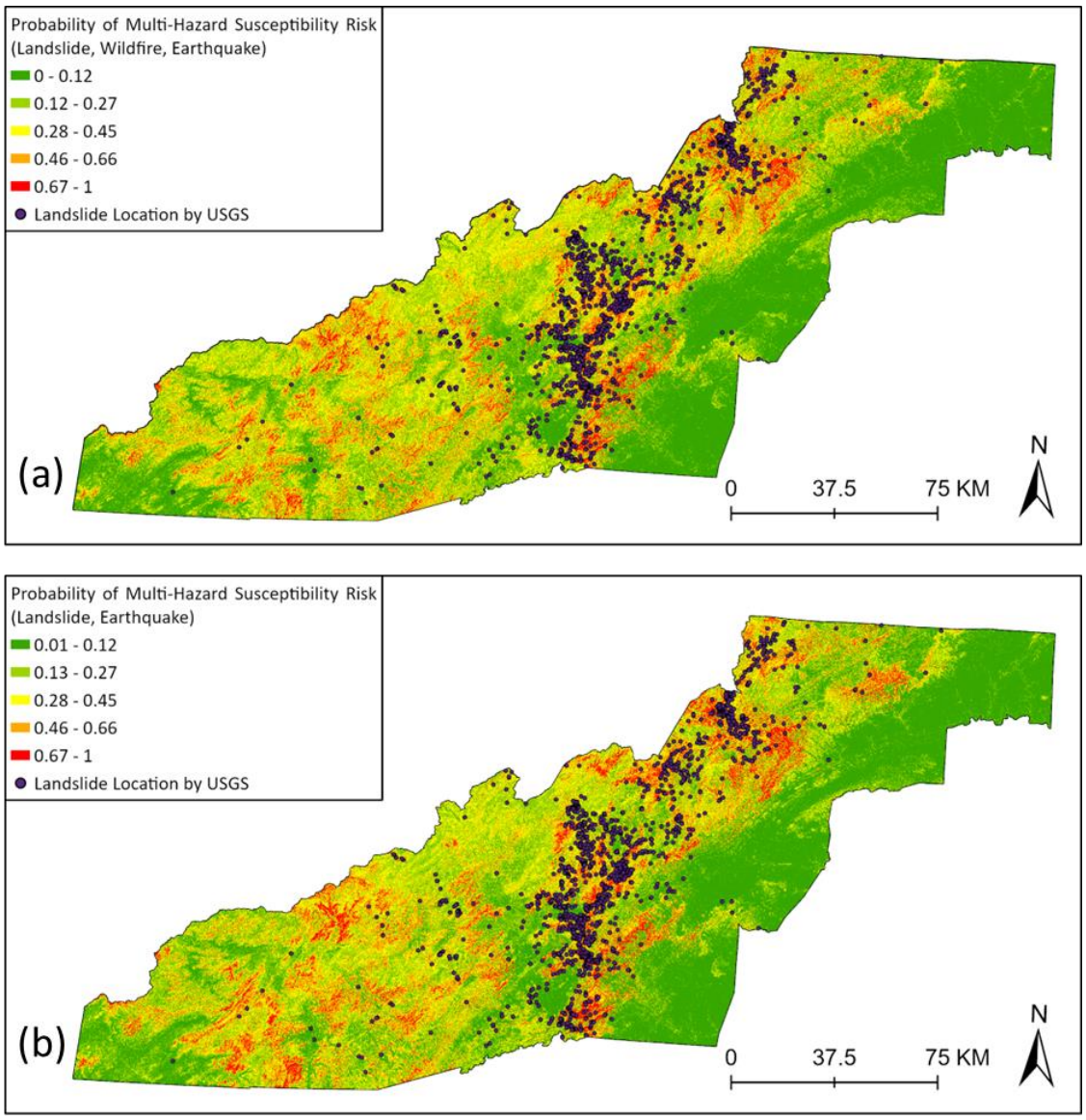

Figure 5-8 Multi-hazard susceptibility map in North Carolina with reported landslide locations (a: landslide, wildfire and earthquake; b: landslide and earthquake).

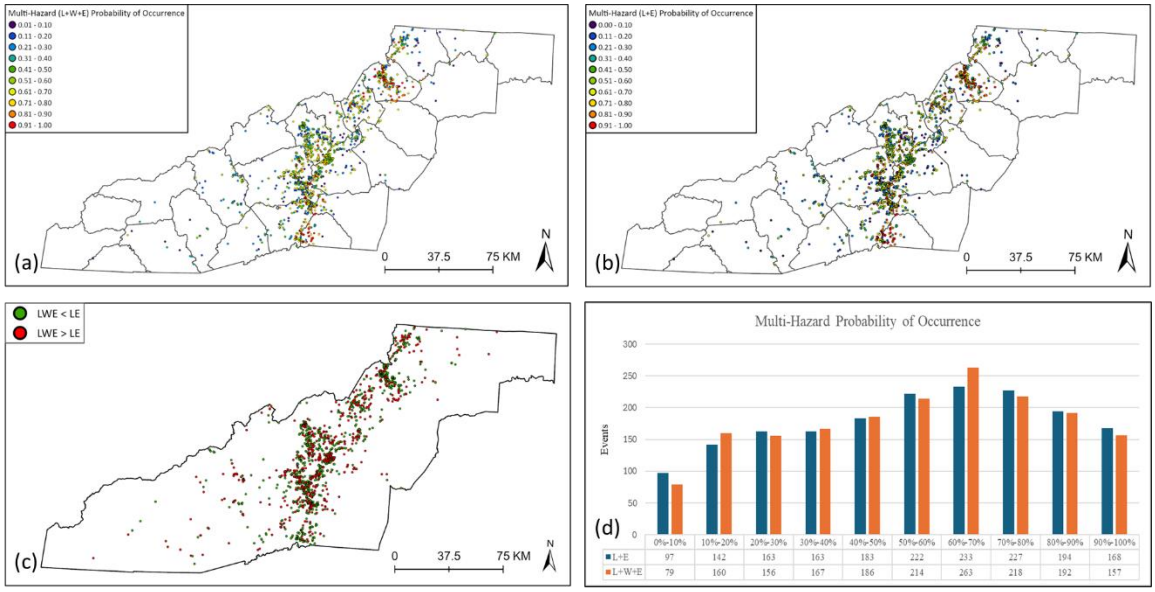

Figure 5-9 Analysis of reported landslides with the corresponding susceptibility probabilities: a) Multi-hazard scenario with wildfire effects; b) multi-hazard scenario without wildfire effects; c) difference between with and without wildfire effects; and d) bar chart comparing the two scenarios by number of slides.

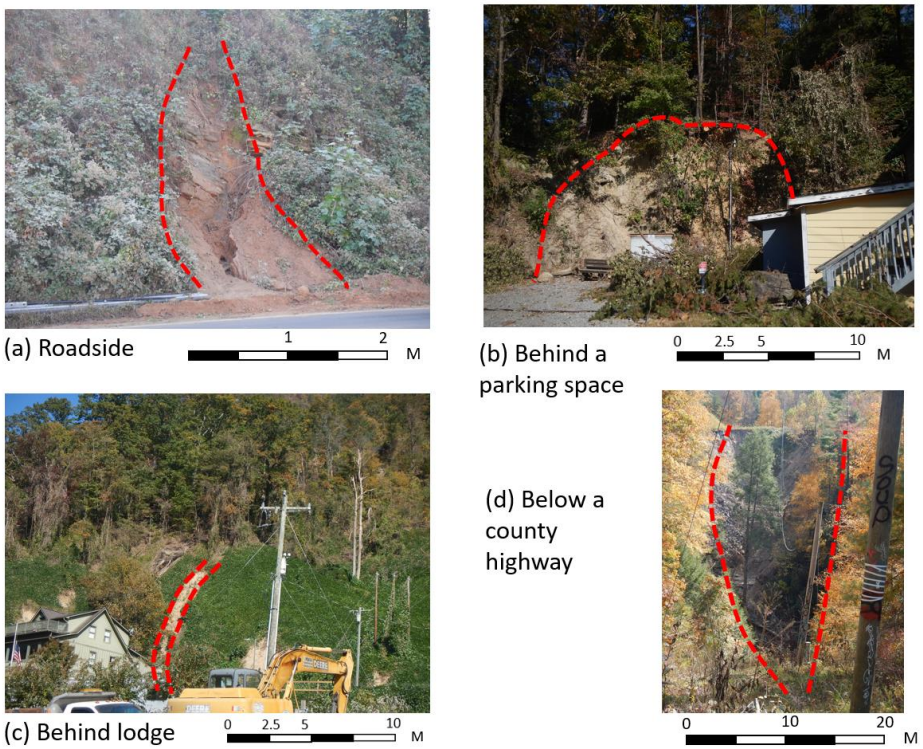

Figure 5-10 Hurricane Helene landslides to transportation structure and facilities: a) By a roadside near lake Lure; b) by a parking space near Chimney Rock; c) near a parking lot in Chimney Rock; d) below a county highway in Henderson Co. (Photo credit: Shen-En Chen, Sophia Lin, and Qifan Zhao)

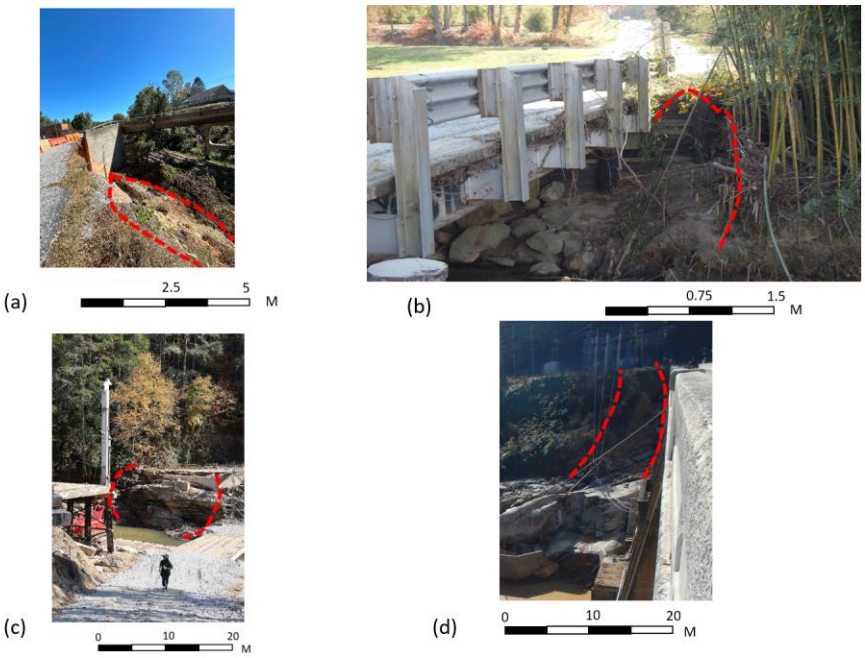

Figure 5-11 Hurricane Helene landslides damages to bridge structures: a) Main Street bridge over railroad, Saluda, NC; b) bridge near Lake Lure; c) ; d) Dam crossing, Lake Lure. (Photo credit: Shen-En Chen, Sophia Lin, and Qifan Zhao)

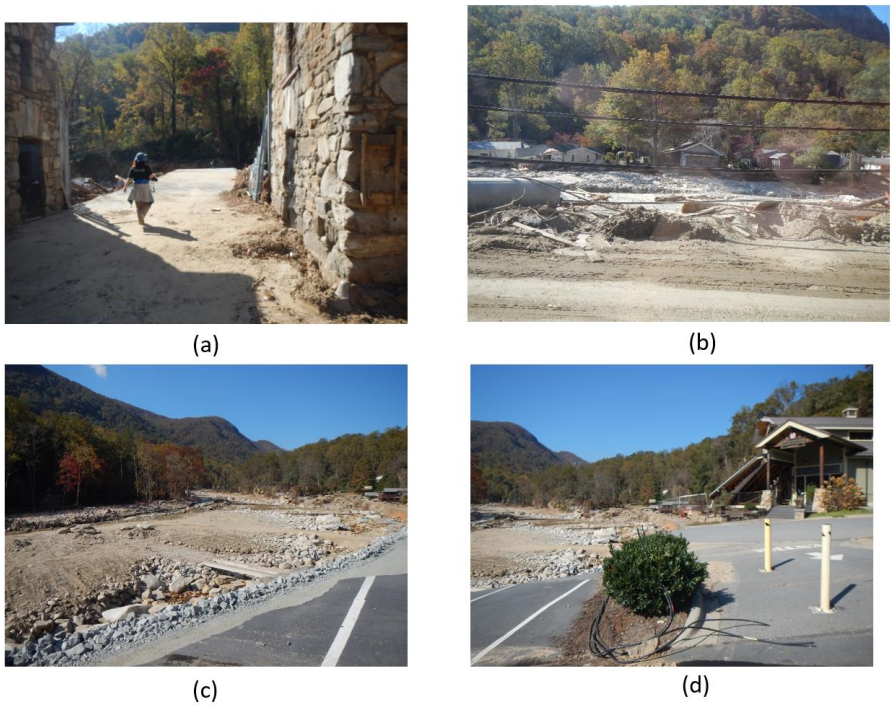

Figure 5-12 Hurricane Helene flood-battered region in Chimney Rock Village, NC: a) Washed away bridge on the Chimney Rock Scenic Road over the Broad River, Chimney Rock, Village, NC; b) from Main Street looking over Broad River; c) scoured Broad River basin in front of Burnshirt Vineyards Bistro on Main Street, Chimney Rock, NC; d) parking lot in front of Burnshirt Vineyards Bistro on Main Street, Chimey Rock, NC. (Photo credit: Shen-En Chen, Sophia Lin, and Qifan Zhao)

5.5 Discussion

Most ML-based landslide susceptibility studies are validated based on only sampled historical data; rarely does one get the opportunity to verify their prediction based on actual events [8, 9, 14, 15, 16, 37-39]. Most of the field surveys are performed to define the landslides [40]. The current research team was given a rare opportunity to validate our study with actual landslide events.

The objectives of this paper are two-fold: 1) To evaluate the performance of the landslide susceptibility mapping in the western mountain regions of North Carolina with the landslides resulting from the severe rainfall due to Hurricane Helene; 2) to report the disaster resulted from Hurricane Helene that pertains to the landslides in the mountains and to correlate the landslides to the damaging mechanisms to the bridges. As such, we will divide the discussion section into two subsections.

5.5.1 Landslide susceptibility mapping validation

One of the challenges in machine modeling for landslide susceptibility assessment is the issue of sampling (Wu et al., 2024). Using the rigorous approach, different sampling and modeling approaches may result in different susceptibility probabilities. Hence, the interpretation of what validates an ML-based susceptibility mapping is difficult to answer. This issue is further complicated by actual field investigation of landslides, since the interpretation of what is a landslide can be difficult due to the significant number of variables, both internal (i.e. lithology, slope angle, slope aspect, and slope profile) and external (e.g., rainfall and anthropogenic actions), that are required to characterize a landslide (Henriques et al., 2015).

As mentioned in section 3.1, the landslides resulting from Hurricane Helene matched different land susceptibility values and the outcomes are very similar for both for both with and without wildfire effects, indicating that wildfire effect may be minimal. Figure 5-8a and Figure 5-8b seem to indicate that there is not a big contrast between the wildfire affected landslides and the non-wildfire affected landslides. Both maps show that the landslides are clustered around the central regions of the maps with the most significant regions are in the Buncombe, Ash and Watauga Counties. Since the state database did not recognize the size of the landslides, it is hard to determine the extent of landslides. Hence, to decide what degree of susceptibility qualifies as a "positive" prediction, Figure 5-13 shows the accumulated distributions of both susceptibility values for both L+E and L+W+E cases. As shown, there are more than 50% of the landslides have higher than 60% (59.99%) landslide susceptibility values. If we define a 50% susceptibility value as a good prediction of landslide, then the confirmed landslides for Hurricane Helene are more than 50%.

A closer look at the landslide data showed that only one landslide has 0% prediction (in Wilkes County), which may be interpreted as a false prediction. There is also one case for 100% prediction (Polk County) for the L+E case. There are 9 cases and 18 cases of landslides that have more than 99% of predictions for both for both with and without wildfire effects cases, respectively. Figure 5-14 shows the locations of these landslides which are predominantly in Watauga, Henderson and Polk counties with one landslide in Avery County for both for both for both with and without wildfire effects cases (the same landslide).

We further plot the landslides against the landslide modeling variables including elevation, slope, aspect, soil type, rainfall, temperature, forest cover, distance to rivers,

distance to faults, distance to roads, distance to high population intensities and probability of wildfires in Figure 5-15. The results show that the landslide distribution is most consistent with rainfall indicating that rainfall may be the most critical independent variable for Hurricane Helene. However, more detailed information from Helene should be included for more precise analysis.

5.5.2 Observations to Helene landslides

Hurricane Helene triggered close to 2,000 landslides which contributed significant waste to the raised river water and flooded several valleys and lowlands in the mountain regions and damaged several bridges. To investigate the damage to the bridges, we computed the AFP described in section 2.2 to determine the flooding potential at each bridge. As shown in Appendix C, most of the damaged bridges have AFP less than 10 m, except bridge ID. 050026 over the North Toe River which has an AFP of 11.91 m. The lowest AFP reported is bridge ID. 040342, which is 0.5 m. With such low AFP, it is very probable that most of the damaged bridges were submerged under the heavy debris-ladened flood water in the river and may have experienced scours at both bridge embankments and bridge piers, which can result in the destabilization of both the bridge super and substructures and ultimately bridge collapses due to deck failure.

To illustrate the damaging effects of scour, Figure 5-16 shows the likely scouring of bridge structure during flooding: Figure 5-16a shows potential scour occurring at both bridge piers and bridge embankments, which can lead to increased stresses at the supporting soil medium around the bridge piers and cause instability to the super structure (Figure 5-16b). It is important to point out that most scour prediction models are either for clear water or for live beds (Figure 5-16c). The dashed line in Figure 5-16 represents the

possible scour from the heavily debris-ladened flood water from Helene. However, the hydrodynamic effects to bridge supporting soil medium remains to be investigated. Pregnolato et al. investigated the flooding impacts to bridge substructures and suggested that some of the flooding forces can damage beam supports and suggested that the consequences of bridge failure should be assessed by the number of days of closure [43].

Finally, to illustrate the difference between landslide and scour at the bridge embankments, we use a landslide over the Hungry River, Flat Rock, NC, as an example. Figure 5-17 shows the landslide with the whole view of the mass movement (Route 1802, Figure 5-17a) and our attempted indication of the debris slide (there is indication of a slip surface) and the scour recognized as deposition of waste (logs and large rocks) near the riverbed (Figure 5-17b). To differentiate landslide versus scour, Wu et al. (Wu et al., 2011) used Figure 5-17c to define a landslide, which ends at a distance, "b", that extends from the slide toe to the stream edge. Similarly, the deep-seated landslide involving rock fall and colluviums in the Kaoping Watershed region, Taiwan, the debris slide at Big Hungry Road Bridge site also involves a long slip plane (Wu et al., 2011). Not shown in the figure is a continuation of the slide above the roadway 1889. However, because of the deposition of debris, it is hard to differentiate the slide toe of the scoured river zone of the Hungry River in Henderson County.

Figure 5-18 shows the washed-out Big Hungry Road Bridge (ID: 4400055) over the Hungry River (upstream from the landslide). As shown, the bridge has severe scours at both abutments and the bridge deck was washed out. At the time of the photograph, construction is underway, and it is shown that the existing bridge abutments were damaged, but the pile foundation remained intact, although the bridge superstructure is gone.

5.6 Conclusions

Hurricane Helene caused a significant disaster in western North Carolina (NC) during September 2024 that the region is still recovering from. This event triggered numerous landslides and flooding due to the heavy rainfall and strong winds brought by the hurricane. Reports and platforms documented 1,792 landslides, 79 damaged bridges, and 102 fatalities, based on data from the USGS, NCDOT, and NC Department of Health and Human Services (NCDHHS) as of November 10th (NCDHHS, 2024; NCDOT, 2008; USGS, 2024). We use data on landslides and damaged bridges to validate our susceptibility maps and conduct ground observations to support the results.

In Figure 5-6 and Figure 5-7, although our two multi-hazard susceptibility maps yield similar results, placing the landslide locations from the USGS platform reveals a notable difference in probability ranges of 0 to 10% and 60 to 70% between the maps (Figure 5-9d). Our multi-hazard susceptibility maps include various variables (elevation, slope, aspect, soil type, rainfall, temperature, forest cover, distance to rivers, distance to faults, distance to roads, distance to high population intensities and probability of wildfires) (Figure 5-15). The distribution of landslide locations appears to be strongly correlated to rainfall (Figure 5-15e). The rainfall factor does not include data from September 25th-28th. Therefore, incorporating this data would enhance the accuracy of our future research.

Ground observations have been made in Macon County, Polk County, Henderson County, Rutherford County, and Buncombe County (Figure 5-3). The observations confirmed those landslides not only damaged roadways and parking facilities but also posed a significant threat to bridge stability, underscoring the vulnerability of infrastructure in high-risk areas. Our investigation revealed that bridge damage in the region was caused

by both landslides and river scours. For most bridges, the damage is at bridge embankments. While landslides, particularly debris flows, resulted from increased soil moisture leading to slope destabilization, river scours resulted from the erosive power of flood water, exacerbated by debris-ladened current. This dual threat contributed to widespread riverbank erosion and infrastructure damage, as observed along the Broad River near Chimney Rock Village. The extensive erosion and sediment deposition at bridge sites highlighted the interaction between landslide debris flows and flooding during Hurricane Helene.

In Appendix C, a lower average flood potential (AFP) bridges were especially vulnerable to submersion and scour, which we based on the damaged bridges from NCDOT. Most of the damaged bridges have AFP less than 10 m.

Differentiating between landslide induced and scour induced damage is essential for understanding the mechanisms that threaten transportation infrastructure in mountainous regions. Our findings demonstrate that assessing and mapping susceptibility to landslides can improve risk management strategies and inform the design of more resilient infrastructure. Future research should focus on refining susceptibility models to incorporate real-time rainfall and hydrological data, enabling more accurate predictions and preventive measures in vulnerable regions.

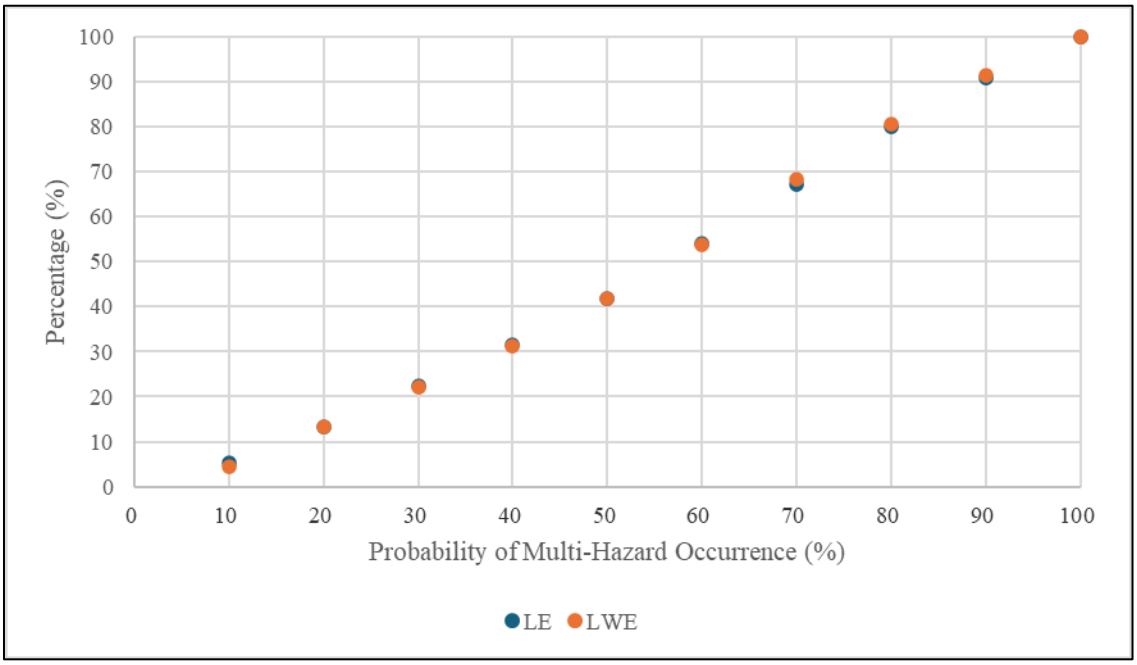

Figure 5-13 Helene landslides and the associated susceptibility values as an accumulated functions.

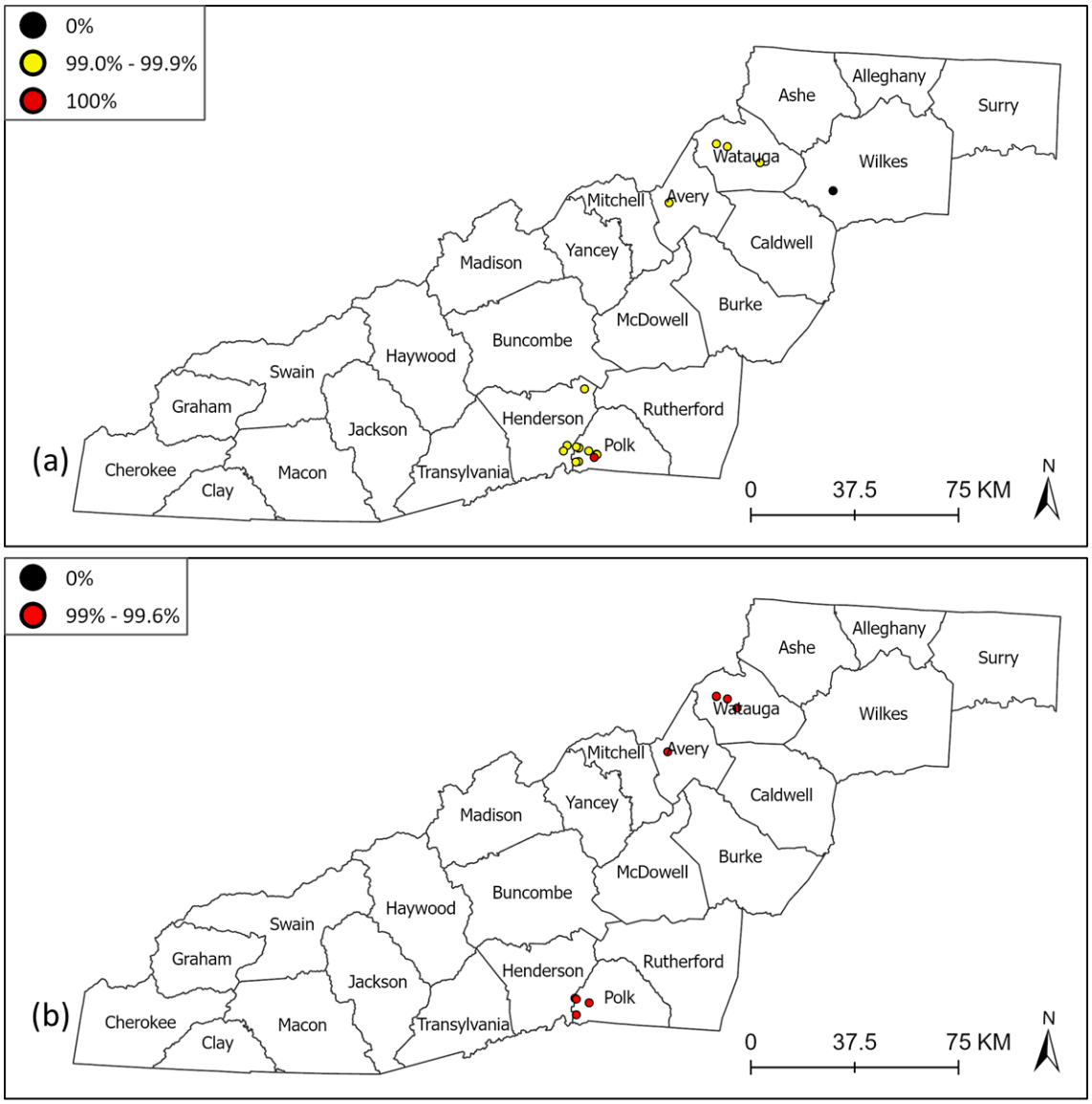

Figure 5-14 Landslides with zero and 99%~100% predictions for a) without wildfire effects; and b) with wildfire effects.

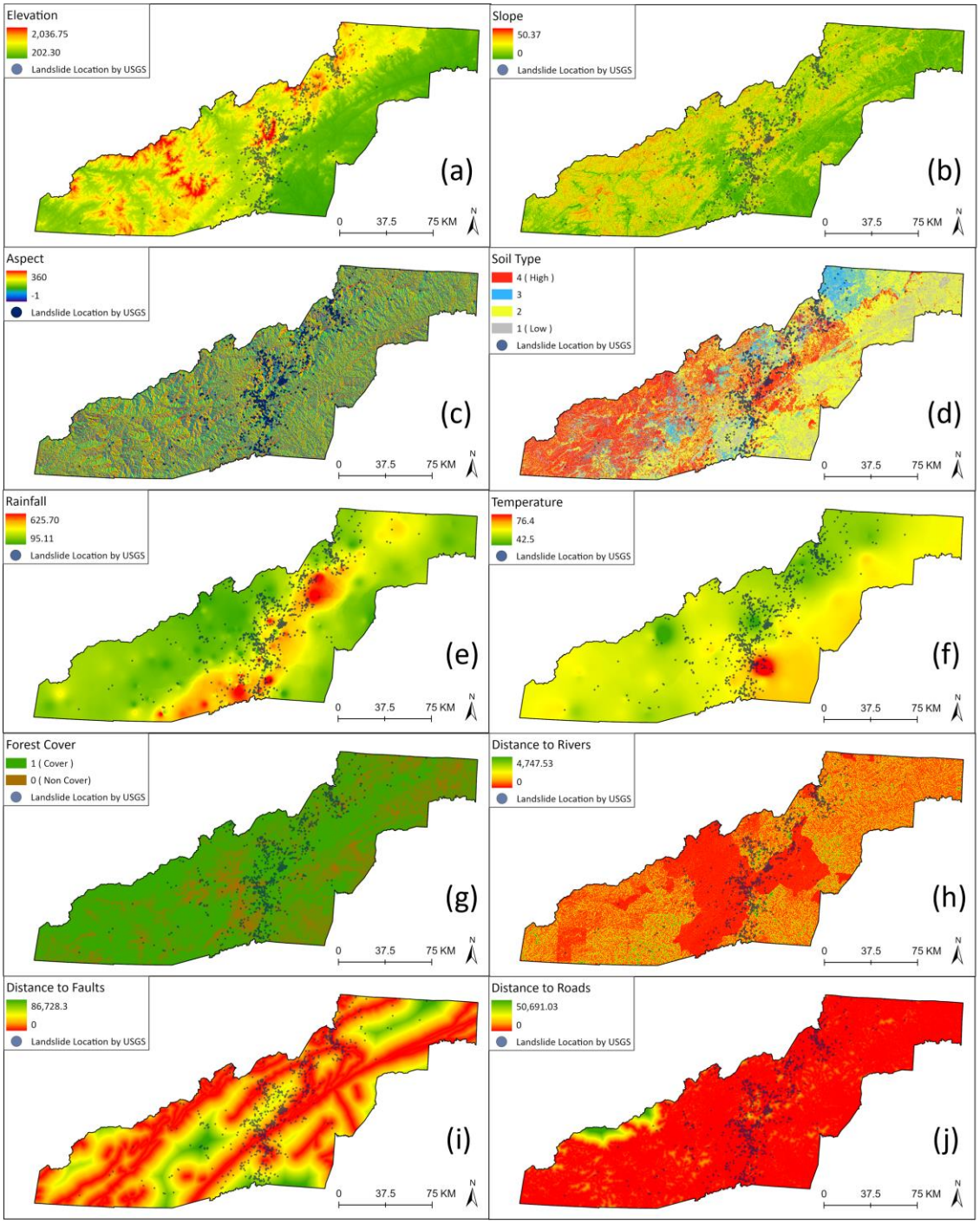
Elevation
2,036.75
202.30
Landslide Location by USGS
(a)
Slope
50.37
0
Landslide Location by USGS
(b)
Aspect
360
-1
Landslide Location by USGS
(c)
Soil Type
4 (High)
3
2
1 (Low)
Landslide Location by USGS
(d)
Rainfall
625.70
95.11
Landslide Location by USGS
(e)
Temperature
76.4
42.5
Landslide Location by USGS
(f)
Forest Cover
1 (Cover)
0 (Non Cover)
Landslide Location by USGS
(g)
Distance to Rivers
4,747.53
0
Landslide Location by USGS
(h)
Distance to Faults
86,728.3
0
Landslide Location by USGS
(i)
Distance to Roads
50,691.03
0
Landslide Location by USGS
(j)
0 37.5 75 KM
N

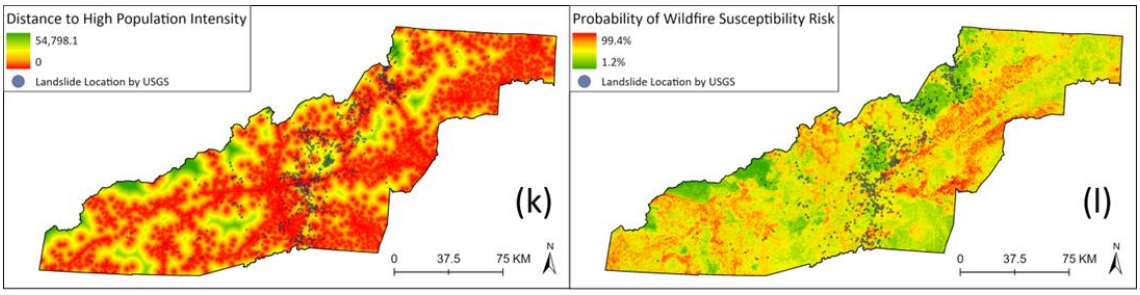

Figure 5-15 Conditioning factors used in this study including reported landslides: a. Elevation, b. Slope, c. Aspect, d. Soil type, e. Rainfall , f. Temperature, g. Forest cover, h. Distance to rivers, i. Distance to faults, j. Distance to roads, k. Distance to high population intensity, l. probability of wildfire occurrence.

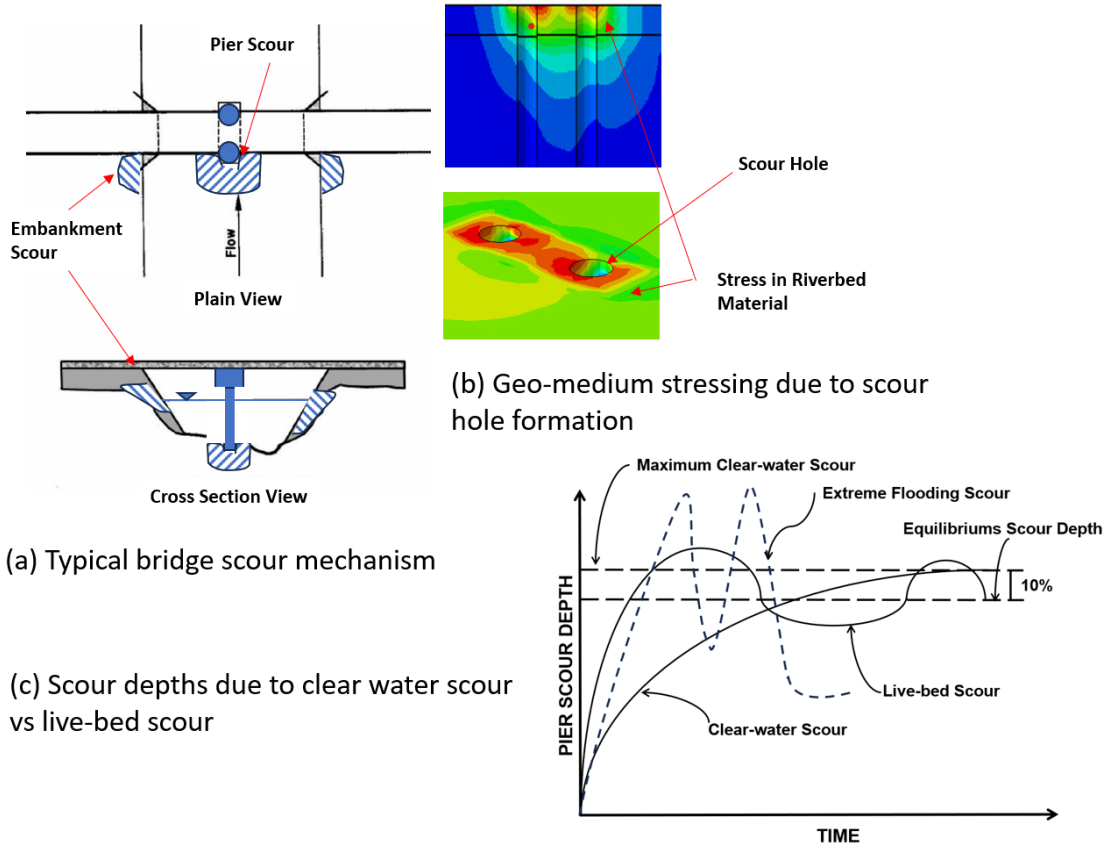

Figure 5-16 Typical bridge scour damage mechanism including the forming of scour holes (local scour) around bridge piers which can result in increased stress in the supporting geo-medium (riverbed material): a) typical scour mechanism; b) geo-medium stressing due to scour hole formation; c) scour depths due to clear water scour vs live-bed scour.

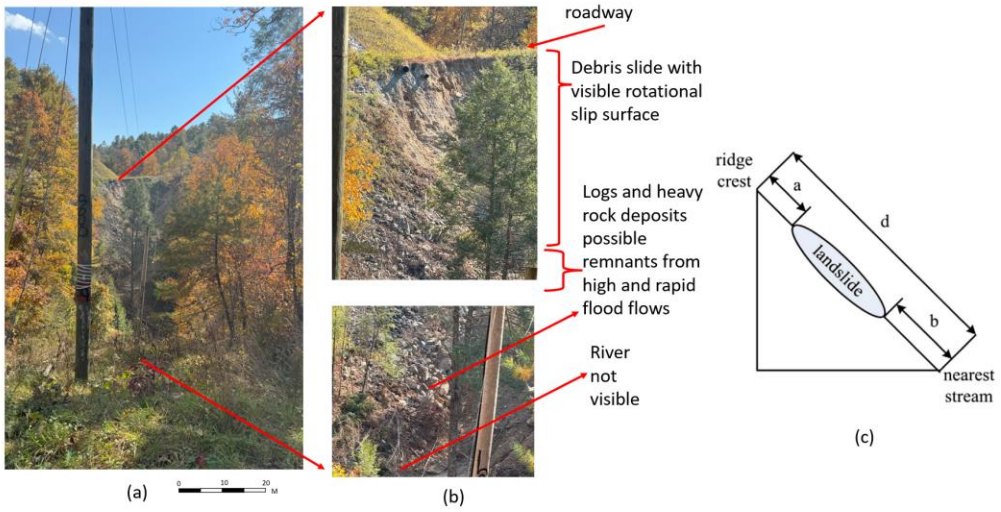

Figure 5-17 Debris slide and scour combined mass waste mechanism of the Hungry River: a) Whole view of the landslide Cord Road (Route 1802); and b) close up of the slide and the river deposits, and c) Landslide assumption by (Wu et al., 2011).

Figure 5-18 The reconstructing Big Hungry Road Bridge a) Flat Rock side; b) Flat Rock side; c) Flat Rock side and d) Opposite of Flat Rock. (Photo credit: Shen-En Chen, Sophia Lin, and Qifan Zhao)

Reference

Abdollahi, M., Vahedifard, F., & Leshchinsky, B. A. (2024). Hydromechanical modeling of evolving post-wildfire regional-scale landslide susceptibility. *Engineering Geology, 335*, 107538.

Arneson, L. A., Zevenbergen, L. W., Lagasse, P. F., & Clopper, P. E. (2012). Evaluating Scour at Bridges: Fifth Edition. Retrieved from https://rosap.ntl.bts.gov/view/dot/42053

Ayalew, L., & Yamagishi, H. (2005). The application of GIS-based logistic regression for landslide susceptibility mapping in the Kakuda-Yahiko Mountains, Central Japan. *Geomorphology*, *65*(1), 15-31. doi:https://doi.org/10.1016/j.geomorph.2004.06.010

Belair, G. M., Jones, E. S., Slaughter, S. L., & Mirus, B. B. (2022). *Landslide Inventories across the United States version 2: U.S. Geological Survey data release*.

Bjånes, A., De La Fuente, R., & Mena, P. (2021). A deep learning ensemble model for wildfire susceptibility mapping. *Ecological Informatics, 65*, 101397.

Breiman, L. (2001). Random Forests. *Machine Learning*, *45*(1), 5-32. doi:10.1023/A:1010933404324

Catani, F., Lagomarsino, D., Segoni, S., & Tofani, V. (2013). Landslide susceptibility estimation by random forests technique: sensitivity and scaling issues. *Natural Hazards and Earth System Sciences, 13*(11), 2815-2831.

Chen, W., Zhang, S., Li, R., & Shahabi, H. (2018). Performance evaluation of the GIS-based data mining techniques of best-first decision tree, random forest, and naïve Bayes tree for landslide susceptibility modeling. *Science of The Total Environment, 644*, 1006-1018.

Culler, E. S., Livneh, B., Rajagopalan, B., & Tiampo, K. F. (2023). A data-driven evaluation of post-fire landslide susceptibility. *Nat. Hazards Earth Syst. Sci., 23*(4), 1631-1652. doi:10.5194/nhess-23-1631-2023

DeBano, L. F., Rice, R. M., & Conrad, C. E. (1979). Soil heating in chaparral fires: effects on soil properties, plant nutrients, erosion, and runoff. *Berkeley, CA: U.S. Department of Agriculture, Forest Service, Pacific Southwest Forest and Range Experiment Station, Res. Paper PSW-RP-145*, 21 p.

Easterbrook, D. J. (1999). Surface processes and landforms. *(No Title)*.

Figueiredo, P., Hill, J., Merschat, A., Scheip, C., Stewart, K., Owen, L., . . . Horton, S. (2022). The Mw 5.1, 9 August 2020, Sparta earthquake, North Carolina: The first documented seismic surface rupture in the eastern United States. *GSA Today*, *32*(3-4).

Gallen, S. F., Wegmann, K. W., Frankel, K. L., Hughes, S., Lewis, R. Q., Lyons, N., . . . Witt, A. C. (2011). Hillslope response to knickpoint migration in the Southern Appalachians: implications for the evolution of post-orogenic landscapes. *Earth Surface Processes and Landforms, 36*(9), 1254-1267.

Hatcher, R. D., Tollo, R., Bartholomew, M., Hibbard, J., & Karabinos, P. (2010). The Appalachian orogen: A brief summary. *From Rodinia to Pangea: The Lithotectonic Record of the Appalachian Region: Geological Society of America Memoir, 206*, 1-19.

He, Q., Jiang, Z., Wang, M., & Liu, K. (2021). Landslide and Wildfire Susceptibility Assessment in Southeast Asia Using Ensemble Machine Learning Methods. *Remote Sensing, 13*(8), 1572. Retrieved from https://www.mdpi.com/2072-4292/13/8/1572

Ho, T. K. (1998). The random subspace method for constructing decision forests. *IEEE transactions on pattern analysis and machine intelligence, 20*(8), 832-844.

Langille, J.M., M. Palmer, and C. Green, *Evidence for Cenozoic topographic rejuvenation associated with the Laurel Creek Lineament in the Spruce Pine 7.5-minute quadrangle, western North Carolina, USA.* Journal of Maps, 2023. **19**(1): p. 2280594.

Leuenberger, M., Parente, J., Tonini, M., Pereira, M. G., & Kanevski, M. (2018). Wildfire susceptibility mapping: Deterministic vs. stochastic approaches. *Environmental Modelling & Software, 101*, 194-203. doi:https://doi.org/10.1016/j.envsoft.2017.12.019

Li, Z.-X., Bogdanova, S., Collins, A., Davidson, A., De Waele, B., Ernst, R., . . . Jacobs, J. (2008). Assembly, configuration, and break-up history of Rodinia: a synthesis. *Precambrian research, 160*(1-2), 179-210.

Lin, S. (2024). *Establishing Highway Bridge Network Resilience Against Multi-Hazards.* (Ph.D). University of North Carolina at Charlotte, Charlotte, North Carolina.

Lin, S., Chen, S.-E., Tang, W., Chavan, V., Shanmugam, N., Allan, C., & Diemer, J. (2024). Landslide Risks to Bridges in Valleys in North Carolina. *GeoHazards, 5*(1), 286-309. Retrieved from https://www.mdpi.com/2624-795X/5/1/15

NASA. (2024). The Landslide Identification Training. *Landslide Reporter's Guide.* Retrieved from https://gpm.nasa.gov/landslides/index.html

NCDHHS. (2024). Hurricane Helene Storm Related Fatalities. *Hurricane Helene Recovery Resources.* Retrieved from https://www.ncdhhs.gov/assistance/hurricane-helene-recovery-resources/hurricane-helene-storm-related-fatalities

NCDOT. (2008). DriveNC/TIMS Incidents data. Retrieved from https://drivenc.gov/?ref=share&type=state&layers=congestion&pins=incidents_planned-road-work,incidents_other-incidents,roads_interstate,roads_us,roads_nc

NCFS. (2024). *Historical Wildfire Information*. Retrieved from: https://www.ncforestservice.gov/fire_control/wildfire_statistics.htm

NWS, W.F.O., Morristown, TN. *Hurricane Helene: Record-Breaking Rainfall and Historic Flooding*. 2024 11/17/2024]; Available from: https://www.weather.gov/mrx/Hurricane_Helene.

Pourghasemi, H. R., Teimoori Yansari, Z., Panagos, P., & Pradhan, B. (2018). Analysis and evaluation of landslide susceptibility: a review on articles published during 2005–2016 (periods of 2005–2012 and 2013–2016). *Arabian Journal of Geosciences, 11*(9), 193. doi:10.1007/s12517-018-3531-5

Rasanen, R.A. and B.W. Maurer, *Probabilistic seismic source inversion from regional landslide evidence.* Landslides, 2022. **19**(2): p. 407-419.

Rasanen, R. A., & Maurer, B. W. (2023). Probabilistic seismic source inversion of the 1886 Charleston, South Carolina, earthquake from macroseismic evidence: A major updating. *Engineering Geology, 312*, 106958.

Regmi, N. R., Giardino, J. R., McDonald, E. V., & Vitek, J. D. (2014). A comparison of logistic regression-based models of susceptibility to landslides in western Colorado, USA. *Landslides, 11*(2), 247-262. doi:10.1007/s10346-012-0380-2

Reinhart, B. (2024). Seven-Day Graphical Tropical Outlook.

Rengers, F. K., McGuire, L. A., Oakley, N. S., Kean, J. W., Staley, D. M., & Tang, H. (2020). Landslides after wildfire: initiation, magnitude, and mobility. *Landslides, 17*(11), 2631-2641. doi:10.1007/s10346-020-01506-3

Services, D. o. A. a. C. (2016). Forest cover. Retrieved from https://www.nconemap.gov/datasets/ncgar:forest-land-cover-2016.

Short, K. C. (2021). Spatial wildfire occurrence data for the United States, 1992-2018 [FPA_FOD_20210617]. 5th Edition (Publication no. https://doi.org/10.2737/RDS-2013-0009.5). Retrieved 07/05/2022

State, N. C. S. o. (2024). Geography. Retrieved from https://www.sosnc.gov/divisions/publications/kids_page_geography

Sun, D., Wen, H., Zhang, Y., & Xue, M. (2021). An optimal sample selection-based logistic regression model of slope physical resistance against rainfall-induced landslide. *Natural Hazards, 105*(2), 1255-1279. doi:10.1007/s11069-020-04353-6

USGS. (2024). Preliminary data for the 2024 Hurricane Helene Landslide Emergency Response: 2024 USGS Provisional Data Release. Retrieved from https://doi.org/10.5066/P1G6Y6HP. Retrieved 11/05/2024.

Wooten, R., Gillon, K., Witt, A., Latham, R., Douglas, T., Bauer, J., . . . Lee, L. (2008). Geologic, geomorphic, and meteorological aspects of debris flows triggered by Hurricanes Frances and Ivan during September 2004 in the Southern Appalachian Mountains of Macon County, North Carolina (southeastern USA). *Landslides, 5*(1), 31-44.

Wooten, R. M., Witt, A. C., Miniat, C. F., Hales, T. C., & Aldred, J. L. (2016). Frequency and magnitude of selected historical landslide events in the southern Appalachian Highlands of North Carolina and Virginia: relationships to rainfall, geological and ecohydrological controls, and effects. *Natural Disturbances and Historic Range of Variation: Type, Frequency, Severity, and Post-Disturbance Structure in Central Hardwood Forests USA*, 203-262.

Wu, C.-H., Chen, S.-C., & Chou, H.-T. (2011). Geomorphologic characteristics of catastrophic landslides during typhoon Morakot in the Kaoping Watershed, Taiwan. *Engineering Geology, 123*(1-2), 13-21.

Appendix C

No	Bridge ID	Stream	Bridge Length (m)	AFP (m)	Report State
1	040342	North Fork New River	28	0.50	underwater
2	040480	North Fork New River	18.8	0.51	underwater
3	040296	North Fork New River	28	0.53	underwater
4	040183	Cranberry Creek	15.2	0.56	underwater
5	040093	North Fork New River	35.9	0.57	wash out
6	040425	Grassy Creek	7.9	0.60	underwater
7	040483	Helton Creek	9.4	0.69	underwater
8	940089	South Fork New River	30.7	0.69	damage
9	040047	Helton Creek	16.7	0.72	wash out
10	040351	South Fork New River	49.3	0.76	underwater
11	040509	South Fork New River	49.3	0.77	wash out
12	040226	South Fork New River	31	0.80	underwater
13	130161	Wilson Creek	14.3	0.82	wash out
14	040354	Big Laurel Creek	9.4	0.83	underwater
15	040466	South Fork New River	37.1	0.85	underwater
16	040206	Helton Creek	28	0.87	underwater
17	040304	Helton Creek	15.5	0.91	underwater
18	040258	Middle Fork Horse Creek	7.6	0.91	damage
19	040463	North Fork New River	50.9	0.94	underwater
20	940178	Cove Creek	15.2	0.95	wash out
21	040048	Helton Creek	12.8	0.99	underwater
22	940271	Watauga River	32.9	1.00	underwater
23	020132	Elk Creek	15.2	1.02	wash out
24	940082	Watauga River	36.8	1.02	underwater
25	040289	Helton Creek	18.5	1.07	underwater
26	040140	Cranberry Creek	18.5	1.11	underwater
27	040121	North Fork New River	73.7	1.14	wash out
28	940161	Watauga River	23.1	1.15	underwater
29	100866	Swannanoa River	42.9	1.25	damage
30	100032	Swannanoa River	34.1	1.28	damage
31	020062	Crab Creek	13.7	1.29	damage
32	940058	Beech Creek	14.6	1.36	wash out
33	040477	South Fork New River	28	1.40	wash out
34	040337	North Fork New River	37.1	1.41	wash out
35	940168	Cove Creek	15.8	1.42	wash out
36	440041	Lewis Creek	10.6	1.49	closed by lane
37	040343	Cranberry Creek	12.8	1.50	underwater
38	040426	Grassy Creek	9.1	1.55	underwater
39	050125	Elk River	40.5	1.56	wash out
40	050101	Elk River	43.2	1.56	wash out
41	940086	Howard Creek	9.4	1.64	underwater
42	580285	North Fork Catawba River	21	1.66	wash out

43	100041	Swannanoa River	18.2	1.71	damage
44	040177	South Beaver Creek	18.8	1.91	underwater
45	050035	Elk River	36.8	1.97	wash out
46	940187	Meat Camp Creek	7	1.98	damage
47	940032	Meat Camp Creek	12.4	1.99	wash out
48	040122	North Fork New River	79.5	2.06	wash out
49	740037	Green River	47.8	2.08	closed by lane
50	430046	Jonathan Creek	29.8	2.10	closed by lane
51	440038	Clear Creek	43.2	2.22	wash out
52	580119	North Fork Catawba River	22.2	2.27	wash out
53	430225	Pisgah Creek	9.4	2.34	wash out
54	940016	Middle Fork S.Frk. New River	20.7	2.35	damage
55	430008	Pisgah Creek	10.9	2.36	wash out
56	440055	Hungry River	41.4	2.51	closed by lane
57	440026	Hoopers Creek	22.8	2.56	wash out
58	100785	Swannanoa River	13.7	2.59	damage
59	440063	Lake Summit	80.1	2.86	wash out
60	100552	Swannanoa River	52.4	2.90	damage
61	100890	Swannanoa River	46.9	3.10	damage
62	440027	Hoopers Creek	32.3	3.12	wash out
63	940280	Brushy Fork Creek	9.4	3.12	wash out
64	580111	North Fork Catawba River	36.8	3.23	closed by lane
65	800313	Broad River	53.6	3.28	wash out
66	130318	Harper Creek	24.9	3.40	damage
67	100380	Swannanoa River	61.5	3.72	damage
68	580083	Buck Creek	35	3.73	wash out
69	430111	East Fork Pigeon River	49.6	4.28	closed by lane
70	990097	South Toe River	48.7	4.50	wash out
71	740112	North Pacolet River	36.8	4.50	wash out
72	800060	Broad River	37.7	4.97	damage
73	990056	South Toe River	61.2	6.27	damage
74	100517	Swannanoa River	61.8	6.48	damage
75	040056	North Fork New River	101.1	6.99	damage
76	110368	Lake James Canal	146.6	7.41	damage
77	440214	Broad River	50.2	7.98	damage
78	990044	Cane River	73.1	8.16	damage
79	050026	North Toe River	85.3	11.91	damage

Chapter 6: Conclusion

This dissertation provides a comprehensive multi-hazard risk assessment model targeting landslide, flood, wildfire, and earthquake vulnerabilities in bridge infrastructure across North Carolina's mountainous regions. By integrating logistic regression (LR) and random forest (RF) modeling within ArcGIS Pro and RStudio, we demonstrated susceptibility maps that pinpoints high-risk bridges (bridge-in-valley), offering actionable insights for proactive maintenance and mitigation strategies. This study's use of extensive geospatial and statistical methods provides a robust framework for understanding infrastructure vulnerability in climate-sensitive landscapes, guiding state transportation departments in risk management and resource allocation.

The destructive impact of Hurricane Helene in 2024 exemplifies the multi-hazard risks faced by bridges under extreme weather events in NC. Field investigations revealed that landslide and scour-induced failures were particularly prevalent at bridge embankments, where sediment deposition and debris flows heightened structural vulnerabilities. This hurricane event further validates the importance of predictive multi-hazard mapping and its role in identifying high-risk infrastructure, enabling more resilient designs and response strategies for future events. Based on our numerical research of the multi-hazard with bridges, the following conclusions and comments can be drawn in the following paragraphs:

In chapter 2, we inspired by the extensive damage to Puerto Rican bridges during Hurricane Maria, a landslide risk susceptibility analysis was conducted for NC, where numerous bridges face multi-hazard threats from landslides and flooding. By applying LR and RF models, a landslide risk map was created, with RF proving more accurate and

sensitive, achieving an 82.7% accuracy rate. This chapter incorporated bridge data and assumed flooding potential (AFP), identified 37 bridges at high risk and in valley from both landslides and flooding. Field observations confirmed these risks, particularly for bridge 740002, affirming the model's reliability as a proactive tool for infrastructure managers. Although this study primarily considered aspect and seismicity variables, future work could include geological and lithological factors to enhance precision. This approach offers a foundation for improving infrastructure resilience and guiding decision-makers in safeguarding vulnerable bridges.

In chapter 3, it conducted a risk susceptibility analysis to identify vulnerable highway bridges in NC's western mountainous region, a necessity underscored by the recent devastation caused by Hurricane Helene in September 2024, which led to fatalities, injuries, and significant bridge and road damage due to flooding and landslides. The multi-hazard analysis focused on landslide and flooding risks and incorporated additional risks from earthquakes and wildfires, forming a comprehensive, nested approach. Using RF model, landslide and wildfire susceptibility maps were generated, achieving higher predictive accuracy (wildfire: 72.9%, landslide (with wildfire): 83.9%). Especially though soil type was included as a landslide predictor, it did not substantially increase model accuracy, suggesting a need for refined soil classifications in future studies. Compared with chapter 2 results, incorporating AFP as an indicator of multi-hazard vulnerability, revealed that the number of bridges with over a 50% probability of multi-hazard risk reduced from 47 to 26. However, four additional bridges were newly identified as high-risk, suggesting increased vulnerability to wildfire-triggered landslides.

In chapter 4, the 2024 hurricane season, marked by Hurricanes Helene and Milton, caused severe infrastructure damage and loss of life, especially in the Appalachian Mountains, where over 1,100 landslides and more than 400 bridge damages were reported. Observations highlight that scouring and landslides at bridge approaches are major contributors to bridge failures, disrupting essential transport and local safety.

In our last chapter, Hurricane Helene caused widespread destruction in western North Carolina in September 2024, triggering 1,792 landslides, damaging 79 bridges, and resulting in 102 fatalities. This study validated susceptibility maps against field observations and USGS data, revealing that bridge damage often occurred at embankments due to landslides and river scour. Landslide debris flows destabilized slopes, while flood-induced scouring eroded bridge foundations, especially along rivers like the Broad River. Findings showed that bridges with lower AFP were particularly vulnerable to submersion and scour. Differentiating landslides induced from scour induced damage is crucial for infrastructure protection, emphasizing the importance of accurate susceptibility mapping.

Chapter 7: Recommended Future Research

1. Developing accurate landslide risk models remains challenging due to the complex interplay of geological, hydrological, topographical, and human factors. While this study provides a foundational tool for proactive bridge management, future research could improve precision by incorporating additional geological and lithological data.
2. To maintain bridge functionality during future storms, extending bridge decks further into roadway sections is recommended to reduce the impact of scouring and landslides on bridge approaches. However, more research are needed to provide quantitative design criteria for future bridges.
3. It should incorporate real-time rainfall and hydrological data to improve predictive accuracy and resilience planning.
4. The findings underscore the urgent need for adaptive infrastructure resilience planning, especially for critical transportation assets like bridges. The insights from this research contribute to a growing body of knowledge in multi-hazard assessment, reinforcing the concept of resilience as central to infrastructure management amidst escalating climate extremes.